Aggregation and toxicity of seipin/*BSCL2* N88S mutant associated with motor neuron degeneration

Verónica Andrade Nogueira
Mestrado em Bioquímica
Departamento de Química e Bioquímica
2021

Orientador
Vitor Teixeira, Ph.D., Investigador Júnior, IBMC/i3S, Universidade do Porto, vitor.teixeira@ibmc.up.pt

Coorientador
Vítor Costa, Ph.D., Professor Associado, ICBAS, Investigador Principal, IBMC/i3S, Universidade do Porto, vcosta@ibmc.up.pt

Todas as correções determinadas pelo júri, e só essas, foram efetuadas.

O Presidente do Júri,

Porto, _____/_____/_____

Acknowledgements

Finalizada uma das etapas mais importantes da minha vida académica, é com enorme satisfação que aqui expresso um profundo agradecimento a todos aqueles que me apoiaram nesta longa caminhada e que, de uma forma ou de outra, tornaram possível a realização deste trabalho.

Primeiramente, queria agradecer ao meu orientador Dr. Vitor Teixeira por, através dos seus aconselhamentos e exigência, orientar o meu trabalho da melhor forma possível. Não posso também deixar de agradecer pela paciência, disponibilidade e por todas as respostas prontas a todas as dúvidas e mais algumas. Todos os ensinamentos partilhados foram, sem dúvida alguma, fundamentais para minha formação científica.

Quero também deixar uma palavra de agradecimento ao meu coorientador Prof. Vítor Costa, pela oportunidade de realizar a minha tese de Mestrado no seu grupo de investigação (Yeast Signalling Networks, i3S), por todos os conhecimentos partilhados e pelo voto de confiança.

Deixo também um agradecimento a todos os restantes membros do meu grupo, pela integração, pelos ensinamentos e por estarem sempre disponíveis para me ajudarem. Agradeço também aos elementos do grupo Phenotypic Evolution, pela companhia, pelos conselhos e pelo excelente ambiente de trabalho.

Como não poderia deixar de o fazer, quero agradecer a todos os meus amigos que me apoiaram em todos os momentos do meu percurso académico, principalmente ao meu colega e amigo Tiago por me ter acompanhado ao longo destes anos de Licenciatura e Mestrado. Obrigada pela amizade, pelo apoio nos momentos mais difíceis e por nunca teres deixado de acreditar em mim. Aos meus amigos de longa data, Rute, Rui Pedro e Nuno Faria, que me apoiaram e estiveram sempre presentes ao longo destes anos, expresso aqui também a minha gratidão.

Ao meu namorado Nuno, pelo apoio incondicional, por todo o amor, amizade, carinho e…paciência! Obrigada por me incentivares a ser uma pessoa melhor todos os dias, por me acalmares quando mais preciso e me fazeres acreditar em mim mesma. Obrigada pela compreensão, por nunca me teres deixado desistir e por estares sempre do meu lado.

Por último, quero agradecer à minha mãe por toda a paciência, por tudo o que sempre fez por mim e por me dar a oportunidade de chegar aqui hoje. Do mesmo modo, agradeço à minha irmã que também sempre me apoiou. Obrigada por acreditaram em mim e me encorajaram a ser melhor. Agradeço o vosso apoio em todas as decisões, mesmo quando têm que aturar as frustrações e reclamações quando as

coisas correm menos bem. Vocês foram fundamentais durante todo o meu percurso académico e sem vocês a realização deste sonho certamente não teria sido possível. A todos os que direta ou indiretamente contribuíram para este trabalho, um sincero obrigada!

Abstract

Gain-of-function N88S mutation in the seipin *BSCL2* gene was identified in a cohort of autosomal dominant motor neuron diseases (MNDs) known as seipinopathies. Previous work has shown that this mutation disrupts *N*-glycosylation, leading to the formation of aggregates into inclusion bodies (IBs) and contributing to severe ER stress and cell death. Importantly, the nature of these aggregates and their contribution to neuron dysfunction is poorly understood.

Our work aimed to establish a humanized yeast model of N88S seipinopathy to study the behavior and the molecular effects of different combinations of human wild-type (WT) and N88S mutant seipin. For this purpose, a Venus-based bimolecular fluorescence complementation assay was employed. As in mammalian systems, our yeast model recapitulates the formation of IBs associated with activation of the unfolded protein response (UPR). We also report the activation of autophagy and of the Hrd1-mediated endoplasmic reticulum-associated degradation (ERAD) in cells expressing mutant homomers and WT-mutant heteromers of seipin. Importantly, the N88S mutation appears to induce changes in ER morphology in association with Kar2p chaperone and Hsp104p disaggregase.

For the first time, we have determined that N88S homo-oligomers expressing cells present reduced viability, decreased antioxidant activity and increased oxidative damage associated with higher ROS levels and lipid peroxidation. This was correlated with the activation of oxidative stress sensor Yap1p. The relationship between ER stress and calcineurin signaling in the context of N88S seipinopathy was also assessed. Our results showed impaired activation of calcineurin signaling in the N88S homomeric strain. Moreover, abrogating calcineurin activity had no effect on ROS levels but increased the formation of IB in all strains, especially in cells expressing the N88S mutation, which indicates that calcineurin is involved in the formation of IBs. Lastly, activation of ERAD and UPR quality control mechanisms were essential for proper cell growth and proved to be crucial to prevent excessive accumulation of IBs and ROS in cells expressing the N88S mutation.

Our work established that the N88S-N88S homo-oligomer is the species that actively contribute to enhance mutant seipin toxicity, resulting in severe cellular oxidative damages and induction of ER stress response that can be modulated, to some extent, by WT seipin. Although much remains to be discovered regarding the mechanisms of molecular pathogenesis of N88S seipinopathies, our study provides new insights into the molecular underpinnings of these diseases.

Keywords: N88S seipinopathy**,** N88S mutant seipin toxicity, *Saccharomyces cerevisiae*, inclusion bodies, endoplasmic reticulum stress, oxidative stress, quality control mechanisms.

Resumo

A mutação de ganho de função N88S, localizada no gene *BSCL2*, está associada ao surgimento de doenças autossómicas dominantes dos neurónios motores (MNDs), também designadas por seipinopatias. Trabalhos prévios demonstraram que esta mutação promove a disrupção do motivo de *N*-glicosilação da seipina, promovendo a formação de agregados em corpos de inclusão, e contribuindo para um estresse severo no retículo endoplasmático e para a morte celular. Todavia, a natureza destes agregados e a sua contribuição para a disfunção dos neurónios permanece desconhecida.

Neste sentido, o nosso trabalho visou estabelecer um modelo humanizado de levedura de seipinopatia N88S e estudar o comportamento e os efeitos moleculares de diferentes combinações de seipina humana WT e seipina humana mutante N88S. Para este fim, recorremos ao ensaio de complementação de fluorescência bimolecular. Tal como observado em modelos de mamíferos, o nosso modelo de levedura recapitula a formação de corpos de inclusão associada à ativação da *Unfolded Protein Response* (UPR). Verificamos, ainda, que ocorre a ativação da autofagia e da degradação associada ao retículo endoplasmático (ERAD) mediada por Hrd1 em células que expressam homómeros N88S-N88S e heterómeros WT-N88S. Além disso, a mutação N88S parece induzir alterações na morfologia do retículo endoplasmático, associadas à chaperone Kar2p e à Hsp104p.

Adicionalmente, determinamos, pela primeira vez, que as células que expressam homo-oligómeros N88S apresentam viabilidade e atividade antioxidante reduzidas e um aumento dos danos oxidativos associados a elevados níveis de espécies reativas de oxigénio (ROS) e peroxidação lipídica. É importante salientar que este aumento dos danos oxidativos está relacionado com a ativação do sensor de estresse oxidativo Yap1p. A relação entre o estresse no retículo endoplasmático e a sinalização mediada pela calcineurina no contexto da seipinopatia N88S também foi avaliada. Os nossos resultados revelaram uma ativação comprometida da sinalização da calcineurina na estirpe homomérica N88S-N88S. Além disso, a disrupção da atividade da calcineurina não teve qualquer efeito nos níveis de ROS, apesar de ter aumentado a formação de corpos de inclusão em todas as estirpes, particularmente nas células que expressam a mutação N88S, sugerindo que a calcineurina está envolvida na formação destes corpos de inclusão. Por fim, a ativação dos mecanismos de controlo de qualidade ERAD e UPR não só demonstraram ser essenciais para um crescimento celular apropriado, como provaram ser cruciais para evitar a acumulação

excessiva de corpos de inclusão e de ROS nas células que expressam a mutação N88S.

O nosso trabalho estabeleceu que os homo-oligómeros N88S-N88S são as espécies que contribuem ativamente para aumentar a toxicidade da seipina mutante, resultando em graves danos celulares oxidativos e indução de resposta ao stress no retículo endoplasmático, que podem ser modulados, até determinado ponto, pela seipina WT. Embora ainda haja muito para descobrir relativamente aos mecanismos de patogénese molecular das seipinopatias N88S, o nosso estudo proporciona novos conhecimentos sobre os fundamentos moleculares deste grupo de doenças.

Palavras-chave: Seipinopatia N88S, toxicidade da seipina N88S mutante, *Saccharomyces cerevisiae*, corpos de inclusão, estresse no retículo endoplasmático, estresse oxidativo, mecanismos de controlo de qualidade.

Table of Contents

Figure List

Table List

List of Abbreviations

ACAT	Acyl-coenzyme A: cholesterol acyltransferases
ACSL	Acyl-CoA synthetase
AGPAT	Acylglycerol- phosphate acyltransferase
ATF6	Activating transcription factor 6
ATGL	Adipose triglyceride lipase
ATP	Adenosine Triphosphate
BiFC	Bimolecular fluorescence complementation
BSCL2	Berardinelli-Seip congenital lipodystrophy type 2
bZIP	Basic leucine zipper Domain
CCT	CTP: phosphocholine cytidylyltransferase
CDP	Cytidine diphosphate
CDRE	Calcineurin-dependent response element
CGL	Congenital generalized lipodystrophy
CHX	Cycloheximide
CMT2D	Charcot-Marie-Tooth disease type 2
CoA	Coenzyme A
COP	Coatamer protein
CPY*	Carboxypeptidase Y
DAG	Diacylglycerol
DGAT	Acyl-CoA: diacylglycerol acyltransferase
DHE	Dihydroethidium
dHMN	Distal hereditary motor neuropathy
DNA	Deoxyribonucleic acid
dNTPs	Deoxynucleotides
DTT	Dithiothreitol
EDTA	Ethylenediaminetetraacetic acid
eIF2α	Eukaryotic translation initiation factor 2

ER	Endoplasmic reticulum
ERAD	ER-associated degradation
ERO1	ER oxidoredutase 1
EV	Empty vectors
FAD	Flavin adenine dinucleotide
FAs	Fatty acids
FFAs	Free FAs
FIT2	Fat storage-inducing transmembrane 2
GFP	Green fluorescent protein
GPAT	Glycerol-phosphate acyltransferase
GSH	Glutathione (reduced form)
GSSG	Glutathione (oxidized form)
HSL	Hormone-sensitive lipase
HSP	Heat shock protein
IB	Inclusion bodies
IRE1	Inositol-requiring protein 1
LA	Lithium acetate
LAL	Lysosomal acid lipase
LB	Lysogeny broth
LBD	Lipid binding domain
LDAF1	Lipid Droplet Assembly Factor 1
LDs	Lipid droplets
LPA	Lysophosphatidic acid
MAGL	MAG lipase
MDA	Malondialdehyde
MGAT	Acyl CoA: monoacylglycerol acyltransferase
MNDs	Motor neuron diseases
NAC	N-acetylcysteine
NADPH	Nicotinamide adenine dinucleotide phosphate

NLs	Neutral lipids
ONPG	O-nitrophenylgalactopyranosyde
ORF	Open reading frame
PA	Phosphatidic acid
PAGE	Polyacrylamide gel electrophoresis
PAP	Phosphatidic acid phosphohydrolase
PBS	Phosphate buffered saline
PC	Phosphatidylcholine
PCR	Polymerase chain reaction
PDI	Protein disulfide isomerase
pDNA	Plasmid DNA
PDS	Post-diauxic shift
PE	Phosphatidylethanolamine
PEG	Polyethylene glycol
PERK	Protein kinase RNA-like ER kinase
PL	Phospholipid
PLIN	Perilipins
QC	Quality control
ROS	Reactive oxygen species
Rpm	Rotation per minute
SC	Synthetic complete
SD	Standard deviation
SDS	Sodium dodecyl sulfate
SEs	Sterol esters
SOD	Superoxide dismutase
TAE	Tris-acetate-EDTA
TAGs	Triacylglycerols
TBS	Tris buffered saline
TE	Tris EDTA

TEMED	N, N, N, N-Tetramethylethylenediamine
TM	Transmembrane
Tris-HCL	Tris-Hydrocloride
TTBS	Tris-tween buffered saline
UPR	Unfolded protein response
UPRE	Unfolded protein response element
UPS	Ubiquitin–proteasome system
VC	C-terminal fragment of Venus
VN	N-terminal fragment of Venus
YNB	Yeast nitrogen base
YPD	Yeast peptone dextrose
YPG	Yeast peptone glycerol

Chapter 1
INTRODUCTION

1. Introduction

1.1. Lipid droplets: structure and function

Lipid droplets (LDs) are ubiquitous cellular organelles of neutral lipids (NLs) storage [1]. These dynamic cytoplasmic organelles consist of a neutral lipid core, mainly of triacylglycerols (TAGs) and sterol esters (SEs) [2], enclosed by a distinctive phospholipid (PL) monolayer (instead of the typical bilayer) that is decorated with integral and peripheral proteins (Figure 1) [1]. LD heterogeneity, defined by distinct number, size, and composition of LDs, has been observed in different cells and usually reflects distinct metabolic states in response to nutrient and environmental cues [1]. LDs are found mostly in the cytoplasm, but in some cell types they are also present in the nucleus [3]. They are generated *de novo* in the Endoplasmic Reticulum (ER) membrane and their degradation occurs through enzymatic hydrolysis mediated by lipases (lipolysis) or through selective form of autophagy (lipophagy) [1, 4].

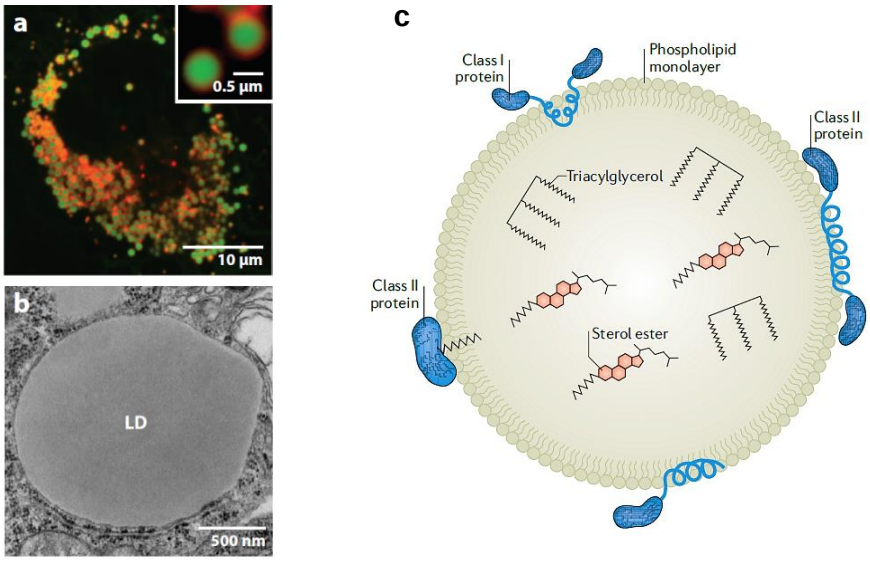

Figure 1. Lipid droplets (LDs) are ubiquitous storage organelles for neutral lipids (NLs) that can be found in most cells, from yeast to man. (a) Fluorescence microscopy image showing LDs (green, labeled with BODIPY 493/503) in mammalian SUM159 cells. Cells carry the LD marker mCherry-LiveDrop (red). **(b)** Electron micrograph showing a LD in *Drosophila* S2 cells. The rough ER bilayer can be seen in proximity. Figures (a) and (b) are adapted from [3]. **(c)** Despite the morphological diversity, all LDs have a similar structural and unique architecture. Instead of the typical phospholipid bilayer, LDs have a phospholipid monolayer surrounding a core filled by NLs, usually triacylglycerol and sterol esters. Adapted from [2].

As a result of the activation of LD breakdown, liberated fatty acids (FAs) can be quickly channeled into the β-oxidation pathway in mitochondria or peroxisomes, possibly through membrane contact sites [5]. These processes strongly reflect cellular metabolism and cycles of nutrient availability: during starvation, lipids stored in conditions of nutrient surplus are mobilized for energy production or for PL synthesis during high demand of membranes [1]. Moreover, LDs have the ability to buffer and

store cellular amounts that are buildup in excess, such as FAs, toxic glycerolipids, PLs and sterols in cell membranes, thus having important roles in preventing lipotoxicity and oxidative stress response [1, 3]. LDs also harbor some proteins/enzymes related to LD metabolism (e.g., specific enzymes of NL synthesis or lipolysis such as DGAT2), or, in some cases, proteins (e.g., histones) that affect transcription and gene expression [3, 6].

During their life cycle, LDs create contacts with several other cellular organelles. The most important organelle is the ER, which supplies LDs with most of their lipid components and plays a key role in their biogenesis. LDs also make contacts with peroxisomes, mitochondria and lysosomes (vacuoles in yeast). All these interactions are closely coordinated and essential for the normal life cycle of LDs and their multiple functions [1, 7].

LDs not only play an important role in regulating intracellular energy storage and FA trafficking but are also involved in a variety of intracellular processes, such as modulation of the ER stress response, host-pathogen interactions and protein degradation and storage [8]. Dysregulation of LD homeostasis is linked with the development of several human disease states, including diseases associated with an excess of LDs, namely obesity, diabetes, hepatic steatosis, arteriosclerosis and cardiovascular disease, or with a deficiency of LDs, namely lipodystrophy and cachexia [9-11]. Mutations in seipin (discussed in detail in Section 1.4.) lead to a severe form of lipodystrophy, namely Berardinelli-Seip lipodystrophy, the most common form of autosomal recessive lipodystrophy [12]. Due to the numerous functional connections with other organelles, dysfunction of LD metabolism is also important for diseases such as cancer and neurodegenerative diseases [10, 11, 13].

1.2. LD biogenesis

Despite recent findings, the molecular mechanisms of LD biogenesis are still not fully understood. The main mechanism of LD biogenesis is *de novo* formation from the ER, where the enzymes of neutral lipid synthesis are localized [3]. However, in yeast, fission of LDs has also been observed [14]. According to the current model, NLs synthesized in the ER accumulate between the bilayer leaflets and cause membrane deformation to the point where it is thermodynamically favorable to coalesce and nucleate into an oil lens at specific ER membrane domains [15]. At these domains, the lens grows until a threshold diameter that promotes its vectorial budding outwards, from the ER membrane. Overall, this process involves three main steps after synthesis of neutral lipids: nucleation, growth and budding, just as in phase separation and

dewetting phenomena, i.e., the process of retraction of a fluid from a non-wettable surface [15].

1.2.1. Neutral lipid synthesis

The first step in the biogenesis of LDs corresponds to the synthesis of NLs such as TAGs (Figure 2) and SEs within the ER bilayer [3]. These NLs are formed by the esterification of an activated fatty acid to diacylglycerol (DAG) or a sterol (such as cholesterol), respectively [1].

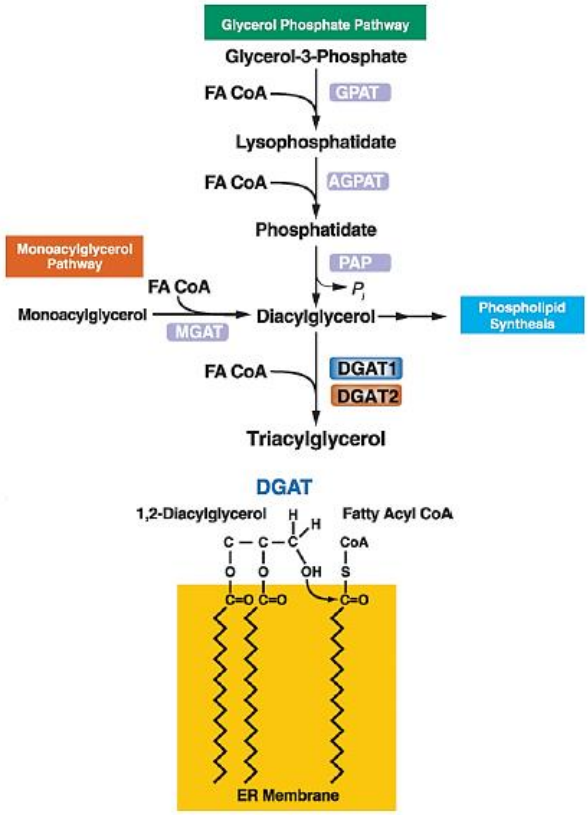

Figure 2. Schematic illustration of *de novo* TAG generation pathway. Triacylglycerols (TAGs) are the end-product of a multi-step pathway. In mammals, glycerol-3-phosphate is converted to lysophosphatidic acid (LPA) via the activity of GPAT enzymes. LPA is converted to phosphatidic acid (PA) via the activity AGPAT enzymes. PA is dephosphorylated to diacylglycerol (DAG) by phosphatidic acid phosphatase (PAP/lipin) enzymes. DAG is esterified to TAG by DGAT1 and DGAT2. DGAT enzymes catalyze the formation of an ester linkage between a fatty acyl CoA and the free hydroxyl group of diacylglycerol. This reaction occurs at the surface of the ER bilayer membrane. DGAT, acyl-CoA: diacylglycerol acyltransferase; GPAT, glycerol-phosphate acyltransferase; AGPAT, acylglycerol- phosphate acyltransferase; PAP, phosphatidic acid phosphohydrolase; MGAT, acyl CoA: monoacylglycerol acyltransferase. Adapted from [16].

Before neutral lipid synthesis reactions occur, the chemically inert FA must be activated by esterification with coenzyme A (CoA). Esterification occurs in an ATP-dependent two-step reaction catalyzed by enzymes of the acyl-CoA synthetase (ACSL) protein family [16]. Kassan et al. have shown that the ER and LD localized acyl-CoA synthetase 3 (ACSL3) appears to be particularly important in the synthesis of NLs for the generation of LD [17].

Distinct enzymes involved in NLs synthesis are localized mainly at the ER [16]. TAGs are the product of diacylglycerol acyltransferase DGAT1 and DGAT2 activity (Dga1p and Lro1p in yeast), while SEs are made by acyl-coenzyme A: cholesterol acyltransferases ACAT1 and ACAT2 (Are1p and Are2p in yeast) [5].

De novo TAG synthesis, one of the two main components of LDs, is performed by the glycerol phosphate pathway, also known as the Kennedy pathway (Figure 2), that initiates by the conversion of glycerol 3-phosphate into lysophosphatidic acid (LPA) by the covalent linking with a fatty acyl-CoA. Subsequently, LPA is converted to phosphatidic acid (PA), which is transformed into DAG by lipin (Pah1p in yeast). In addition, DGAT enzymes catalyze the last reaction of the *de novo* TAG synthesis, by linking DAG with a fatty acyl-CoA [18]. On the other hand, *de novo* TAG synthesis can occur through the monoacylglycerol pathway (Figure 2), in which monoacylglycerol is covalently joined with fatty acyl-CoA to produce DAG, and subsequently TAG. In yeast, TAG can also be synthesized through an acyl-CoA-independent reaction, in which PLs can act as the acyl donor. This reaction is catalyzed by phospholipid/diacylglycerol acyltransferase, encoded by Lro1p in yeast and found exclusively in the ER [19], while Dga1p is localized both in the LD and ER [20].

Yeast cells lacking all enzymes of neutral lipid synthesis (Dga1p, Lro1p, Are1p and Are2p) are completely devoid of LDs [21]. In fact, expression of each of these four enzymes is sufficient for the formation of LD in yeast, suggesting that formation of these organelles can be triggered by either TAGs or SEs, although the assembly of LDs stimulated by TAGs has been studied in more detail in both yeast and higher eukaryotes [1].

1.2.2. Oil lens formation

Newly synthesized NLs deposit between the leaflets of the ER bilayer and are initially free to move between the leaflets of the ER [22]. As their concentration increases, the NLs coalesce and form an oil lens in a process of demixing, since the energy cost of interacting with each other is lower than that of interacting with other membrane components such as PLs or proteins [15, 23]. The subsequent growth of such lens-like structures leads to deformation of the ER bilayer, resulting in budding out of a small nascent LD towards the cytoplasmic side (Figure 3) [1].

The membrane curvature strain, the surface tension and membrane lateral pressure are altered by specific changes in lipid composition, and all of these factors have a major effect on the budding of nascent LD towards the cytosol and also on the LD size [24]. Therefore, a significant change in lipid content must occur at the sites where the nascent LD is formed to promote budding and efficient packing of TAG/SEs into LDs [5].

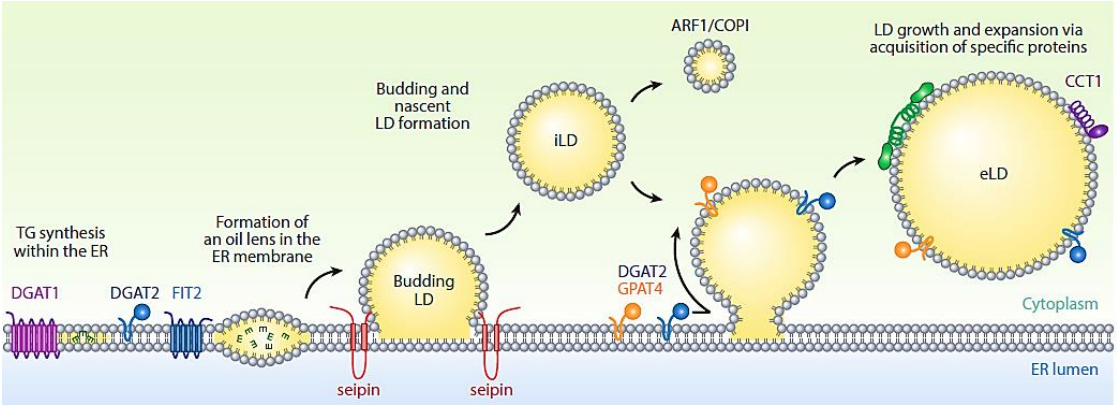

Figure 3. Steps in LD biogenesis. LDs emerge from the ER. Fat storage-inducing transmembrane 2 (FIT2) protein and other ER-resident proteins are important for the maintenance of morphology and lipid composition of the ER membranes. Step 1: Triacylglycerol synthesis and cholesterol ester synthesis enzymes deposit NLs in between the leaflets of the ER bilayer. Beyond a certain concentration, the NLs demix and coalesce into a lens. Step 2: seipin and other LD biogenesis factors are recruited to the lens structure and facilitate the growth of the nascent LD by forming ER-LD contact sites. The emergence of the LD into the cytosol is affected by differences in surface tension of the luminal and cytosolic leaflets of the ER bilayer, possibly determined by asymmetrical protein binding and phospholipid composition. Step 3: in mammalian cells, LDs bud from the ER and grow through fusion or local lipid synthesis. DGAT, acyl-CoA: diacylglycerol acyltransferase; GPAT, glycerol-3 phosphate acyltransferase; eLD, expanding LD; iLD, initial LD; TG, triacylglycerol. Adapted from [3].

Earlier studies suggested that LD formation occurs at defined sites in the ER, possibly to minimize disruption of other ER functions [17]. In fact, there is now evidence for discrete LD-forming ER subdomains supporting LD biogenesis [25]. Seipin and Lipid Droplet Assembly Factor 1 (LDAF1) are known to mark sites for LD formation in mammalian cells [26]. More recently, in yeast, seipin (Fld1p/Sei1p) and Nem1 (the catalytic component of the Nem1p-Spo7p phosphatase complex), were also described to localize to such discrete ER subdomains (Figure 4) [25]. Sei1p/Nem1p sites require the activity of Fat storage-inducing transmembrane 2 (FIT2) protein Yft2p, and Pex30p (an ER and peroxisomal membrane protein involved in ER-derived organelle budding and ER membrane tubulation) to ensure proper recruitment of the TAG synthases Dga1p and Lro1p to LD-forming nucleation sites [25]. This indicates that all four proteins (Sei1p/Nem1p/Yft2p/Pex30p) might work together in establishing ER subdomains permissive for localized TAG synthesis and lens formation (Figure 4) [25]. By accumulating at these sites, these proteins may help in nascent LD stabilization and facilitate bilayer deformation and LD budding, possibly through protein crowding effects [25].

Importantly, FIT proteins exhibit PL-remodeling functions, suggesting that they may change PL composition to adjust surface tension of the inner leaflet of the ER membrane and thus facilitate directional budding of LDs to the cytoplasmic side [27, 28]. These proteins may also play a role in recruiting TAG synthases to locally control DAG accumulation, since they are able to bind DAG and TAG *in vitro* [29, 30].

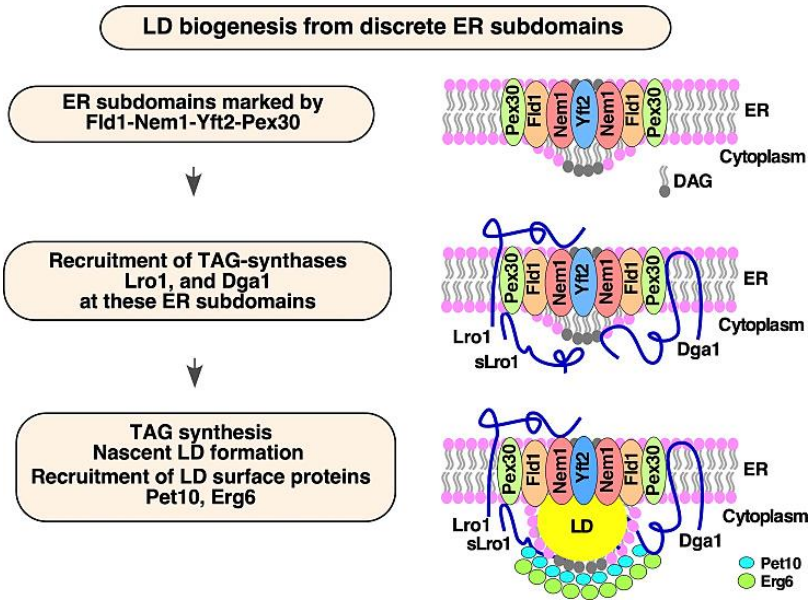

Figure 4. Model of LD formation at discrete ER subdomains defined by Fld1 and Nem1. Representation showing the order of events that occur at specific ER subdomains for efficient LD formation. ER subdomains marked by seipin Fld1 and Nem1 undergo sequential enrichment with LD biogenesis factors, thus promoting localized TAG synthesis and droplet assembly. Adapted from [25].

Lastly, other ER-shaping proteins modulate LD assembly, including spastin, receptor expression- enhancing protein 1 (REEP1), spartin and atlastin-1. These proteins may facilitate the deformation of the ER bilayer at LD-forming sites to accommodate the NLs that are synthetized [31, 32]. The deformation of the ER bilayer could facilitate nucleation and trigger LD assembly at specific sites determined by seipin at ER tubules [33].

1.2.3. Budding and nascent LD formation

Expansion of the NLs lens results in LD budding from the ER membrane. However, it is unknown if all LDs, or only some, remain connected to the ER. In mammalian cells, at least some LDs appear to be completely separated from the ER, while in yeast a significant portion of LDs remains physically connected with the ER [34]. Budding of secretory vesicles from the ER requires the involvement of membrane curvature-inducing coat proteins, such as COPII. However, these proteins are not involved in the budding of LDs. Instead, *in vivo* studies suggested that ER membrane PL composition is critical for LD budding [35-37], as well as membrane surface tension [15, 24]. Surface tension is defined by the energy cost of exposing NLs to the aqueous cellular environment and seems to be especially important for the acquisition of the rounded shape of LDs [24]. On the other hand, PL composition affects budding efficiency mainly through geometric effects: conically shaped molecules, such as DAG

or phosphatidylethanolamine (PE) disfavor budding, whereas molecules with opposite geometry, such as lysophospholipids, promote budding [30].

Even though LD budding from the ER is a biophysical process of emulsion formation, specific ER proteins mark and modulate the sites of LD budding in the ER. These proteins act as gatekeepers for the formation of domains with specific protein and PL compositions that allow the budding of nascent LDs [3]. In cells, LD budding is mediated by FIT proteins, which belong to an evolutionarily conserved family of ER integral membrane proteins [38]. Two highly related FIT proteins, FIT1 and FIT2, are present in mammals, whereas other metazoan and yeast exclusively express FIT2-related proteins [38]. Depletion of FIT-related proteins in yeast (Scs3p and Yft2p) and mammalian cells inhibits LD budding, resulting in the accumulation of NL lenses embedded in the ER membrane [39]. These proteins may also be important in regulating the directionality of the budding reaction toward the cytosol and away from the ER lumen [39]. Besides, specific lipids may also have a role in LD budding. For instance, dephosphorylation of PA by the yeast enzyme Pah1p, a protein related to mammalian lipin, to generate DAG, seems to be important for packaging of TAGs into LDs [35].

Perilipins (PLIN), some of the most abundant LD-coating proteins, have also been implicated in establishing LD formation sites [40]. PLIN1 and PLIN2 are LD-resident proteins, while PLIN3, PLIN4, and PLIN5 are cytosolic or enriched at ER [41]. PLIN1 regulates both lipolysis and lipid storage, depending on the metabolic status of the cell [41], and cytoplasmic perilipin proteins, especially PLIN3, may sense the increased local concentration of NLs or DAG at the ER, which is consistent with the fact that PLIN3 and PLIN4 bind early to droplets [37, 42]. In yeast, ER-LD budding is facilitated by Pln1p (also known as Pet10p), the yeast orthologue of mammalian PLIN3. Like other perilipins, Pln1p is recruited from the cytosol to the LD monolayer [43]. This protein may facilitate budding by changing the balance of tension between the two membrane monolayers. Interestingly, the binding and stabilizing effect of Pln1p on LDs depends on the presence of TAGs, since it does not recognize droplets containing only SEs [43]. During the biogenesis process, LD targeting occurs at very early stages for Pln1p, and this protein functionally interacts with others like seipin and FIT2, suggesting that Pln1p plays an important role in LD budding. In fact, cells lacking *PLN1* show a significant delay in LD budding [43].

Seipin, which corresponds to the Sei1p/Ldb16p complex in budding yeast, is another protein crucial for efficient LD budding [44]. This protein seems to mark sites that are related with the initial growth of nascent budded LDs [12]. Seipin also plays a key role in stabilizing ER-LD contact sites by creating a diffusion barrier, which helps to

regulate LD surface tension during budding and growth, apart from regulating the profile of acyl chains in PL [45-48]. Seipin also regulates abundance and size of LDs [44, 47, 48]. Predictably, mutations in seipin lead to aberrant LD biogenesis, morphology, and dynamics in a variety of cells, resulting in 'supersized' LDs or clusters of abnormally small and misshapen LDs [48]. Moreover, seipin modulates the activity of Glycerol-phosphate acyltransferase (GPAT), which catalyzes the conversion of glycerol-3-phosphate and long-chain acyl-CoA to lysophosphatidic acid, a precursor of PA (Figure 2) [49]. In mammalian cells, seipin interacts with GPAT3 and GPAT4 and participates in the regulation of LD expansion and adipogenesis [49]. Seipin might also be necessary for membrane remodeling, or it could help to control the content of the negatively charged PA at the contact sites, by targeting GPATs [50]. In fact, previous studies showed that the β-sandwich structure of human seipin has the capacity to bind to anionic PL. Seipin also directly regulates TAG synthesis through physical interaction with 1-acylglycerol-3-phosphate O-acyltransferase 2 (AGPAT2) and Lipin-1, which are crucial enzymes of the TAG biosynthetic pathway [51]. More recently, seipin was shown to associate with yeast LD organization (Ldo)16 and Ldo45 isoforms [52, 53], the latter orthologous to human LDAF1 (Figure 5) [26].

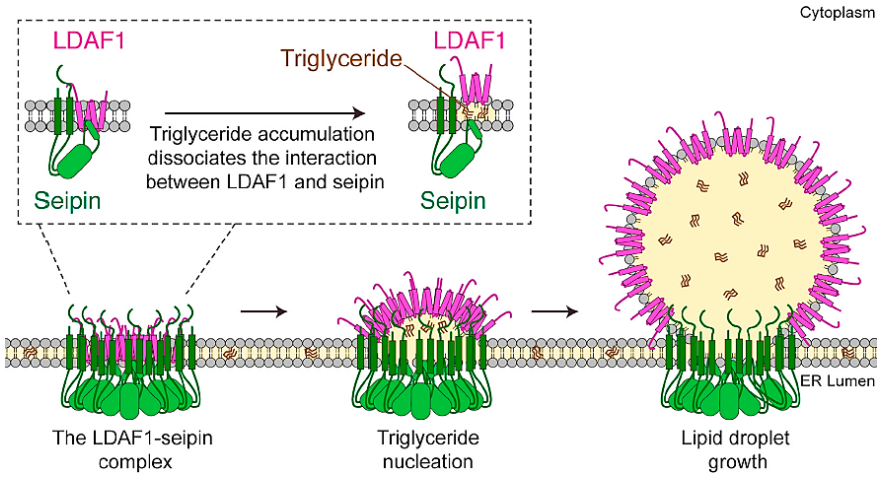

Figure 5. **Model LD Formation at LDAF1-Seipin Complex Sites.** Oligomers of LDAF1 and seipin form a large protein complex (~600 kDa) composed of 66 transmembrane domains and 11 seipin hydrophobic helices in the ER bilayer. The assembly of hydrophobic helices may direct nucleation and TAG lens formation. TAG accumulation in the complex causes dissociation of the complex and redistribution of LDAF1 to the growing LD surface as LDs grow. LDAF1 redistribution to LD surfaces may lower LD surface tension, enabling efficient budding and growth of LDs. Adapted from [26].

Chung et al. demonstrated that human seipin forms a complex with LDAF1 and collectively they establish sites for LD formation in the ER bilayer [26]. LDAF1 activates seipin at ER-LD contact sites and during LD maturation, this complex is dissociated. Whereas seipin stays at ER-LD interface, LDAF1 moves to the surface of the LD, possibly to regulate LD proteome [26].

1.2.4. LD growth and maturation

After formation, LDs can grow in size via acquisition of more NLs to its core and simultaneous expansion of the LD monolayer. This occurs via three identified mechanisms: flux of NLs through the ER-LD contact sites [17, 47, 54, 55], synthesis of NLs at the LD PL monolayer [3, 55] and lipid transfer between LDs and/or ripening [23, 34].

The ER is an essential source of additional material for LD expansion, with newly synthesized lipids transported to the LD via ER-LD membrane bridges. These ER-LD contacts were first observed in plant cells by electron microscopy [56] and were more recently shown to participate in localization of TAG enzymes to the LD surface [55]. Both nascent and mature LDs can acquire enzymes for growth from the ER. Once ER-LD bridges are established, specific enzymes required for *de novo* TAG generation (such as GPAT4, AGPAT3, DGAT2) use the connections to relocalize from the ER to LD surface (Figure 3), where they assist LD expansion by catalyzing TAG synthesis [55]. In fact, depletion of DGAT2 or GPAT4 prevents the expansion of LDs [55]. ER-LD connections are thus crucial for LD growth. Moreover, factors maintaining ER structure, such as atlastin, a GTPase that mediates membrane fusion to connect ER tubules, play a key role in regulating LD size [57].

It is currently unclear how the LD diversity is achieved. The Arf1/COPI machinery was shown to be necessary for GPAT3 localization to LDs. Coatomer protein (COP)-I machinery, localized on the LD surface, plays an essential role in establishing connections to the ER [58]. These proteins remove PLs at LD surfaces, thus increasing LD surface tension and promoting the fusion of LDs with other membranes [59]. Alterations of the LD surface tension could then allow these enzymes to diffuse from the ER to LDs via ER-LD bridges.

The expansion of the LD core by TAG synthesis and of the PL surface are tightly associated. Although the most abundant PLs in the LD monolayer are phosphatidylcholine (PC) and PE, PC is crucial for coating LDs and preventing their coalescence [60]. Consequently, the expansion of droplets leads to an increased need of PC on the surface of LDs. Synthesis of PC comprises three enzymatic steps, the second of which is a rate-limiting step catalyzed by CTP: phosphocholine cytidylyltransferase (CCT). CCT uses phosphocholine and cytidine triphosphate (CTP) to form CDP-choline, which is combined with DAG by cytidine diphosphate (CDP)-choline:1,2-diacylglycerol cholinephosphotransferase (CPT) in the ER to generate PC. During LD expansion, CCT is translocated from the cytosol to LD surface and becomes activated, suggesting that PC synthesis increases in response to local demands [60].

Since CPT, the last enzyme of the PC synthesis pathway, is exclusively localized at the ER, newly synthesized PC needs to be relocated to expanding LDs.

Lastly, LDs can grow by lipid transport from one LD to another, which typically happens between adjacent LDs [23]. This can be achieved via two distinct mechanisms: LD-LD fusion, which is a quick merging/coalescence of droplets, that occurs within seconds, and Ostwald ripening, a molecular diffusion process that occurs over minutes-hours, by which smaller droplets continuously transfer material to bigger ones through a connecting phase [15, 23]. Both processes can be modulated by factors that influence LD-LD clustering, such as microtubule and actin cytoskeleton networks [61] and proteins that induce LD clustering [62]. Following LD coalescence, the total volume of fusing LDs remains the same, whereas the surface area decreases. Moreover, cells deficient in PL synthesis often contain larger LDs via an increased rate of LD-LD fusion [63].

1.3. LD breakdown

The major function of LDs is to store energy in the form of energy-dense NLs. These organelles are dynamically synthesized and broken down in response to cellular needs and environmental signals [5]. Upon times of cellular demand, the NLs of the LD core can be broken down to release free FAs that can be used by mitochondria through β-oxidation pathway for energy production or membrane synthesis [5]. LD consumption is achieved via lipolytic enzymes, hydrolyzing NLs at the LD monolayer, or via engulfment of LD constituents into degradative vesicles in a specialized form of selective autophagy, termed lipophagy (Figure 6) [64].

The lipolytic enzymes are recruited and activated at the surface of LDs and promote TAG breakdown to FAs that are liberated in the cytosol, resulting in gradual LD shrinkage [22]. In mammals, adipose triglyceride lipase (ATGL) is responsible for the first step of lipolysis, namely the hydrolysis of TAG to form DAG and a FA [65]. After the formation of DAG, the hormone-sensitive lipase (HSL) hydrolyses DAG to monoacylglycerol (MAG) and FA [66]. MAG lipase (MAGL) then converts MAG to glycerol and FA [67].

In addition to the gradual LD consumption in the cytosol by lipolysis, during nutrient deprivation, LD turnover can also be mediated by lipophagy [68]. This process involves several steps and starts with phagophore formation, with subsequent phagophore expansion and formation of the limiting membrane; then occurs the formation of a double membrane autophagosome and sequestration of LDs or LD portions by autophagosomes. Finally, a phagolysosome is generated via autophagosome-lysosome fusion [69]. Once the phagolysosome is formed, lysosomal

lipases, such as lysosomal acid lipase (LAL), gain access to internalized LDs, and catalyzes TAG breakdown to FFAs [69]. Lipophagy has also been described in yeast cells. Instead of a macrolipophagy process like in mammals, yeast lipophagy is mediated by microautophagy. In this process, LDs are engulfed and degraded by vacuoles (yeast lysosome equivalent) [69].

Lipophagy is induced especially in stationary growth phase, when yeast cells are in starvation conditions, and in response to other types of nutrient stress [70]. It is currently accepted that both lipolysis at the LD surface and lipophagy are necessary for maximal LD breakdown efficiency [71]. Curiously, recent studies in hepatocytes suggest that LD size may determine which type of breakdown dominates, with larger LDs being more susceptible to breakdown by lipases and smaller LDs to lipophagy [72].

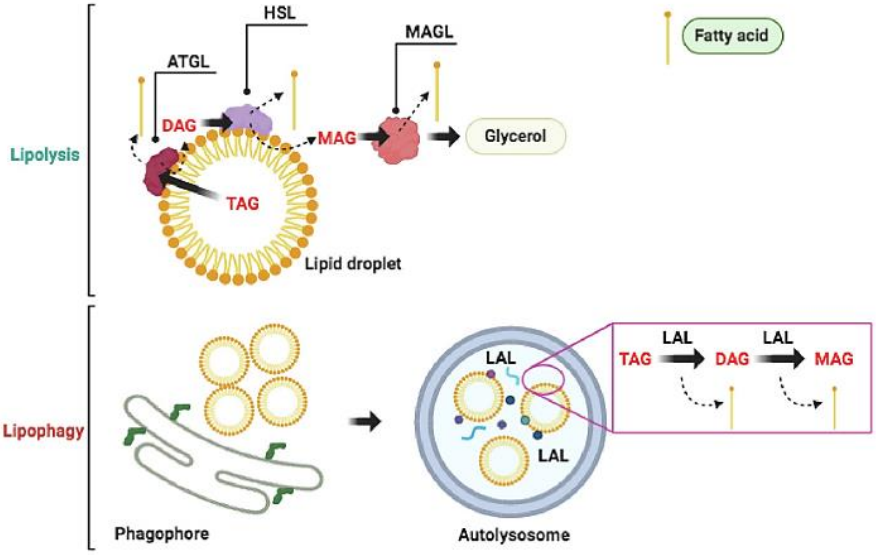

Figure 6. Free fatty acids (FFAs) can be released by LD breakdown in a process mediated by lipolysis (upper panel), at the surface of LDs, or by lipophagy (lower panel). TAG lipolysis is mediated by three enzymes that act successively: adipose triglyceride lipase (ATGL), hormone sensitive lipase (HSL) and monoacylglycerol lipase (MAGL). Lipophagy is an autophagic process in which LDs are engulfed by autophagosomes to be delivered to lysosomes, where the lysosomal acid lipase (LAL) catalyzes TAG breakdown to FFAs. Adapted from [5].

1.4. Seipin

Seipin is a ubiquitous homo-oligomeric ER transmembrane protein involved in LD biogenesis by establishing ER-LD contacts [12]. In humans, this protein is encoded by the *Berardinelli-Seip congenital lipodystrophy type 2* (*BSCL2*) gene [12, 73], which was originally identified as a loss-of-function gene for the rare autosomal recessive disease congenital generalized lipodystrophy (CGL) [12] (see Section 1.5). Subsequent studies have uncovered other seipin mutations leading to motor neuron diseases (MNDs), such as hereditary spastic paraplegias (HSP) and a severe form of

encephalopathy with fatal outcomes at a young age [74]. Although its function is not fully elucidated, it is clear that seipin is required for adipogenesis, and studies in a variety of model organisms have shown that this protein plays a critical role in LD formation, as mutations in seipin lead to aberrant LD biogenesis, morphology, and dynamics in a variety of cells [46-48].

1.4.1. Seipin structure

Seipin is an integral ER membrane protein with two transmembrane (TM) domains, a large highly conserved luminal loop that is glycosylated in mammals, and two cytosolic termini (N- and C-termini) (Figure 7) [75]. The luminal region of the human seipin contains a conserved *N*-glycosylation site (amino acids (aa) N88-S90, an N-X-V/S site). Although the exact functional importance of this site is unclear, the missense mutations located in this domain have been associated with autosomal dominant MND (N88S and S90L), and to the recessive CGL2 (A212P) (discussed below in more detail) [76]. Moreover, *N*-glycosylation deficient seipin protein has been shown to aggregate in cells, with increased localization to ER domains near to LDs [76].

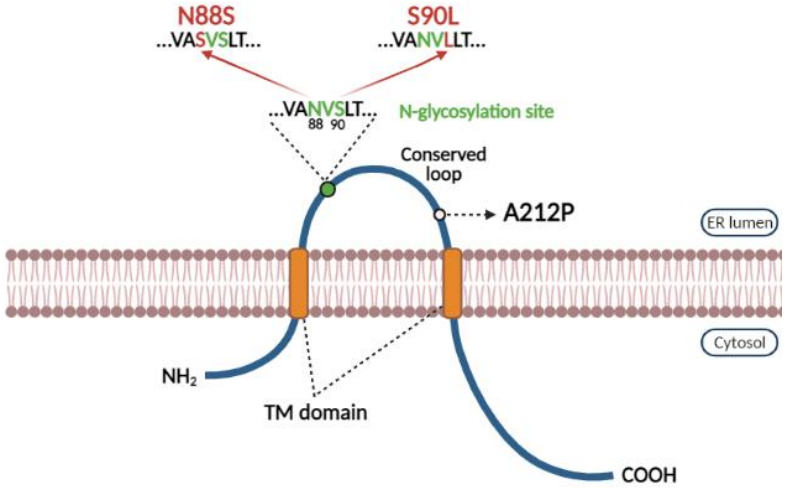

Figure 7. Structure and mutations of seipin/*BSCL2*. Schematic illustration of human seipin protein containing two hydrophobic domains (orange). N- and C-termini of seipin are localized in the cytoplasm and its loop region in the ER lumen. Glycosylation motifs (green) and mutations in seipinopathy (red) and CGL2 (black). Adapted from [76].

In humans, the *BSCL2* gene is ubiquitously and highly expressed in the testis and some regions of the human brain, particularly in motor neurons of human spinal cord, cortical neurons of human frontal lobe, and regions related to the regulation of energy balance, such as the hypothalamus and brainstem [77]. *BSCL2* gives rise to three transcripts that produce three seipin isoforms: isoform 1 (398 aa), isoform 2 (287 aa) and isoform 3 (462 aa) [78]. Isoforms 1 and 3 contain the intraluminal loop and both TM domains, while isoform 3 has an extended N-terminal sequence compared to isoform 1. Isoform 2 differs from the others in its C-terminal sequence and may

completely lack the second TM [78]. In addition, its expression appears to be restricted to the central nervous system, and to date there is no evidence for its existence at the protein level [74, 79]. The functional importance of these different isoforms is unknown. However, isoform 1 appears to be the major isoform of seipin. Indeed, it is the most studied isoform in the literature, and its sequence provides the nomenclature for more than 30 seipin mutations [78].

The seipin homologue in *Saccharomyces cerevisiae* is Fld1p, more recently renamed as Sei1p [36, 48]. The orthologs share a central region of about 250 aa conserved in the secondary structure, corresponding to two transmembrane domains and a large ER luminal loop [80, 81]. However, in budding yeast, seipin function is only complemented when Sei1p forms a functional complex together with Ldb16p, a transmembrane protein in the ER [48]. The stability of Ldb16p requires Sei1p, since Ldb16p is subjected to ER-associated degradation (ERAD) in the absence of Sei1p. On the other hand, in the absence of Ldb16p, Sei1p is stable but non-functional [82].

Recent cryo-electron microscopy structures of the luminal region of *Drosophila* and human seipin reported ring-shaped homo-oligomers with twelve and eleven subunits, respectively (Figure 8), and a preliminary report suggests that yeast seipin is a homo-oligomer of about nine subunits with a toroid shape [83-85]. The conserved luminal domain of *Drosophila melanogaster* seipin was resolved at high resolution, and this domain was found to contain several hydrophobic α-helices positioned at the inner rim of the seipin ring towards the ER bilayer, possibly having an anchoring function [85].

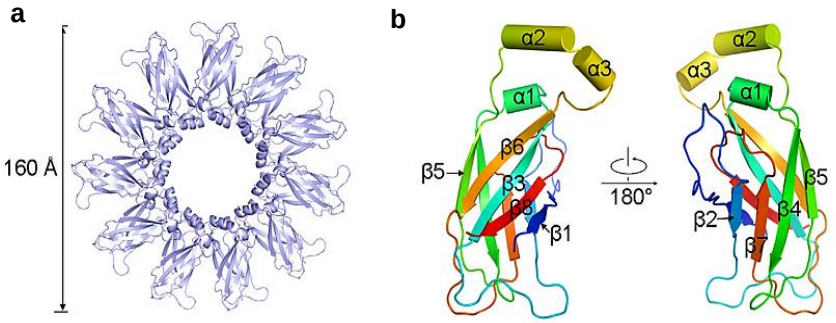

Figure 8. Structure of human seipin. (a) The structure colored in silver gray contains 11 identical protomers with a diameter of 160 Å. **(b)** The monomeric structure of seipin. The structure is colored in rainbow with the amino and carboxyl termini colored in blue and red, respectively. Adapted from [50].

Moreover, it also contains a β-sandwich domain with similarity to lipid-binding proteins, such as Niemann-Pick type C2 protein [85]. Indeed, the binding of this seipin domain to anionic PLs has been demonstrated *in vitro*, and PA has been indicated as a potential ligand of this domain [50]. Curiously, the binding to PA was dependent on the acyl-

chains of PA, with seipin showing high affinity for PA containing oleate and palmitate fatty acid chains [50]. Furthermore, a designed mutant, harboring two aa substitutions in the hydrophobic cleft of the beta sandwich, was unable to complement the seipin knock-out (KO) LD phenotype in cells [85], which suggests that this putative lipid binding domain (LBD) is essential for seipin function. Nevertheless, which lipids seipin binds or interacts with in intact cells remains to be determined.

1.4.2. Seipin function

Seipin is a key regulator of LD cellular dynamics by assisting on their biogenesis and maturation [47, 73]. Despite having a clear role in both adipogenesis and LD formation, the exact molecular role(s) of this protein remains to be identified. In fact, different hypotheses about the molecular role of seipin have been proposed. Considering the ring shape of seipin oligomers and its localization within the lipidic connection between LD and ER, seipin may support LD growth and/or anchoring [86]. Moreover, seipin could also have a structural role at the LD-ER contact site, maintaining mature LDs through physical stabilization of the lipidic bridge or through a gatekeeper function by establishing correct partitioning of specific molecules between LDs and ER, maintaining the identity of the surfaces of both organelles. In fact, LDs of seipin mutants display altered lipid composition as well as loss of typical LD surface proteins [46].

Furthermore, Sui et al. suggested a novel model for the mechanistic role of seipin in LD biogenesis [85]. According to this model, seipin oligomers move within the ER membrane and scan its surface from both sides with the hydrophobic α-helices searching for the membrane packing defects induced by small NL lenses. When the oligomer detects such a lens, it stops scanning and becomes immobilized, now functioning as a structural anchor that maintains the connection between the ER membrane and the surface of the developing LD. This model is supported by previous studies that describe highly mobile seipin foci that move within the ER membrane until they eventually merge with nascent LDs [44]. The N-terminal cytosolic α-helix might mediate stable docking of the LD onto the ER membrane, thus preventing aberrant formation of tiny LDs through premature physical separation from the parent organelle [3]. In fact, in absence of seipin, cells exhibit an aberrant LD morphology phenotype of tiny and clustered LD aggregates, probably due to failed and premature growth, or a reduce number of supersized LDs, which likely result of coalescence of smaller LDs [3, 47, 48]. In budding yeast, *fld1*Δ*, ldb16*Δ and *fld1*Δ*ldb16*Δ cells exhibit the same two LD phenotypes in the indicated conditions [48, 87]. Consistent with these results, mutations in seipin promote an increase of NLs content in the ER [31] and alterations in PL levels, particularly elevation of PC and phosphatidylinositol [31], resulting in clustering and

formation of supersized LD [75]. However, in wild-type (WT) cells, increased NLs often lead to an increase in the number but not the size of LD [48]. It is known that seipin deficiency increases PA levels, which may contribute to LD fusion, explaining the supersized LDs in mutated cells [36]. Seipin may thus play a role in the formation and maintenance of LDs through modulation of PL metabolism.

Finally, the presence of an LBD-like domain within the luminal part of seipin is intriguing and points toward functional implications and not only a mere structural role of this protein [50]. LBDs can fulfill diverse functions, including transfer of lipids from one place to another, lipid scavenging, lipid sensing, and presentation of lipids to other proteins. Thus, potential roles of the putative seipin LBD include lipid sorting at the LD-ER interface, but also involvement in localized lipid metabolism reactions as well as regulatory or signaling roles [50]. For instance, a possible lipid-mediated conformational switch of the seipin complex at some point during LD biogenesis, or the lipid-based integration of an external signal [50].

1.5. Seipin-related diseases

Mutations in seipin give rise to distinct disease states in humans. Several loss-of-function mutations give rise to BSCL2, the most severe form of congenital lipodystrophy in humans [12]. BSCL2 is a rare autosomal recessive disease associated with severe lipoatrophy, insulin resistance, hypertriglyceridemia and mental retardation [88, 89]. Most seipin mutations associated with lipodystrophy contain non-sense, frameshift, or aberrant splicing mutations that produce truncated, non-functional proteins [80, 90].

In contrast, dominantly inherited, gain-of-function mutations in the *N*-glycosylation site of seipin give rise to MND, hereditary spastic paraplegias with variable phenotypes, collectively known as seipinopathies [12]. Finally, mutations resulting in skipping of exon 7 of seipin, either homozygously or in combination with a *BSCL2*-causing mutant, cause an early-onset, fatal neurodegenerative disorder named Celia's encephalopathy [12].

1.6. Seipinopathy motor neuron disease

Seipin related seipinopathies represent a spectrum of dominantly inherited motor neuronal disorders caused by gain-of-function mutations in the ER luminal *N*-glycosylation motif of seipin, namely mutations N88S (Asparagine 88 to Serine) and S90L (Serine 90 to Leucine) [74, 76, 89].

Seipinopathies are rare disorders defined by progressive decline of upper and lower neurons, typically without major afflictions in sensory neurons, with distinct clinical manifestations [74, 91, 92]. Even though seipinopathy refers to the genetic diagnosis, patients may clinically be diagnosed with Silver syndrome (main phenotype: weakness and wasting in the small hand muscles and spasticity of the lower limbs), distal hereditary motor neuropathy (dHMN) type V (weakness and wasting in the small hand muscles), HSP (spastic paraplegia in the lower limbs) or Charcot-Marie-Tooth disease type 2 (CMT2D) (distal muscle weakness, wasting of the upper and lower limbs) [74, 76, 88, 93]. Moreover, it is implicated in progressive encephalopathy with or without lipodystrophy (PELD) or Celia's encephalopathy, characterized by developmental regression of motor and cognitive skills in the first years of life, generally culminating in death in the first few decades [94].

1.6.1. Seipinopathy: a conformational disease?

To date, there have been few studies on the mechanistic details of seipinopathy, so the molecular pathogenesis remains unclear. However, there is increasing evidence that this disease may arise via toxic accumulation of the mutant protein, which could be particularly deleterious in sensitive cells, such as motor neurons [76, 95, 96]. Indeed, protein misfolding, aggregation and accumulation in the affected brain regions are a common pathological feature in other neurodegenerative diseases such as polyglutamine diseases, Parkinson’s disease and Alzheimer’s disease [95, 97-100].

Exactly how the disruption of *N*-glycosylation in seipin leads to neuropathy and how it affects nervous system function in general is not fully understood. Previous studies have shown that seipinopathy-related mutations lead to an accumulation of unfolded proteins in the ER, resulting in the activation of the unfolded protein response (UPR) and cell death. This indicates that seipinopathies are closely associated with the buildup of toxic protein aggregation and ER stress (Figure 9) [76, 89, 95].

To gain more insight into the etiology of N88S seipin neuropathology, a transgenic mouse was recently established [101]. Overexpression of N88S seipin in mice leads to motor neuron dysfunction with upregulation of the ER stress response in neurons, but curiously, no neuronal death was observed [101]. This supports the idea that ER stress protects cells from more severe damage. It is also striking that neuronal death does not appear to be necessary for disease, suggesting that ER stress alone is sufficient for the development of motor phenotypes of seipinopathies [96]. However, another study in transgenic mice reported that overexpression of N88S induces cell death in the spinal cord associated with increased autophagy, which may be a compensatory response to accelerate the degradation of mutant seipin aggregates and

protect motor neurons from apoptosis, thus delaying the progression of motor phenotypes [102]. Importantly, the nature of these seipin aggregates remains largely elusive. Both yeast and mammalian seipin can form homodimeric protein species, interacting with itself, and with N88S mutant seipin, forming heterodimeric protein species [87]. These protein species can then assemble into higher order oligomers (homomers or heteromers) [87].

Previous studies have also reported that disruption of the *N*-glycosylation motif by the N88S mutation promotes the accumulation of misfolded proteins in inclusion bodies (IB) [95]. Whether the formation of these IB is protective or pathogenic in seipinopathy remains to be determined (Figure 9).

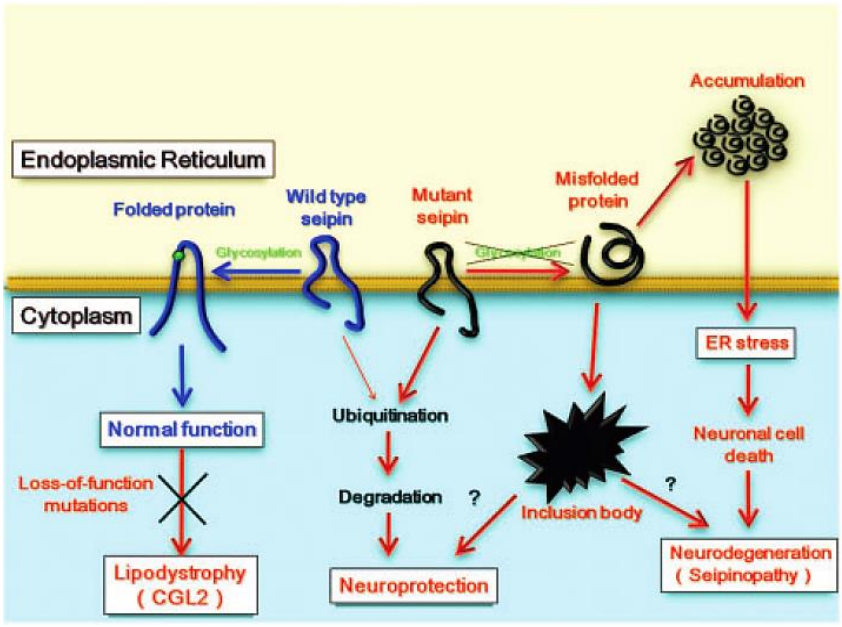

Figure 9. Possible mechanisms of seipinopathy. Wild type (WT) seipin is glycosylated and correctly folded by chaperones at the ER. A small amount of WT seipin is misfolded, ubiquitinated and degraded by ubiquitin–proteasome system (UPS), while mutations that disrupt the *N*-glycosylation motif enhance ubiquitination and lead to the formation of inclusion bodies. Mutant and incorrectly folded seipin accumulates in the ER, causing ER stress and eventually neuronal cell death. On the other hand, loss-of-function mutations in the seipin gene lead to lipodystrophy. Adapted from [76].

1.7. ER stress

The ER is an essential cellular organelle in eukaryotes. It plays an important role in protein biosynthesis and post-translational modification processes by ensuring proper folding and maturation of secretory and membrane proteins through post-translational processes, such as disulfide bonding and *N*-glycosylation [101]. Numerous studies have shown that any disruption in the protein biosynthesis, such as abnormal increase in protein biosynthesis, inhibition of disulfide bond formation, metabolic energy depletion, and perturbation of *N*-glycosylation can lead to the generation of misfolded proteins that accumulate in the ER [89].

Under normal conditions, the ER has an advanced protein quality control mechanism to refold and/or remove misfolded proteins that otherwise would accumulate in the ER lumen. However, ER homeostasis can be compromised when the protein misfolding rate exceeds the normal refolded threshold, leading to an accumulation of misfolded proteins and consequently causing ER stress [103]. Therefore, the fate of the cell under ER stress depends on the balance between two opposing pathways: adaptation and cell death [103]. To relieve the cell from ER stress, a highly evolutionarily conserved intracellular signalling pathway known as UPR is activated [89]. This signaling pathway was first described in the budding yeast *S. cerevisiae* in the early 1990s [104], following the discovery by Sambrook and co-workers [105] and Walter and co-workers [106] of an unfolded protein response element (UPRE) in the yeast *KAR2* promoter. Indeed, the UPRE is essential and sufficient to confer ER stress inducibility on a heterologous reporter gene [107]. The UPR triggers multiple mechanisms to reduce unfolded protein load through general attenuation of translation, transcriptional upregulation of molecular chaperone genes that promote protein folding, secretion and activation of ERAD that enhances degradation of unfolded proteins [108]. However, if ER homeostasis cannot be restored, severe or prolonged UPR triggers pro-apoptotic signaling cascades involving mitochondria-dependent or -independent mechanisms [108].

Recently, disruption of ER homeostasis and upregulation of the UPR have been observed in several neurological diseases, including Alzheimer's disease, Parkinson's disease, amyotrophic lateral sclerosis (ALS), prion disease, expanded polyglutamine tract diseases, Charcot-Marie-Tooth disease and stroke [108]. Nevertheless, there is no direct evidence in *in vivo* models that ER stress alone can lead to neurodegeneration, and some critics have suggested that ER stress may not be central to the mechanism of neurodegeneration, but rather a secondary pathological phenomenon among the complicated degenerative processes that modifies the progression and severity of these diseases [108].

1.8. Transduction of the unfolded protein signal across the ER membrane

The established mammalian UPR pathway has three transmembrane proteins that transduce the unfolded protein signal across the ER membrane. Inositol-requiring protein 1 (IRE1) and protein kinase RNA-like ER kinase (PERK) belong to the ER luminal domains of the type I, and the third is the type II transmembrane protein ATF6 (activating transcription factor 6) (Figure 10) [109]. PERK contains a large ER luminal

stress-sensing domain that is functionally similar with the IRE1 luminal domain and a cytosolic domain that phosphorylates the α subunit of eukaryotic translation initiation factor 2 (eIF2α) [110]. ATF6 is a transcription factor with an N-terminal basic leucine zipper (bZIP) domain in the cytosol and a C-terminal ER luminal domain to sense stress [110]. Importantly, only PERK and IRE1 exhibit a degree of conservation throughout all eukaryotes and no ATF6 orthologue has been found in yeast until now. In mammals, the counterpart of yeast Ire1p has two isoforms: IRE1α and IRE1β. Whereas IRE1α is expressed in most cells and tissues, IRE1β expression is mostly restricted to the intestinal epithelial cells [111]. IRE1 contains an N-terminal ER stress-sensing domain in the ER lumen, an ER transmembrane domain, a serine/threonine kinase domain and a C-terminal endoribonuclease domain in the cytosol [112].

Recent studies demonstrate that the ER chaperone protein BiP binds to the luminal domains of these ER stress sensors under unstressed conditions, thereby keeping them inactive [113]. BiP is a peptide-dependent ATPase and belongs to the heat shock 70 protein family (HSP70) that binds transiently to newly synthesized proteins translocated to the ER and more permanently to underglycosylated, misfolded or unassembled proteins, thus serving as a master regulator of the UPR [113]. When misfolded proteins accumulate in the ER lumen, BiP dissociates from proximal signal transducers and supports protein folding. Sequestration of BiP by unfolded proteins promotes the dimerization/oligomerization, *trans*-autophosphorylation and subsequent activation of IRE1 and PERK [103, 114].

The calnexin/calreticulin cycle and recognition of unfolded proteins by BiP play a key role in the regulation of activity of the proximal stress transducer ATF6 [115]. Release of ATF6 from BiP allows ATF6 transport to the Golgi compartment where it is cleaved to generate the cytosolic domain of ATF6 that translocates to the nucleus to activate transcription [110]. Thus, this BiP-regulated activation provides a direct mechanism for all three UPR transducers to sense the stress in the ER and an auto-regulatory mechanism by which the UPR is shut off upon increased expression of BiP [113].

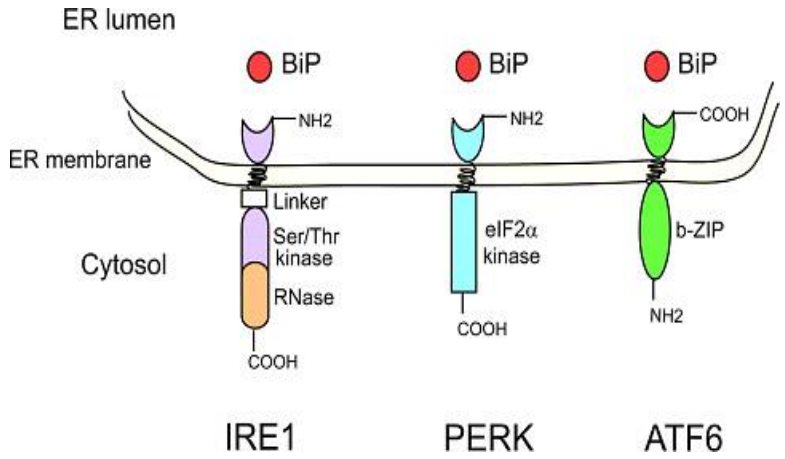

Figure 10. Illustration of three UPR transducers and one master regulator in mammalian cells. The domain structures of IRE1, PERK, and ATF6 and their associations with BiP are shown. Adapted from [113].

1.8.1. UPR signaling mediated by IRE1 in yeast

In yeast, the UPR is a simple linear pathway, with transcriptional regulation entirely mediated by the Ire1p-Hac1p pathway, through the induction of chaperones and ERAD [116]. This pathway is characterized by exclusive features in stress signal transduction and is observed in all eukaryotes. The *IRE1* gene was identified in a forward genetic screen for mutations linked to the activation of an *UPRE*::*LACZ* reporter by ER stress [105, 106]. The product of the gene, Ire1p, is an atypical type I transmembrane ER protein, with an N-terminal luminal domain that senses the ER stress and a C-terminal cytoplasmic domain required for *KAR2* (the yeast orthologue of BiP) expression [116]. Ire1p also has a C-terminal endoribonuclease (RNase) homology domain that is essential for UPR signaling [116]. The substrate for the RNase activity of Ire1p is the mRNA encoding the bZIP transcription factor *HAC1* that activates transcription of the UPR target genes [116].

Accumulation of unfolded proteins in the ER lumen, experimentally induced by agents such as tunicamycin, a natural inhibitor of *N*-linked glycosylation, or dithiothreitol (DTT), which impairs disulfide bond formation, promotes the dimerization and *trans*-autophosphorylation of Ire1p [116]. This activates its RNase activity and induces the cleavage of both 5'- and 3'-exon-intron splice site junctions in *HAC1* mRNA, leading to the formation of 5'-OH and 3'-cyclic PO4 ends (exons), that are joined by tRNA ligase [117]. This spliceosome-independent splicing of *HAC1* mRNA removes a large intron of 252 bp, located in the 3'-end of the mRNA, and thereby replaces the carboxy-terminal 10 aa in the *HAC1* protein with a new 18 amino acid tail. This leads to the expression of an alternative C-terminus with high transcriptional activation potential and to the removal of a translational attenuator from *HAC1* mRNA [117]. Then, Hac1p translocates to the nucleus and activates transcription of several UPR target genes by

binding to a DNA sequence motif termed UPRE (consensus motif: CAGCGTG) in the promoter regions of genes encoding ER-resident chaperones, such as *KAR2* and *PDI1* [117]. Although there are not readily recognizable UPREs in the promoters of the genes associated with ERAD, Hac1p also activates transcription of these genes [118, 119]. After suppression of protein synthesis in ribosomes, ER chaperones are induced to correct protein conformation, by refolding unfolded proteins. The remaining unfolded proteins are then eliminated from the ER to the cytosol through retrograde transport and degraded by the proteasome via ERAD [120].

1.9. Endoplasmic reticulum-associated degradation (ERAD)

There are several quality control (QC) mechanisms in the secretory pathway that aim to counteract protein misfolding and maintain protein homeostasis, namely ERAD, ER-phagy, Golgi QC, and plasma membrane QC. All these processes are regulated by the UPR and/or the heat shock response and are responsible for the control of protein synthesis, chaperone levels and activity of protein degradation pathways [121].

ERAD is an important catabolic cellular process that serves to remove terminally misfolded proteins from the membrane or the lumen of the ER and selectively degrade them, thereby maintaining ER homeostasis [122]. This pathway is conserved in eukaryotes and has been well studied in *S. cerevisiae* [123]. Work primarily in budding yeast has shown that ERAD functions according to a conserved principle in which misfolded proteins in the lumen of the ER are recognized through the detection of specific domains, such as unpaired cysteines or exposed hydrophobic regions, and are ubiquitinated by either the ERAD-L (ERAD of substrates with misfolded lesions within the ER lumen), ERAD-C (cytoplasm), or ERAD-M (membrane) pathway, depending on the location of the misfolded lesion [121].

ERAD requires several ER-resident factors, such as ubiquitin-protein ligases (E3s), which in yeast are Hrd1p and Doa10p [121]. ERAD-L/ ERAD-M substrates, which are soluble or integral membrane proteins with a luminal lesion, interact with the Hrd1p complex. In contrast, substrates that follow the ERAD-C pathway use a complex containing the ubiquitin ligase Doa10p [124]. After selection, ERAD-L substrates are delivered to the Hrd1 complex, which contains Yos9p, Hrd3p, Der1p, Usa1p, and Hrd1p [125]. The RING domain of Hrd1p, which is required for its ubiquitin ligase activity, is localized on the cytosolic side of the ER. Therefore, ERAD-L substrates must be retrotranslocated from the ER to the cytosol via the translocon [126].

Sec61p forms the conducting channel in the translocon through which proteins are imported into the ER lumen. Moreover, this protein could also act in the reverse direction and function as a retrotranslocon [121]. In addition to Sec61p, Hrd1p is also a prime candidate for ERAD retrotranslocon for substrates with lumenal lesions. After retrotranslocation, substrates are polyubiquitinated and recognized by proteasome subunits and subsequently degraded [121].

1.10. Oxidative stress

A phenotype commonly associated with age-related diseases and a potential consequence of ER stress is the accumulation of oxidative damage due to increased levels of reactive oxygen species (ROS) [127]. ROS are partially reduced metabolites of oxygen with strong oxidizing abilities that contribute to diseases related to cell metabolism, survival, and death. At low concentrations, ROS maintain cellular homeostasis as secondary signaling molecules. However, at high concentrations, ROS can cause severe oxidative damage to proteins, lipids and DNA [127]. The overall level of ROS in a cell at a given time is the result of the sum of the activity of all production and detoxification systems [127]. The main sources of ROS are ROS-producing enzymes involved in processes in various compartments of the cell, which include the mitochondrial electron transport system, fatty acid β-oxidation in peroxisomes, membrane-localized nicotinamide adenine dinucleotide phosphate (NADPH) oxidases, and oxidative protein folding in the ER [128].

Mitochondria are indispensable cellular organelles for the maintenance, adaptability, and survival of eukaryotic cells and are a critical component of diverse signaling pathways [129]. Several neurodegenerative diseases have been linked to mitochondria dysfunction, and in fact a loss of mitochondrial function occurs naturally during the normal aging process, making it one of the major sources of ROS [130]. The level of superoxide production in mitochondria, caused mainly by complexes I and III, depends on several factors that vary widely, such as O_2 availability, proton motive force, $NADH/NAD^+$, and CoQH2/CoQ ratios [131]. Although mitochondria have the reputation of being the major ROS-inducing organelles of the cell, oxidative protein folding in the ER generates large amounts of ROS [127].

Under normal physiological conditions and in response to ROS production, antioxidant enzymes, such as catalase, superoxide dismutase (SOD), and glutathione peroxidase maintain redox homeostasis by converting ROS to water and oxygen [128]. Other antioxidant molecules, including reduced glutathione (GSH), vitamin E and NADH, can also inactivate ROS (Figure 11). At the ER, ROS can also be produced by NADPH oxidases downstream of protein disulfide-isomerase PDIA1 activity [132, 133]. However, in a disease state, the underlying systemic and cellular perturbations enhance ROS production and impair antioxidant mechanisms, leading to accumulation of ROS and redox imbalance, which in turn causes oxidative stress.

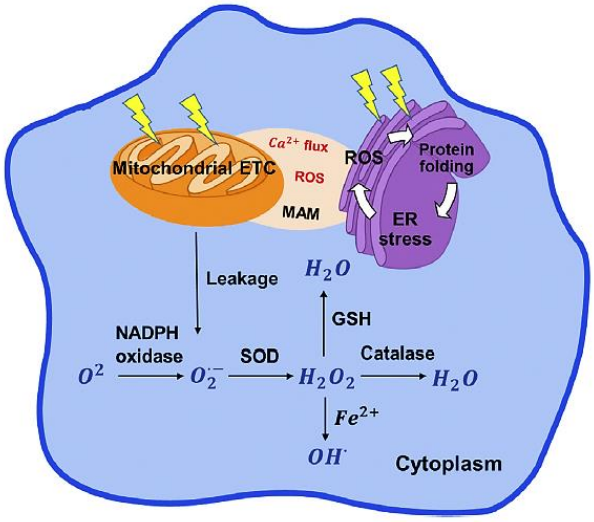

Figure 11. Overall ROS production in the mitochondria, cell cytoplasm and ER. ROS are produced based on cell requirements and extracellular stimuli. Mitochondria and ER are the two major organelles that control ROS signaling. ETC, electron transport chain; ER, endoplasmic reticulum; MAM, mitochondria-associated ER membrane; NADPH, nicotinamide adenine dinucleotide phosphate; ROS, reactive oxygen species; SOD, superoxide dismutase. Adapted from [128].

1.11. ER stress and oxidative stress: a vicious cycle

The relationship between ER stress and oxidative stress is not fully understood. However, recent studies have shown that ER protein folding pathways are strongly correlated with ROS production [134]. In the ER, redox homeostasis is critical for the protein folding process and disulfide bond formation. Any alteration in ER-regulated protein folding pathways can lead to ROS imbalance and stimulate ROS production, disrupting both redox and ER homeostasis [135]. Consequently, ROS have a profound effect on the ER protein folding process and several oxidants can even pathologically trigger the UPR [127].

In the protein folding process, the formation of disulfide bonds is crucial for the stabilization of protein structure and promotes the assembly of functional, mature and uniquely tertiary structured proteins [136]. The protein folding process is extremely sensitive to redox homeostasis, as its redox state is tightly modulated by numerous redox mechanisms such as the GSSG (oxidized glutathione) / GSH (reduced glutathione) cycle and the Protein Disulfide Isomerase (PDI) reaction [136].

Importantly, the oxidizing environment of the ER is maintained by the GSH/GSSG ratio to allow protein folding [128]. GSH is a non-protein thiol that can be oxidized and converted to GSSG [137]. The balance between GSH and GSSG is critical for maintaining redox homeostasis. The ratio of GSH to GSSG is about 1:1 in the ER lumen and it is approximately 50:1 in the cytoplasm [137]. Therefore, it has been suggested that a highly oxidized environment enhances disulfide bond formation, although this also creates an unfavorable environment for the antioxidant mechanism since the interaction between GSH and ROS is essential for the maintenance of ER redox homeostasis [137]. Moreover, this oxidized environment disrupts the activities of ER-resident proteins and promotes the formation of misfolded proteins, thus contributing to ER stress [137].

Disulfide bonds are also critical to the process of protein folding. Cysteine mispairing and improper disulfide bonding can lead to increased protein misfolding [138]. GSH can react and reduce non-native disulfide bonds, which contributes to the refolding of misfolded proteins. However, the process of protein refolding is slow because it requires electron acceptors and is also highly dependent on the redox reaction [139]. During ER stress, the GSH/GSSG ratio is disturbed, increasing ROS production and altering the ER redox environment [136].

To alleviate ER stress due to the accumulation of misfolded proteins, molecular chaperones such as PDI and ER oxidoreductase 1 (ERO1) provide refolding of these misfolded proteins [108]. PDI is an oxidoreductase protein involved in the oxidative protein folding process and is responsible for catalyzing the formation of disulfide bonds [140]. During the oxidative protein folding process, the cysteine residues in the active site of PDI capture electrons from free thiols in nascent polypeptides to form a disulfide bond that oxidizes the polypeptide chain substrate and reduces the active sites of the PDI protein [140]. Moreover, ERO1 plays a crucial role in assisting PDI in the oxidative folding process. Once PDI accepts the electrons from the polypeptide substrate chain, these electrons are transferred to the membrane-bound ERO1 [140]. ERO1 recruits Flavin Adenine Dinucleotide (FAD) to perform a redox reaction on PDI [140]. The redox reaction transfers the electrons to molecular oxygen molecules and generates hydrogen peroxide (H_2O_2) (Figure 12), which is toxic to the cell and can lead to apoptosis [127, 128, 141].

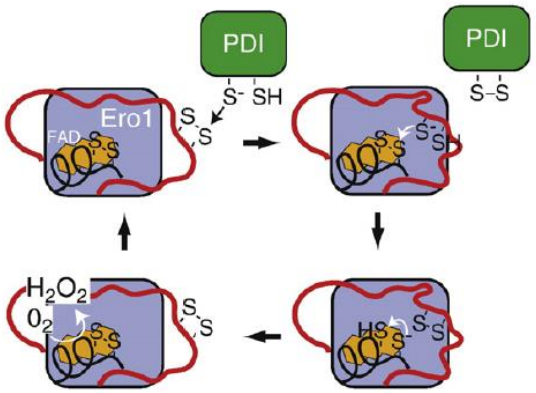

Figure 12. This oxidizing environment of the ER promotes nascent protein folding and disulfide bond formation. ERO1 is a key mediator of disulfide bond formation in the ER. Reduced polypeptides are oxidized by PDI, which transfers its electrons to ERO1. ERO1 is reoxidized by oxygen and produces H_2O_2. Shuttle cysteines (red region), active-site cysteines (black), and FAD cofactor (orange) are shown. Thin arrows reflect electron flow. Adapted from [141].

Furthermore, the redox imbalance disrupts the protein folding pathway through the production of ROS, leading to the upregulation and accumulation of misfolded proteins and thus inducing ER stress [142].

In eukaryotes, the ER is responsible not only for secreted and membrane-bound protein folding, but also for calcium (Ca^{2+}) storage [128]. In addition, ER stress can cause the release of Ca^{2+} from the ER into the cytosol. Mitochondria uptake the released Ca^{2+}, causing physical and metabolic changes. High Ca^{2+} ion levels enhance mitochondrial Krebs cycle dehydrogenases and nitric oxide synthase activities, both leading to an increase in ROS levels. Plus, ROS induces the release of cytochrome c into the cytoplasm, inhibiting the activity of the complex III and further inducing ROS in the form of a ubisemiquinone radical intermediate [127]. In a vicious cycle, ER-induced mitochondrial ROS may accelerate the release of Ca^{2+} from the ER, further increasing mitochondrial oxidative stress [127]. Mitochondrial dysfunction also alters ATP generation required for protein folding and bond formation in the ER, thus aggravating overall stress sensed by the cell [127].

1.12. *Saccharomyces (S.) cerevisiae* as a model organism for research in seipinopathy

The budding yeast *S. cerevisiae* is the best-studied eukaryotic cell, both at the genetic and physiological levels. Yeast models are crucial to our current understanding of various biological processes, such as regulation of gene expression, signaling pathways, stress responses, and cell death [143]. Most of the general cellular and molecular mechanisms are conserved between mammalian cells and yeast cells. In fact, 20-30% of all human genes have orthologs in yeast [143]. Therefore, yeast is an invaluable model for studying conserved molecular mechanisms underlying aging and various human diseases. In the particular case of neurodegenerative diseases, yeast

models have been able to recapitulate several important features of complex and devastating disorders, such as Huntington's disease and Parkinson's disease [144].

The simple genetic manipulation of *S. cerevisiae* has established this model in several research areas. This manipulation is facilitated by the high transformation efficiency of these cells and by the presence of a very efficient homologous recombination pathway that makes it relatively easy to insert, delete or mutate any genomic sequence up to the chromosome level [144]. The complete sequencing of the yeast genome allowed the creation of the yeast deletion collection by deleting all open reading frames (ORF). In this collection, each gene is replaced by a drug-resistance gene, making each deletion selectable [143]. The yeast *S. cerevisiae* is widely used in medical, industrial and pharmaceutical research. Compared to other model systems, yeast has a number of advantages, such as low cost of culture media, short generation time, and ease of genetic manipulation, as mentioned earlier. Therefore, yeast has become a reliable model organism to study the relationship between genotype and phenotype in eukaryotes [143].

Importantly, the human seipin gene (*BSCL2*) can functionally complement LD defective phenotypes observed in Fld1p/Ldb16p-disrupted yeast cells, suggesting that the activities of Fld1p and Ldb16p are shared with the mammalian seipin protein [82]. This opened the possibility of using yeast as a model for N88S seipinopathy. The yeast model for N88S seipinopathy was obtained by deleting the entire open reading frame of *FLD1* and *LDB16* (*fld1Δldb16Δ*), mimicking a complete loss-of-function of seipin. Subsequently, human WT seipin and human N88S mutant seipin were expressed in yeast, resulting in yeast-humanized strains that were used to explore the nature of N88S seipinopathy.

1.13. Aims of this project

Previous work reported that the N88S mutation disrupts the *N*-glycosylation motif of seipin, leading to the formation of seipin aggregates in inclusion bodies (IBs) [89]. Importantly, the nature of these IBs and their contribution to neuronal dysfunction remain largely unresolved.

The aim of this work was to establish a humanized yeast model of N88S seipinopathy to study the cell biology, behavior and molecular effects of different combinations of human WT and N88S mutant seipin. To this end, a Venus-based bimolecular fluorescence complementation (BiFC) assay was used, in which Venus fragments, VN and VC, were fused to the C-terminus of WT/N88S seipin. The BiFC assay allows the study of homo- or heterodimeric protein species by fluorescence microscopy and enables the analysis of intracellular IB formation. This work aimed to

investigate the effects of homo- and heteromeric combinations on LD dynamics, the aggregation landscape (IB formation), stress response, in particular ER stress response and oxidative stress response (ROS production), on cellular quality control mechanisms and potentially relevant signaling pathways.

Chapter 2
MATERIALS AND METHODS

2. Materials and methods

2.1. Yeast strains and plasmids

The *S. cerevisiae* strains used in this study resulted from the W303α parental strain and are described in Table 1.

Table 1. Yeast strains used in this study.

Strain	Genotype	Source/Reference
W303α	MATa *ura3Δ1 leu2Δ3 his3Δ11 trp1Δ1 ade2Δ1 can1Δ100*	EUROSCARF
fld1Δldb16Δ	W303α *ldb16Δ*::natNT2 *fld1Δ*::hphmx4	This study
***fld1Δldb16Δ* EV**	W303α *ldb16Δ*::natNT2 *fld1Δ*::hphmx4 pRS306-GPD-MCS-CYC1t pRS413	This study
WT-VN WT-VC	W303α *ldb16Δ*::natNT2 *fld1Δ*::hphmx4 pRS306-GPDpr-WThBSLC2-VN-CYC1t pRS413-GPDpr-WTseipin-VC-CYC1t	This study
N88S-VN WT-VC	W303α *ldb16Δ*::natNT2 *fld1Δ*::hphmx4 pRS306-GPDpr-N88ShBSLC2-VN-CYC1t pRS413-GPDpr-WTseipin-VC-CYC1t	This study
N88S-VN N88S-VC	W303α *ldb16Δ*::natNT2 *fld1Δ*::hphmx4 pRS306-GPDpr-N88ShBSLC2-VN-CYC1t pRS413-GPDpr-N88Sseipin-VC-CYC1t	This study
***fld1Δldb16Δ* EV rho^0**	W303α *ldb16Δ*::natNT2 *fld1Δ*::hphmx4 pRS306-GPDpr-MCS-CYC1t pRS413 rho^0	This study
WT-VN WT-VC rho^0	W303α *ldb16Δ*::natNT2 *fld1Δ*::hphmx4 pRS306-GPDpr-WThBSLC2-VN-CYC1t pRS413-GPDpr-WTseipin-VC-CYC1t rho^0	This study
N88S-VN WT-VC rho^0	W303α *ldb16Δ*::natNT2 *fld1Δ*::hphmx4 pRS306-GPDpr-N88ShBSLC2-VN-CYC1t pRS413-GPDpr-WTseipin-VC-CYC1t rho^0	This study
N88S-VN N88S-VC rho^0	W303α *ldb16Δ*::natNT2 *fld1Δ*::hphmx4 pRS306-GPDpr-N88ShBSLC2-VN-CYC1t pRS413-GPDpr-N88Sseipin-VC-CYC1t rho^0	This study
fld1Δldb16Δ* EV *aim14Δ	W303α *ldb16Δ*::natNT2 *fld1Δ*::hphmx4 pRS306-GPDpr-MCS-CYC1t pRS413 *aim14Δ*::KANMX6	This study

WT-VN WT-VC *aim14*Δ	W303α *ldb16*Δ::natNT2 *fld1*Δ::hphmx4 pRS306-GPDpr-WThBSLC2-VN-CYC1t pRS413-GPDpr-WTseipin-VC-CYC1t *aim14*Δ::KANMX6	This study
N88S-VN WT-VC *aim14*Δ	W303α *ldb16*Δ::natNT2 *fld1*Δ::hphmx4 pRS306-GPDpr-N88ShBSLC2-VN-CYC1t pRS413-GPDpr-WTseipin-VC-CYC1t *aim14*Δ::KANMX6	This study
N88S-VN N88S-VC *aim14*Δ	W303α *ldb16*Δ::natNT2 *fld1*Δ::hphmx4 pRS306-GPDpr-N88ShBSLC2-VN-CYC1t pRS413-GPDpr-N88Sseipin-VC-CYC1t *aim14*Δ::KANMX6	This study
***fld1*Δ*ldb16*Δ EV *cnb1*Δ**	W303α *ldb16*Δ::natNT2 *fld1*Δ::hphmx4 pRS306-GPDpr-MCS-CYC1t pRS413 *cnb1*Δ::KANMX4	This study
WT-VN WT-VC *cnb1*Δ	W303α *ldb16*Δ::natNT2 *fld1*Δ::hphmx4 pRS306-GPDpr-WThBSLC2-VN-CYC1t pRS413-GPDpr-WTseipin-VC-CYC1t *cnb1*Δ::KANMX4	This study
N88S-VN WT-VC *cnb1*Δ	W303α *ldb16*Δ::natNT2 *fld1*Δ::hphmx4 pRS306-GPDpr-N88ShBSLC2-VN-CYC1t pRS413-GPDpr-WTseipin-VC-CYC1t *cnb1*Δ::KANMX4	This study
N88S-VN N88S-VC *cnb1*Δ	W303α *ldb16*Δ::natNT2 *fld1*Δ::hphmx4 pRS306-GPDpr-N88ShBSLC2-VN-CYC1t pRS413-GPDpr-N88Sseipin-VC-CYC1t *cnb1*Δ::KANMX4	This study
N88S-VN WT-VC *hrd1*Δ	W303α *ldb16*Δ::natNT2 *fld1*Δ::hphmx4 pRS306-GPDpr-N88ShBSLC2-VN-CYC1t pRS413-GPDpr-WTseipin-VC-CYC1t *hrd1*Δ::KANMX6	This study
N88S-VN N88S-VC *hrd1*Δ	W303α *ldb16*Δ::natNT2 *fld1*Δ::hphmx4 pRS306-GPDpr-N88ShBSLC2-VN-CYC1t pRS413-GPDpr-N88Sseipin-VC-CYC1t *hrd1*Δ::KANMX6	This study
***fld1*Δ*ldb16*Δ EV *ire1*Δ**	W303α *ldb16*Δ::natNT2 *fld1*Δ::hphmx4 pRS306-GPDpr-MCS-CYC1t pRS413 *ire1*Δ::KANMX4	This study
WT-VN WT-VC *ire1*Δ	W303α *ldb16*Δ::natNT2 *fld1*Δ::hphmx4 pRS306-GPDpr-WThBSLC2-VN-CYC1t pRS413-GPDpr-WTseipin-VC-CYC1t *ire1*Δ::KANMX4	This study
N88S-VN WT-VC *ire1*Δ	W303α *ldb16*Δ::natNT2 *fld1*Δ::hphmx4 pRS306-GPDpr-N88ShBSLC2-VN-CYC1t pRS413-GPDpr-WTseipin-VC-CYC1t *ire1*Δ::KANMX4	This study
N88S-VN N88S-VC *ire1*Δ	W303α *ldb16*Δ::natNT2 *fld1*Δ::hphmx4 pRS306-GPDpr-N88ShBSLC2-VN-CYC1t pRS413-GPDpr-N88Sseipin-VC-CYC1t *ire1*Δ::KANMX4	This study

MCS, multiple cloning site; **GPDpr**, GPD promoter; **CYC1t**, CYC1 terminator; **VN**, Venus N-terminal fragment; **VC**, Venus C-terminal fragment.

Plasmids used in this study are listed in Table 2. Plasmids 5903 and 6007 [82] (Table 2) were cut with *Bam*HI and *Sal*I to remove the coding region of human *BSCL2* (h*BSCL2*). The remaining plasmid VT1 (Table 2) contains both GPD promoter (*Sac*I-*Xba*I) and CYC1 terminator (*Xho*I-*Kpn*I). Amplification of h*BSCL2* (WT/N88S) without the stop codon was performed using plasmids 5903 and 6007 as templates, and primers hBscl2_XbaI Fw and hBscl2_BamHI_Rv (Table 3). The resulting *Xba*I-*BamH*I fragment was cut and inserted into *Xba*I and *BamH*I sites of plasmid VT1, generating pRS306-GPDpr-WThBSLC2-CYC1t and pRS306-GPDpr-N88ShBSLC2-CYC1t plasmids with hBSCL2 gene without stop codon. Amplification of the C-terminal fragment of Venus (VC) was performed using pFA6a-VC-HIS3MX6 plasmid (P30556, EUROSCARF) as template and primers VC_BamHI_Fw and VC_SalI_Rv (Table 3). For amplification of the N-terminal fragment of Venus (VN), plasmid pFA6a-VN-kanMX6 (P30559, EUROSCARF) and primers VN_BamHI_Fw and VN_SalI_Rv were used (Table 3). To generate plasmids pRS306-GPDpr-WThBSLC2-VN-CYC1t (VT2) and pRS306-GPDpr-N88ShBSLC2-VN-CYC1t (VT3), a VN *BamH*I-*Sal*I fragment was integrated into *BamH*I and *Sal*I sites of the previously generated plasmids based on VT1. Similarly, plasmids pRS306-GPDpr-WThBSLC2-VC-CYC1t (VT4) and pRS306-GPDpr-N88ShBSLC2-VC-CYC1t (VT5) were developed by inserting a VC *BamH*I-*Sal*I fragment. To obtain plasmids pRS413-GPDpr-WTseipin-VC-CYC1t (VT6) and pRS413-GPDpr-N88Sseipin-VC-CYC1t (VT7), GPD-WThBSLC2-VC-CYC1t and GPD-N88ShBSLC2-VC-CYC1t fragments were amplified using VT4 and VT5 as templates and primers GPDpr_SacI_Fw and CYC1T_SacI_Rv (Table 3). Both fragments were then cut with *Sac*I and inserted into the *Sac*I site of pRS413. The fidelity of the cloning was confirmed by Sanger sequencing.

For the cloning of *GFP-ATG8* in the pRS315 vector, pRS416-GFP-ATG8 plasmid [145] was digested with *Sac*I and *Sal*I, and the resulting insert (GFP-ATG8 under the endogenous *ATG8* promoter) was cloned into *Sac*I and *Sal*I restriction sites of the pRS315 vector.

For the cloning of *UPRE-lacZ* in the pRS315 vector, pJT30 (pRS316 harboring an UPRE-lacZ reporter [146]) was digested with *Hind*III, and the resulting insert (*UPRE-lacZ* under the endogenous *UPRE* promoter) was cloned into *Hind*III restriction sites of pRS315 vector.

For the cloning of *CDRE-lacZ* in the YEplac181 vector, plasmid pAMS366 [147] was digested with *Psi*I, and the resulting insert (*CDRE-lacZ* under the endogenous *CDRE* promoter) was cloned into *Sma*I restriction sites of YEplac181 vector.

The digested products were analyzed by electrophoresis and the band corresponding to the insert was excised and purified following the instruction of the Gel Band Purification Kit (GE Healthcare, Life Sciences). The reaction mix used in each ligation reaction contained 1x ligase buffer (Thermo Scientific), 2 mM of rATP (Thermo Scientific), 2 U of DNA ligase (Thermo Scientific), pDNA and insert for a reaction ratio of 3:1 (insert: vector). Lastly, *E. coli* competent cells (lab made from DH5α) were transformed with the cloning product (as described in section 2.6). The plasmid was extracted using NZYTech Miniprep Kit and the cloning was confirmed by enzyme restriction reaction, followed by electrophoresis analysis.

For amplification of plasmid DNA, *E. coli* cells carrying the plasmid were grown aerobically at 37 °C in a gyratory shaker at 180 rpm. Cells were grown in lysogeny broth (LB) medium supplemented with ampicillin [1% (wt/vol) tryptone (LabM), 1% (wt/vol) NaCl (Merck), 0.5% (wt/vol) yeast extract, 0.1% (vol/vol) ampicillin (Sigma Aldrich)]. Plasmid was extracted using a commercial Kit (NZY miniprep Kit) following the kit manufacturer instructions.

Table 2. Plasmids used in this study.

Plasmids	Backbone	Description	Source/ Reference
5903	pRS306	pRS306-GPDpr-WThBSLC2-CYC1t	[82]
6007	pRS306	pRS306-GPDpr-N88ShBSLC2-CYC1t	[82]
VT1	pRS306	pRS306-GPDpr-MCS-CYC1t	This study
VT2	pRS306	pRS306-GPDpr-WThBSLC2-VN-CYC1t	This study
VT3	pRS306	pRS306-GPDpr-N88ShBSLC2-VN-CYC1t	This study
VT4	pRS306	pRS306-GPDpr-WThBSLC2-VC-CYC1t	This study
VT5	pRS306	pRS306-GPDpr-N88ShBSLC2-VC-CYC1t	This study

VT6	pRS413	pRS413-GPDpr-WTseipin-VC-CYC1t	This study
VT7	pRS413	pRS413-GPDpr-N88Sseipin-VC-CYC1t	This study
VN1	pRS315	pRS315-UPRE-LacZ	This study
VN2	pRS315	pRS315-*GFP-Atg8*	This study
AP-1 LacZ	pRS415	pRS415-AP-1-CYC1-LacZ	[148]
Yap1-9Myc	pRS315	pRS315-Yap1-9Myc	[148]
VN3	YEplac181	YEplac181-CDRE-lacZ	This study
CPY*HA	pRS315	pRS315-CPY*HA	[149]
Kar2-mCherry	pYX242	pYX242-Kar2(1-135)-mCherry-HDEL	[150]

Table 3. Primers used for the construction of Venus based plasmids.

Primer	Sequence (5'→ 3')
hBscl2_XbaI Fw	TAAGCATCTAGAATGGTCAACGACCCTCCAGTACCTGC
hBscl2_BamHI_Rv	TGCTTAGGATCCGGAACTAGAGCAGGTGGGGCGCTGTCGGAGAG
VC_BamHI_Fw	TAAGCAGGATCCAACCACGACAAGCAGAAGAACGGCAT
VC_SalI_Rv	TGCTTAGTCGACCTACTTGTACAGCTCGTCCATGCCGAGAG
VN_BamHI_Fw	TAAGCAGGATCCGTGAGCAAGGGCGAGGAGCTGTTCACCGGG
VN_SalI_Rv	TGCTTAGTCGACCTACTCGATGTTGTGGCGGATCTTGAAGT
GPDpr_SacI_Fw	TAAGCAGAGCTCAGTTTATCATTATCAATACTCGCCATTTCAAAGAA
CYC1T_SacI_Rv	TGCTTAGAGCTCGGCCGCAAATTAAAGCCTTCGAGCGTCCCAAAACCT

2.2. Culture media and growth conditions

The yeast cells were grown aerobically at 26 ºC in a gyratory shaker at 140 rpm using Erlenmeyer flasks. A 1:5 proportion of growth media to flask volume was used. The liquid growth media used for yeast grown were: Yeast peptone dextrose (YPD) [1% (wt/vol) yeast extract (Conda Pronadisa), 2% (wt/vol) bacto peptone (LabM) and 2% (wt/vol) glucose (Fisher Scientific)], yeast peptone glycerol (YPG) [1% (wt/vol) yeast extract (Conda Pronadisa), 2% (wt/vol) bacto peptone (LabM) and 3% (vol/vol) glycerol (VWR Chemicals)], and synthetic complete (SC) medium [2% (wt/vol) glucose (Fisher Scientific) and 0.67% (wt/vol) yeast nitrogen base (YNB) without aa (BD BioSciences), supplemented with appropriate aa and nucleotides: (0.008% (wt/vol) histidine (Sigma Aldrich), 0.008% (wt/vol) tryptophan (Sigma Aldrich), 0.04% (wt/vol) leucine (Sigma Aldrich), 0.008% (wt/vol) uracil (Sigma Aldrich) and 0.008% (wt/vol) adenine (Sigma Aldrich)]. For solid medium, 1.5% (wt/vol) agar (Conda Pronadisa) was added. For growth assays on solid medium (SC), the cells were grown in selective SC-glucose to exponential phase (OD_{600}=0.5-0.6), diluted to an OD_{600}=0.1 and fivefold dilutions were spotted on SC-glucose plates.

2.3. Construction of yeast mutants

Protein tagging and individual gene knockout (KO) (Table 1) were based on the following polymerase chain reaction (PCR) protocol. Polymerase chain reactions were performed in 20 µL reaction mixes containing NZYTech Proof polymerase mix and 200 ng of plasmid or 400 ng of DNA extract. PCR was performed in a T100 Thermo Cycler (Bio-Rad) with a heated lid using the following conditions: Initial denaturation step at 95ºC for 3 min, secondary denaturation step at 95 ºC for 45s (where PCR cycling starts), a primer annealing step with a temperature adjusted according to primer melting point for 45s, an elongation step at 72ºC for 1kb of PCR product/min (where PCR cycling ends) and a final elongation step of 10 min at 72ºC. Primers were designed using Primers-4-Yeast [151] for pFA6 [152] and pYM [153] plasmid sets. Primers used in this work are described in Table 4.

Table 4. Primers used for the generation of KO mutants and C-terminal tagging.

Primer	Sequence (5'→ 3')
LDB16 KO NAT Fw	TGTAGGAGGAGAAAGCAGGTATATAACTAGCCGCAATATGCGT ACGCTGCAGGTCGAC
LDB16 KO NAT Rv	TTCACTTGTTAGTGCATGAGAAGAAGTAATTGCAATATCAAATG GCGAGTATTGATAAT

FLD1 KO HYGB Fw	AAGGTTTCAAGAAAATAAGATAAAGTGAATAGGAAGGATGATCTGTTTAGCTTGCCTTGTCC
FLD1 KO HYGB Rv	TAGGTTTTAAAATTATATAGCGAGAAGTACAATTCTATCAGAATTCGAGCTCGTTTTCGAC
AIM14 KO pFA6 Fw	GCCAGAAACTTCTAATTTGGTAAGCCTTCCAATAAATATGCGGATCCCCGGGTTAATTAA
AIM14 KO pFA6 Rv	ATATTGCGTAAGACATTATTATTCTTTTCTTTTCCCCTCAGAATTCGAGCTCGTTTAAAC
Amplif_CNB1_Fw	CAATGGTGATCAGAATCCATAGAAGCATTTTTATTTCTTAAAATG
Amplif_CNB1_Rv	AAAATATTGGCATACCATAAATGAATGAAGTGTCCCCTAGTCTTA
HRD1 KO pFA6 Fw	AATTTGTAAGAGAAGGGGAGAAAGACAAAATAATAATATGCGGATCCCCGGGTTAATTAA
HRD1 KO pFA6 Rv	CTTTAAAAAAAACTATGTATAATATAAAACATGCAATCTAGAATTCGAGCTCGTTTAAAC
IRE1 KO pFA6 Fw	GCATATCTGAGGAATTAATATTTTAGCACTTTGAAAAATGCGGATCCCCGGGTTAATTAA
IRE1 KO pFA6 Rv	ATAATCAACCAAGAAGAAGCAGAGGGGCATGAACATGTTAGAATTCGAGCTCGTTTAAAC
HSP104 Ctag Fw	CGATAATGAGGACAGTATGGAAATTGATGATGACCTAGATGACGGTGCTGGTTTAATTAAC
HSP104 Ctag Rv	CTTGTTCGAAAGTTTTTAAAAATCACACTATATTAAAGAATTCGAGCTCGTTTAAAC

All PCR reaction products were analyzed by nucleic acid electrophoresis at 125V, using 1% (w/v) agarose gels with GreenSafe premium 0.04 µL/mL (NZYtech) and TAE buffer (40 mM Tris, 20 mM acetic acid, 1 mM EDTA). DNA bands were visualized through UV fluorescence and extracted from the gel using the NZYgelpure kit (Nzytech) according to the manufacturer's instructions. DNA quantification was done using Nanodrop 1000 (Thermofisher).

The parental strain used in this work was W303α *ldb16*Δ::natNT2 *fld1*Δ::hphMX*4*, thus generating a seipin null background (*fld1*Δ*ldb16*Δ). For *LDB16* and *FLD1* deletion, natNT2 cassette was amplified with flanking regions of *LDB16* from plasmid pYM-N16, and hphMX4 cassette was amplified with flanking regions of *FLD1* from plasmid pFA6a-6xGLY-3xFLAG-hphMX4. Strains *fld1*Δ*ldb16*Δ EV, WT-VN WT-VC, N88S-VN WT-VC and N88S-VN N88S-VC were generated by transformation (as described in section 2.5) using the following plasmids (please refer to Tables 2 and 5):

Table 5. Venus-based plasmids used for the construction of the main strains of this study (based on table 2).

Strain	Plasmid *URA3* (cut with *Stu*I)	Plasmid *HIS3*
***fld1*Δ*ldb16*Δ EV**	VT1	pRS413
WT-VN WT-VC	VT2	VT6
N88S-VN WT-VC	VT3	VT6
N88S-VN N88S-VC	VT3	VT7

2.4. Genomic DNA extraction

Yeast cells (10 mL of YPD medium) were grown overnight at 26 ºC to stationary phase. The cells were harvested by centrifugation at 4000 rpm for 5 min, resuspended in 1 mL of deionized H_2O and transferred to a microtube. Following centrifugation at 14000 rpm for 1 min, the pellet was resuspended in 100 µL of lysis solution (2% (v/v) Triton X- 100, 1% (wt/vol) SDS, 100 mM NaCl, 10 mM Tris.HCl pH 8.0, 1 mM EDTA and 100 µL of phenol: chloroform: isoamyl alcohol (50:48:2). Cells lysis was achieved by the addition of glass beads and vigorous vortexing for 5 min. After centrifugation (5000 rpm for 5 min), the aqueous phase was transferred to a new tube containing 100 µL of chloroform and 100 µL of 1x TE (10 mM Tris, 1mM EDTA pH 8.0). The mixture was homogenized by vortexing 5 min and centrifuged at 13400 rpm for 5 min. The aqueous phase was transferred to a new microtube and gently mixed with 1 mL of 100% ethanol (-20 °C). The solution was placed at -20 ºC for 30 min and centrifuged at 13400 rpm for 5 min. The pellet was resuspended in 100 µL 1x TE and incubated with 1 µL RNase A (20 mg/ml) for 5 min at 37 °C. Next, 10 µL of 4 M ammonia acetate and 1 mL of 100% ethanol (-20 °C) were added and mixed. The mixture was placed at -20 ºC for 10 min and then centrifuged at 13400 rpm for 5 min. Finally, the DNA pellet was resuspended in 50 µL of sterile water. Genomic DNA was quantified using a Nanodrop spectrophotometer (ND-1000, Thermo Scientific).

2.5. Yeast transformation

Yeast cells were transformed using a modified version of the lithium acetate (LA)/ single-stranded carrier DNA/ Polyethylene glycol (PEG) method [154]. Cells were grown overnight in YPD medium or SC selection medium to an OD_{600}= 0.3-0.4 and then harvested by centrifugation, washed and resuspended in 700 µL of a mix of 1.0 M lithium acetate (Sigma Aldrich), 10X Tris-EDTA (TE) pH 7.4 and water. After the washing step, 120 µL of cells were incubated with the transformation mix, containing 700 µL 40% (w/v) polyethylene glycol 3350 (PEG 3350) (Sigma Aldrich), 20 µL single-

stranded carrier DNA (ssDNA) (5 mg/mL) and the appropriate amount of DNA. The mixture was vortexed, incubated at 26ºC for 30 min and then switched to 42ºC for another 30 min. Then, YPD medium was added, and the mixture was incubated for 3 hours at 26ºC. Finally, cells were harvested by centrifugation, resuspended in selective media and spread in selective media plates.

In the case of plasmids, the protocol was simplified: 3 µL of plasmid and 3 µL of salmon sperm DNA (ssDNA) were added to 100 µL of transformation mix, containing 80 µL 50% (wt/vol) PEG 3350 (Sigma Aldrich), 10 µL of 1.0 LA (Sigma Aldrich) and 10 µL 10X TE pH 7.4. A small portion of culture from the plate was added to the mixture and was incubated for 4 hours at 26ºC.

2.6. *E. coli* transformation

For the transformation of *E. coli* cells, competent cells were chemically made by calcium soaking protocol and then were slowly thawed on ice. 50 µL of the chemically competent cells were mixed with 2 µL of plasmid DNA and incubated on ice for 30 min. Next, the mixture was incubated at 42 ºC for 1 min and 30 sec, for heat shock transformation, and then placed back on ice for 2 min. Following heat shock, transformed cells were cultured with 900 µL ampicillin-free LB and were incubated at 37ºC for 1 hour for recovery. After the recovery period, cells were plated in LB agar plate with ampicillin and were grown overnight at 37 ºC.

2.7. ROS and neutral lipid (NL) levels

To assess ROS and NL levels, cells at logarithmic and stationary phase were incubated with 5 µg/mL dihydroethidium (DHE) and 5 µg/mL of Nile Red, respectively, for 10 min at room temperature in the dark. Then, cells were centrifuged, washed and resuspended in PBS 1x. Flow cytometry analysis was performed with λex= 488 nm excitation and FL3 (670 LP) filter and FL1 (533/30) (BD Accuri C6 Flow cytometer) for 50000 events, respectively. Data were evaluated with FlowJow software (v. 10.6.1).

2.8. Generation of rho^0 cells

Cells carrying their mitochondrial DNA (RHO+) were grown to saturation in SC-glucose medium lacking histidine plus 25 µg/mL ethidium bromide (EtBr; Sigma). Cultures of EtBr-treated were grown for approximately 24h at 26°C. Then 25 µL of the cell culture were harvested by centrifugation and resuspended in fresh medium containing 25 µg/mL EtBr and allowed to grow for an additional 24 h time period. Cells were plated on SC-glucose lacking histidine plates for individual colonies, and rho^0

clones were checked for growth defects on a nonfermentable carbon source (SC medium lacking histidine and supplemented with 3% glycerol).

2.9. Growth in glycerol plates

In order to assess mitochondrial function, yeast cells were grown overnight in SC-glucose to exponential phase (OD_{600}=0.6). Cultures were then diluted to an OD_{600}=0.1 and fivefold serial dilutions were plated on SC-glucose and SC-glycerol (3%) medium containing 1.5 % agar (w/v). Cells were incubated for 3-5 days at 26ºC.

2.10. Lipid peroxidation assay

For lipid peroxidation analysis, cells were grown in SC-glucose lacking histidine to stationary phase. Yeast extracts were prepared in 20 mM sodium phosphate buffer (pH 7.2), by vigorous shaking of the cell suspension, in the presence of glass beads, for 5 min. Trichloroacetic acid (10% w/v) was added and two more pulses of 1 min were performed. Total protein levels were quantified by the Lowry method using a bovine serum albumin standard curve. Lipid peroxidation was assayed in 600 µL of 1% (w/v) thiobarbituric acid, 0.05 M NaOH, 0.025% (w/v) butylated hydroxytoluene, 100 µL of 0.1 M EDTA, and 100 µL of total protein extract. Malondialdehyde (MDA) concentration was determined spectrophotometrically at 532 nm and expressed as nanomoles of MDA. $(mg\ of\ protein)^{-1}$ [155].

2.11. β-Galactosidase activity assay

Cells harboring pRS315-UPRE-LacZ, pRS415-AP-1-CYC1-LacZ and YEplac181-CDRE-lacZ plasmids were grown in SC-glucose lacking histidine and leucine until logarithmic phase and post-diauxic shift (PDS) phase. Cells were harvested by centrifugation, resuspended in breaking buffer (100 mM Tris, 1 mM DTT, 10 % (v/v) glycerol) and protease inhibitors (Complete mini EDTA-free Protease cocktail inhibitor tables) and mechanically lysed with zirconium beads for 5 min. Debris were pelleted at 12044g for 15 min at 4 ºC and the supernatant was collected for protein quantification. Total protein levels were quantified by the Lowry method using a bovine serum albumin standard curve. Volumes corresponding to 20-80 µg of total extract protein were diluted up to 800 µL with β-galactosidase buffer (60 mM Na_2HPO_4, 40 mM NaH_2PO_4, 10 mM KCl, 1 mM $MgSO_4$, 50 mM β-mercaptoethanol). Then, samples were incubated at 30 ºC for 5 min and 200 µL of o-nitrophenylgalactopyranosyde (ONPG) were added to initiate the reaction, followed by short vortexing of the solutions. When color became yellow, the reaction was stopped by addition of 400 µL of 1M Na_2CO_3.

Ortho-nitrophenol absorbance was measured at 420 nm and β-galactosidase activity was calculated according to the following equation:

$$\beta - \text{Galactosidase activity} = \frac{\text{Abs}420nm \times 1.40}{0.0045 \times \text{protein(mg)} \times \text{t(min)}}\, nmol.min^{-1}mg^{-1}$$

2.12. Enzymatic activities

For the analysis of antioxidant defenses, yeast cells were grown to PDS phase and harvested by centrifugation for 5 min at 4000 rpm (4 ºC). Cells were resuspended in 50 mM sodium potassium phosphate buffer (pH 7.0) containing protease inhibitors (Complete, EDTA-free Protease Inhibitor Cocktail, Roche). The protein extracts were obtained by mechanical disruption of the cells by vortexing in the presence of glass beads for 5 min. Cell debris was removed by centrifugation at 14000 rpm for 15 min at 4 ºC and protein concentration was determined by the method of Lowry, using bovine serum albumin as a standard. The activity of superoxide dismutase (SOD) was analyzed *in situ* after separation of the proteins (90 µg) by native PAGE at 4 ºC, using 10% polyacrylamide gels. Native gels were incubated with 2.5 mM 4-nitrobluetetrazolium chloride (NBT) (Sigma Aldrich) for 20 min and then with the staining solution [28 mM N, N, N', N'-Tetramethylethylenediamine (TEMED) (NZYTech), 86 µM riboflavin and 36 mM potassium phosphate buffer pH 7.8] for 15 min. Then, the gel was exposed to a 60 W lamp until the appearance of achromatic bands that are proportional to enzyme activity [156]. Gel imaging was performed using a GS800 densitometer (Bio-Rad).

For catalase activity, we employed a spectrophotometric assay as previously described [157]. This method permits to evaluate catalase activity by following the degradation of H_2O_2 by cell lysates. Briefly, cells were grown to PDS phase in YPD medium supplemented with adenine at 26 ºC. Next, cells were harvested by centrifugation, resuspended in 50 mM of phosphate buffer pH 7.0 and protease inhibitors (Complete mini EDTA-free Protease cocktail inhibitor tables) and mechanically lysed with zirconium beads for 5 min. Debris were pelleted at 12044x*g* for 15 min at 4 ºC and the supernatant was collected for protein quantification. Total protein levels were quantified by the Lowry method using a bovine serum albumin standard curve. Catalase activity was measured using 40 µL of the cell extract, before measuring Lowry protein concentration. Then normalization to concentration was made to calculate the mass. Proteins were incubated with 30 mM of H_2O_2 in 50 mM of phosphate buffer pH 7.0 for 1 min. Catalase activity was expressed as units of catalase per

milligram of proteins (U/mg), being one unit the amount of enzyme required for degradation of 1 µmol of H_2O_2 /min. Absorbance at 240 nm was measured against a blank and catalase activity was calculated according to the following equation:

$$\text{Specific activity (mU/mg)} = \frac{\Delta\text{Abs}240nm/min \times 1000}{43.6 \times \text{protein(mg)}}$$

Lastly, reduced glutathione (GSH) levels were measured using the GSH/GSSG Ratio Detection Assay Kit (Fluorometric - Green) (ab138881, Abcam). For this purpose, cells were grown to PDS phase in YPD medium supplemented with adenine at 26 ºC. Next, cells were harvested by centrifugation, resuspended in 100 mM of phosphate buffer 2 mM EDTA pH 7.4 and mechanically lysed with zirconium beads for 5 min. Debris were pelleted at 12044x*g* for 15 min at 4 ºC and the supernatant was collected. 20 µL of TCA 100% was added to 100 µL of supernatant and the mixture was gently mixed and incubated in ice for 10 min. Then, the samples were centrifuged at 13400 rpm for 5 min at 4 ºC and the supernatant was collected and neutralized to pH 4-6 with 2 M KOH. The samples were centrifuged at 13400 rpm for 5 min at 4 ºC and processed according to the manufacturer´s instructions.

2.13. Western blotting analysis

For analysis of autophagy flux, *fld1*Δ*ldb16*Δ EV, WT-VN/WT-VC, N88S-VN/WT-VC and N88S-VN/N88S-VC strains expressing GFP-Atg8p were grown in SC-glucose medium lacking histidine and leucine at 26 ºC. The cells were harvested at PDS and stationary phase by centrifugation for 4 min at 4000 rpm (4 ºC). Cells were resuspended in 50 mM sodium potassium phosphate buffer (pH 7.4) containing protease inhibitors. The protein extracts were obtained by mechanical disruption of the cells as described above. The samples were centrifuged at 14000 rpm for 15 min at 4 ºC, the pellet was discarded, and the total protein content in the supernatant was determined by the method of Lowry, using bovine serum albumin as standard. Protein samples (25/30 µg) were prepared in 3x Laemmli sample buffer (6% SDS; 30% glycerol; 10% 2-mercaptoethanol, 0.3% bromophenol blue and 0.5 M Tris HCl, pH 6.8) and heated at 95 ºC for 7 min. Proteins were separated by SDS-PAGE, using 10% polyacrylamide gels, and transferred to nitrocellulose membranes (Hybond-ECL GE Healthcare) in a semi-dry system at 45 mA/cm^2 for 1 hour. Protein transfer to the nitrocellulose membrane was confirmed by Pounceau S staining (0.5% (wt/vol) Pounceau S, 5% (vol/vol) acetic acid). Membranes were blocked with 5% (wt/vol) nonfat dry milk in TTBS (20 mM Tris, 140 mM NaCl, 0.05% (vol/vol) Tween-20 pH 7.6) for 1 hour. Next,

membranes were incubated with primary antibodies: mouse anti-GFP antibody (1:3000, Roche Diagnostics) or mouse anti-PGK1 (1:30000, Molecular Probes). After washing with TTBS, membranes were incubated with the secondary antibody, anti-mouse IgG-peroxidase (1:5000, Molecular Probes). Immunodetection was performed by chemiluminescence using WesternBright ECL reagent (Advansta) and exposing the membranes to LucentBlue X-ray films (Advansta). For stripping, membranes were washed in TTBS and incubated with stripping buffer (62.5 mM Tris-HCl pH 6.8, 2% (wt/vol) SDS, 10 mM 2-mercaptoethanol) for 30 min at 50 ºC. Membranes where washed several times for complete removal of β-mercaptoethanol.

To evaluate protein degradation by ERAD, cells harboring pRS315-CPY*HA were grown in SC-glucose medium lacking histidine and leucine to early exponential phase. Yeast cells were treated with 200 µg/mL cycloheximide (CHX). One OD_{600} unit of cells were collected at 0, 15, 30 and 60 min and cells were harvested by centrifugation at 13 4000 rpm for 3 min and washed once with water. Proteins were extracted by alkaline lysis. Briefly, cells were resuspended in 150 mM NaOH, vortexed, incubated on ice for 10 min and centrifuged at 13400 rpm for 2 min. Then, 50 µL of 3x Laemmli sample buffer (6% SDS; 30% glycerol; 10% 2-mercaptoethanol, 0.3% bromophenol blue and 0.5 M Tris HCl, pH 6.8) was added to the pellet and the mixture was heated at 95 ºC for 7 min. Proteins were separated by SDS-PAGE, using 10% polyacrylamide gels, and transferred to nitrocellulose membranes (Hybond-ECL GE Healthcare) in a semi-dry system at 45 mA/cm^2 for 1 hour. Protein transfer to the nitrocellulose membrane was confirmed by Pounceau S staining. Membranes were blocked with 5% (w/v) nonfat dry milk in TTBS for 1 hour. Next, membranes were incubated with primary antibodies: rabbit anti-HA antibody Y-11 (1:5000, sc-805 Santa Cruz Biotechnology) or mouse anti-PGK1 (1:10000, Molecular Probes). After washing with TTBS, membranes were incubated with the secondary antibody, anti-rabbit IgG-peroxidase (1:5000, Molecular Probes) and anti-mouse IgG-peroxidase (1:10000, Molecular Probes). Immunodetection was performed by chemiluminescence using WesternBright ECL reagent (Advansta) and exposing the membranes to LucentBlue X-ray films (Advansta).

2.14. Fluorescence microscopy

To examine the intracellular localization of IBs using the Venus signal upon reconstitution of the VN and VC fragments, cells were grown to exponential or stationary phase in SC-glucose lacking histidine. To determine whether these IBs colocalize with Kar2p and Hsp104p protein, cells harboring the plasmid pYX242-Kar2-mCherry-HDEL were grown to exponential phase in SC-glucose lacking histidine and

leucine, and cells expressing *HSP104* C-terminally tagged with mCherry were grown to exponential phase in SC-glucose lacking histidine. Cells were washed with PBS and immobilized in agarose beds before observation by fluorescence microscopy (Zeiss Axio Imager Z1 Apotome or Leica TCS SP8). Z-stacks were acquired for DIC, mCherry and Venus channels. The output final images and colocalization analysis were performed using ImageJ 1.51k software.

2.15. Statistical analysis

Data were analyzed in GraphPad Prism Software v9.0 (GraphPad Software). Values were compared by Student's t-test and are expressed as mean values ± SD of at least three independent experiments. The 0.05 probability level was chosen as the point of statistical significance throughout.

Chapter 3

RESULTS

3. Results

3.1. Characterization of Venus-based constructs

To assess the formation of WT and mutant seipin homomers and heteromers, we used the BiFC assay [158]. In this assay, fluorescence requires interaction between two proteins, each of which is fused to non-fluorescent, truncated fragments of the Venus fluorescent protein. The BiFC assay thus allows the study of homo- or heterodimeric protein species, which may then assemble into higher order oligomers (homomers or heteromers) [158].

We generated several combinatorial strains on a yeast seipin-depleted *fld1Δldb16Δ* background that differentially express the human WT/N88S forms of seipin, either fused to the 3' region of the N-terminus (VN) or to the C-terminus (VC) of the Venus protein (Figure 13). We obtained the following combinatorial strains: N88S-VN/WT-VC; WT-VN/WT-VC; N88S-VN/N88S-VC and *fld1Δldb16Δ* EV strain expressing the corresponding empty vectors (EV; Table 1).

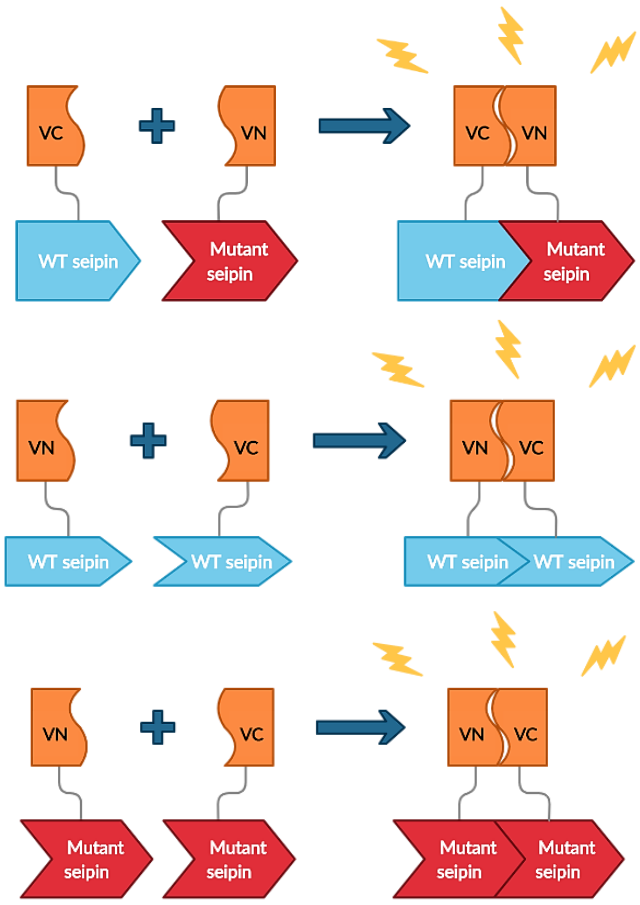

Figure 13. Potential combinations and outputs of human seipin-associated Venus-based constructions Schematic representation of the BiFC assay. In the case of heterodimers, WT hSeipin was fused to N-terminal of VC fragment of Venus fluorescent protein (WT seipin-VC) and N88S mutant seipin was tagged to C-terminal of VN fragment (VN-mutant seipin). To obtain WT hSeipin homodimers, cells contained VN-WT seipin instead of VN-mutant seipin. To obtain mutant seipin homodimers, cells contained mutant seipin-VC instead of WT seipin-VC.

To characterize the Venus-based constructs, we first performed LD-staining using the Nile Red dye and confirmed that the supersized LD phenotype of seipin-null cells (Figure 14A, marked with arrows) was suppressed into multiple, clustered LDs upon heterologous expression of human WT and N88S (Figure 14A). Venus (YGFP) protein fluorescence was then monitored by fluorescence microscopy to examine IB formation.

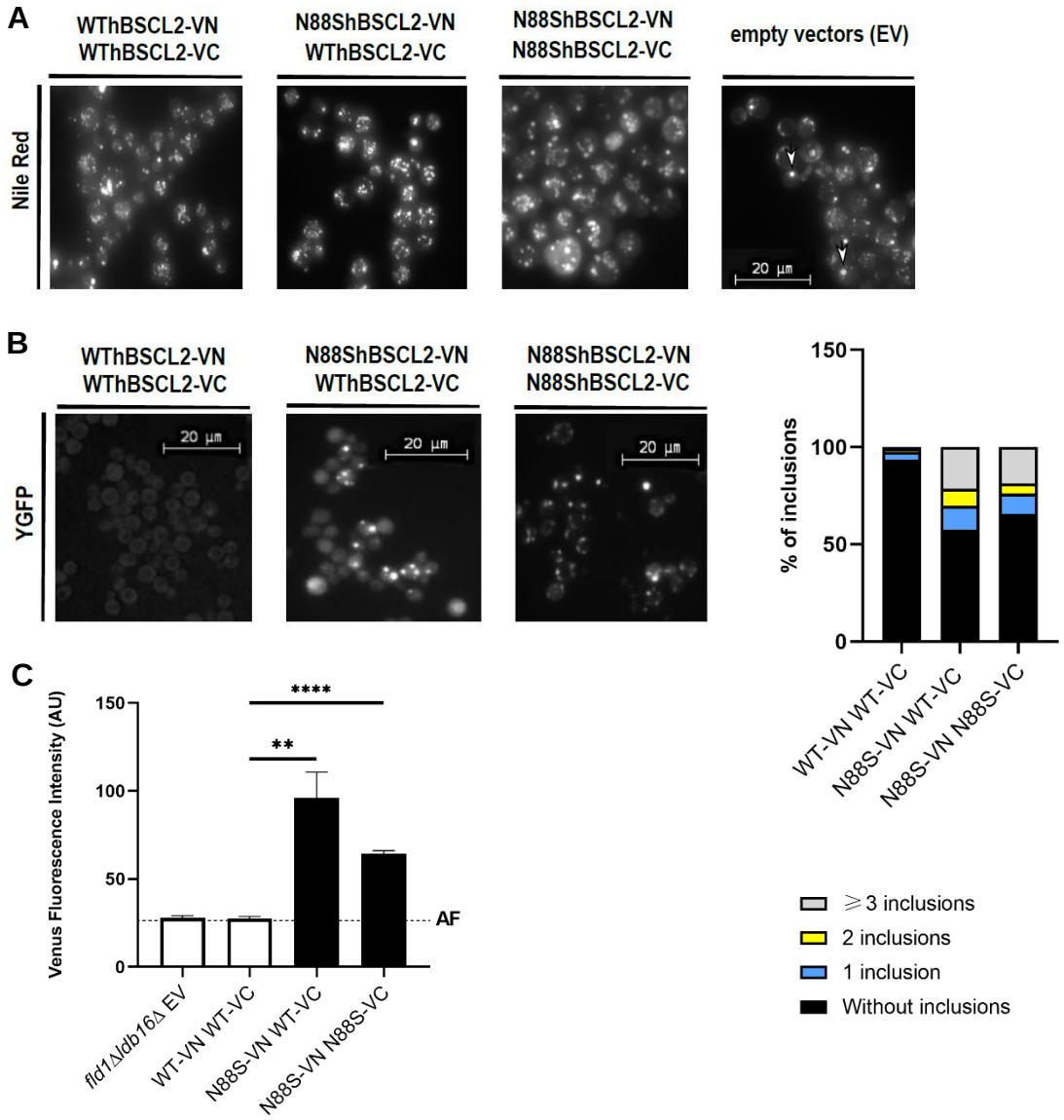

Figure 14. Characterization of Venus-based constructs. Cells were grown in SC-glucose lacking histidine to exponential phase. **(A)** Cells with the indicated genotypes were stainded for LD dye Nile Red. The supersized LD phenotype (markes with arrows) observed in seipin-null cells expressing empty vectors (EV) is supressed to multiple, clustered LDs observed upon expression of WT and gain-of-function N88S mutant seipin. WThBSCL2-VN/WThBSCL2-VC, N88ShBSCL2-VN/WThBSCL2-VC and N88ShBSCL2-VN/N88ShBSCL2-VC are therein named as WT-VN WT-VC, N88S-VN WT-VC and N88S-VN N88S-VC strains. Bar scale, 20 µm. **(B)** Formation of IBs was monitored by fluorescence microscopy using the YFP//Venus channel (left panel) and quantification of the number of IB puncta is defined as percentage of IB foci (n>100 cells; right panel). The number of IB was classified in 3 different groups: black, blue, yellow and grey bars represent the percentage of cells without any inclusion, with 1 inclusion, 2 inclusions and cells with at least 3 inclusions, respectively. Data were combined from at least 3 independent experiments. Bar scale, 20 µm. **(C)** Formation of IBs was monitored by flow cytometry using the FL1 channel and quantification of the Venus fluorescence intensity, normalized to cell number, was determined. Auto-fluorescence (AF) is expressed as the background signal defined by the *fld1*Δ*ldb16*Δ expressing EV. ***p*<0.01; *****p*<0.0001.

As shown in Figure 14B, we observed the formation of IBs as previously reported for mammalian cells [95], and we showed that these IBs can be composed of mutant homomers or WT-mutant heteromers, demonstrating that WT seipin can also interact with N88S seipin to generate these inclusions. Importantly, their formation was not observed in cells expressing only WT seipin (Figure 14B). The fact that WT protein homomers do not accumulate in unstressed cells, although they are constantly produced, is due in part to the existence of the cellular quality control machinery that suppresses the accumulation of excess or less stable protein [159]. Steric hindrance of the fusion protein affecting seipin homomerization could also explain this feature. However, we discard this possibility as WT homomers can abolish the LD supersized phenotype, and therefore form stable and functional seipin complexes (Figure 14A) that restores neutral lipid content (data not shown) of the *fld1*Δ*ldb16*Δ strain. We also observed that approximately 30-40% of cells expressing the mutant N88S form of seipin displayed inclusions. The number of inclusions per cell was comparable for both strains expressing the mutant seipin (Figure 14B, right panel). In view of these results, we performed quantitative analysis for IBs using a flow cytometry based assay, which allows quantification of Venus fluorescence intensity (Figure 14C). The results show that the formation of IBs can be followed with this approach, as the quantification of Venus fluorescence perfectly matches the fluorescence microscopy results, showing a signal significantly above the background signal (defined by the *fld1*Δ*ldb16*Δ EV strain) in the N88S-VN WT-VC and N88S-VN N88S-VC strains, in which the formation of IB was detected. Importantly, the Venus fluorescence intensity for WT-VN WT-VC cells was essentially the same as in seipin-null cells (*fld1*Δ*ldb16*Δ EV), which is consistent with our microscopy results, as we did not observe IB formation in cells expressing only WT seipin (Figure 14B). Taken together, these results indicate that the N88S mutation is responsible for the formation of IBs, which can be composed of seipin N88S homomeric and heteromeric species (with WT seipin).

3.2. UPR is activated in cells expressing the N88S mutation

Previous studies have shown that mutations associated with seipinopathy lead to accumulation of unfolded seipin in the ER lumen, suggesting that seipinopathies are closely associated with ER stress [76, 89]. When the capacity of the ER to fold proteins properly is compromised or overwhelmed, the UPR pathway is activated in order to restore ER homeostasis.

Since seipinopathy is an age-related disease, we assessed the activation of the ER stress response during growth from exponential to post-diauxic shift (PDS) phase. For this purpose, *fld1*Δ*ldb16*Δ EV, WT-VN WT-VC, N88S-VN WT-VC and N88S-VN N88S-VC strains were transformed with an UPRE-*lacZ* gene reporter (based on pJT30) and β-galactosidase (β-Gal) activity was measured (Figure 15). At the exponential phase, expression of the mutant N88S form of seipin (in N88S-VN WT-VC and N88S-VN N88S-VC cells) increased β-Gal activity when compared to WT-VN WT-VC cells (Figure 15), indicating that the UPR was activated in these cells. Importantly, in all tested strains, β-Gal activity increased during growth to PDS phase when respiratory metabolism is stimulated after glucose exhaustion (Figure 15). Importantly, aged cells expressing N88S-N88S homomers displayed an almost 2-fold increase compared to cells expressing only WT seipin at PDS phase (Figure 15). In addition, N88S-VN WT-VC cells also experienced higher ER stress during aging, although not as markedly as observed for cells carrying N88S homomeric species (Figure 15). Overall, these results suggest that the formation of N88S-N88S homomers is associated with higher ER stress during aging, which essentially recapitulates the observations made in mammalian cells expressing the N88S mutation [101].

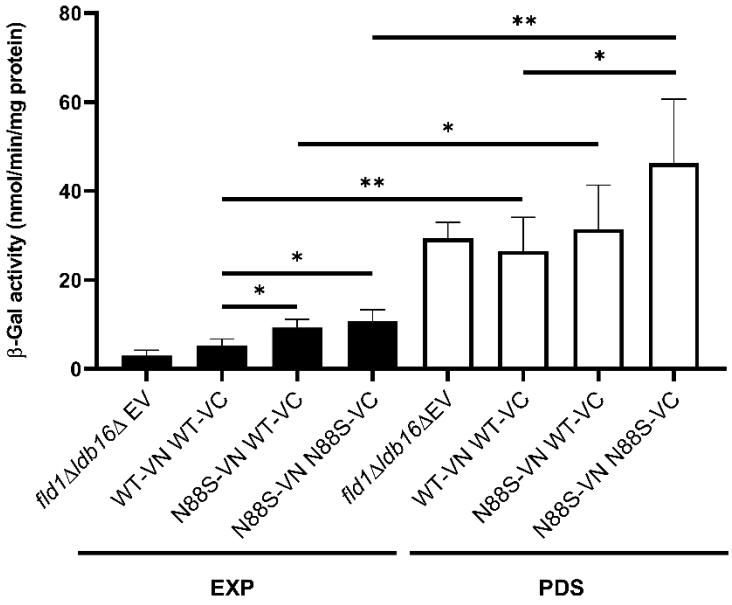

Figure 15. Seipin N88S mutation promotes ER stress. Cells with the indicated genotypes harboring pRS315-UPRE-LacZ reporter were grown in SC-glucose lacking histidine and leucine to exponential phase and to post-diauxic shift (PDS) phase. β-galactosidase activity was determined. Values are represented as a mean ± SD of at least three independent experiments. *p<0.05. **p<0.01.

3.3. N88S seipinopathy is not associated with impairment of ERAD

A failure in the polypeptide chain to adopt its native conformation may lead to activation of protein degradation pathways, including the ERAD mechanism [160]. In this process, a misfolded protein is retro-translocated across the ER membrane into the cytosol, where it is ubiquitylated and targeted for degradation by the 26S proteasome. Thus, a defect in proteasome degradation could explain IB accumulation in cells expressing the N88S mutation (Figure 14B). To test if ERAD is compromised in these cells, we challenged cells with a well-characterized misfolded version of carboxypeptidase Y called CPY* that is degraded by ERAD [149]. For this, cells carrying pRS315-CPY*HA were treated with cycloheximide (CHX) to monitor CPY*HA stability over time.

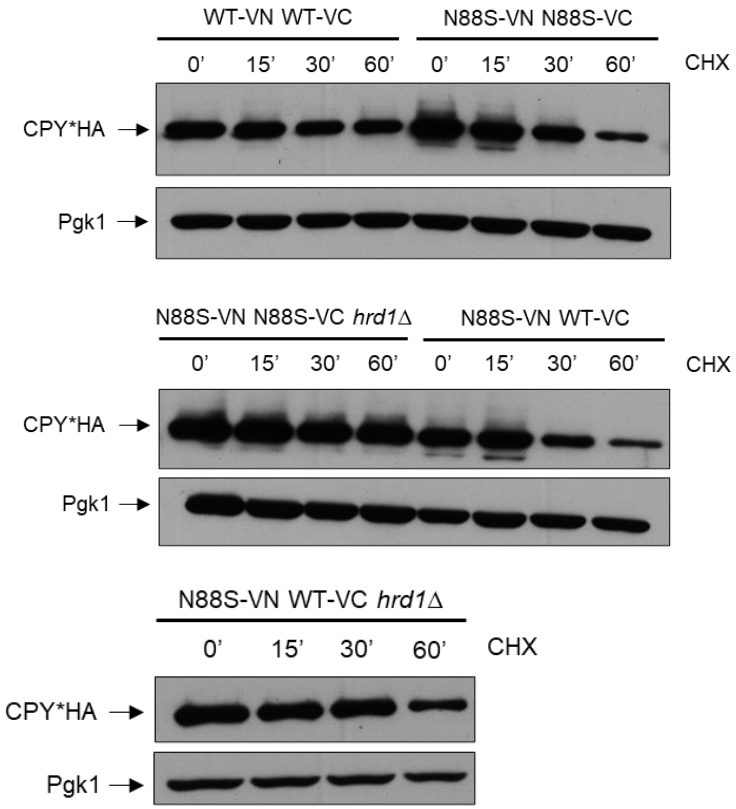

Figure 16. Analysis of ERAD (CPY* stability) upon seipin WT and N88S mutation. Cells with the indicated genotypes harboring pRS315-CPY*HA were grown in SC-glucose lacking histidine and leucine to exponential phase. Subsequently, cells were treated with 200 µg/mL cycloheximide (CHX) for 0, 15, 30 and 60 min. Cells were lysed, and protein extracts were separated by SDS-PAGE and analyzed by immunoblotting, using anti-HA and anti-Pgk1 (loading control) antibodies.

Our preliminary results indicate that after the CHX pulse, a fraction of CPY* was slightly degraded after 60 minutes in WT-VN WT-VC cells (Figure 16). In contrast, in cells expressing N88S mutant seipin, CPY*HA was processed at a faster kinetics over time

than WT-VN WT-VC cells. This indicates that ERAD was fully efficient in cells expressing the N88S mutant seipin. Importantly, loss of *HRD1* in cells expressing mutant homomers significantly stabilized CPY*HA protein over time (Figure 16) as expected, since Hrd1p is the E3 ligase involved in the degradation of ERAD-L substrates, which includes CPY*HA [161]. Overall, these results indicate that UPR and ERAD are fully functional and become activated in response to N88S mutant seipin.

3.4. IB formation landscape

Accumulation of misfolded proteins in the ER activates the UPR stress signaling pathway. To enhance secretory protein folding and promote adaptation to stress, the UPR stimulates the expression and activity of ER chaperone proteins [162]. Molecular chaperones and heat shock proteins are specialized in controlling the quality of the proteins in the cell, in particular by supporting proper folding, dissolution and clearance of already formed protein aggregates [163].

KAR2 encodes an essential protein that is a member of the HSP70 family of molecular chaperones [164]. During ERAD, a misfolded substrate is firstly recognized by several proteins members of the Hrd1p complex, including Yos9p (luminal lectin), Der1p (transmembrane protein), Kar2p or directly by Hrd1p. Non-glycosylated misfolded substrates may be recognized by Kar2p. Both Yos9p and Kar2p bind to the luminal domain of Hrd3p, while unfolded and extended polypeptide segments may be recognized by the luminal domain of Hrd3p [164, 165]. Unlike most chaperones that prevent proteins from aggregating, Hsp104p, a general protein disaggregase of the *HSP100* gene family, operates coordinately with the chaperone Hsp70p (Ssa1p) and co-chaperone Hsp40 Ydj1p to disassemble protein aggregates that accumulate under stress conditions [163].

To gain more insight into the process of IB formation, we generated N88S-VN WT-VC and N88S-VN N88S-VC cells either expressing endogenous Hsp104p C-terminally tagged with mCherry or carrying pYX242-Kar2(1-135)-mCherry-HDEL and monitored the localization of intracellular inclusions (Venus) and chaperones (mCherry) by fluorescence microscopy. We observed that Kar2p formed ER-localized foci that colocalize with N88S mutant heteromers and mutant homomers, with at least on foci per cell in all cells (Figure 17A). Additionally, Hsp104-mCherry also colocalized or could be found in close proximity with N88S-containing inclusions (Figure 17B). Indeed,

approximately 80% of cells expressing N88S homomers or heteromers showed colocalization with at least one Hsp104-mCherry foci (Figure 18).

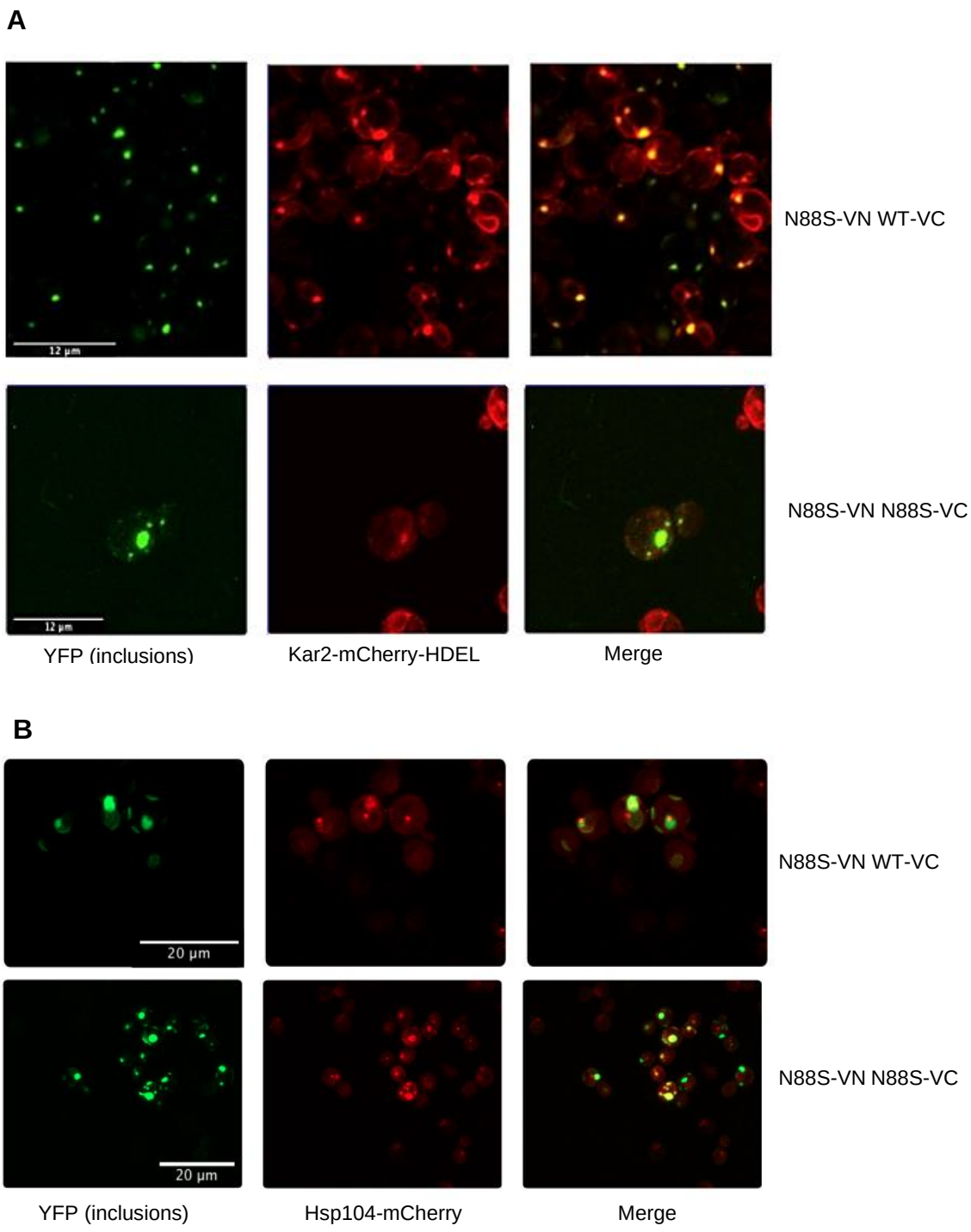

Figure 17. N88S mutation induces changes in ER morphology associated with Hsp104 disaggregase. (A) Cells with the indicated genotypes expressing pYX242-Kar2(1-135)-mCherry-HDEL were grown to exponential phase in SC-glucose lacking histidine and observed by fluorescence microscopy. Z-stacks were taken for DIC, mCherry and Venus channels. The overlay of YFP (green) and mCherry (red) signals is also shown (merge). Bar scale, 12 µm. **(B)** Cells endogenously expressing Hsp104p C-terminally tagged with mCherry were grown to exponential phase in SC-glucose lacking histidine and observed by fluorescence microscopy. Z-stacks were taken for DIC, mCherry and Venus channels. The overlay of GFP and mCherry is also shown (merge). Bar scale, 20 µm.

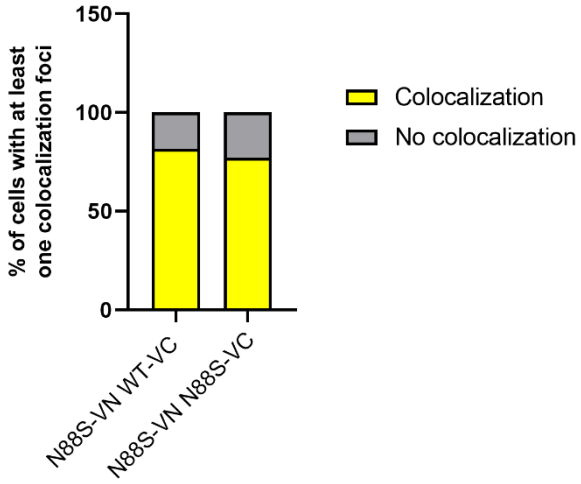

Figure 18. Hsp104p colocalizes with seipin aggregates. Colocalization of Hsp104-mCherry and Venus protein was monitored by fluorescence microscopy using the mCherry and YFP/Venus channels. Yellow and grey bars represent the percentage of cells with at least one Hsp104-mCherry foci that colocalizes and do not colocalize with YFP protein, respectively (n>100 cells). Data were combined from at least 3 independent experiments.

These findings suggest that the N88S homomers and heteromers are recognized and associate with Kar2p and Hsp104p disaggregase. We conceive that Kar2p, as a member of the Hrd1p complex, may be involved in the degradation of mutant seipin by ERAD. Hsp104p presumably colocalizes with IBs composed of N88S mutant protein to rescue misfolded proteins from an aggregated state.

3.5. Autophagy is induced in cells expressing mutant N88S-N88S homomers

Autophagy is one of the major systems for cytoplasmic protein degradation and an overactivation of autophagic response can lead to progressive neurodegeneration [102]. Previous studies in transgenic mice reported N88S overexpression to increase autophagy, which might be a compensatory response to accelerate the removal of mutant seipin aggregates and to protect cells from apoptosis, and thus delaying the progression of motor phenotypes [102]. To test if autophagy is similarly induced, we used the GFP-Atg8p processing assay as a reporter assay for autophagy activation [166].

Atg8p is an ubiquitin like protein, homolog of mammalian LC3-II, involved in the formation of autophagosomes [167]. When autophagy is induced, GFP-Atg8p is delivered to the vacuole within the inner vesicle of the autophagic body. Atg8p is degraded upon lysis of the autophagic body, but the GFP moiety is relatively resistant to the vacuolar degradation. Hence, monitoring free GFP processed from GFP-Atg8p reflects the level of autophagy [166]. GFP-Atg8p and free GFP can be easily detected

by Western blotting using a GFP-specific antibody (Figure 19). For this purpose, cells were grown to PDS phase, a condition known to promote the induction of autophagy under nutrient scarcity [168]. We showed that GFP-Atg8p was processed in aged cells carrying pRS315-GFP-*ATG8* (Figure 19). This result essentially recapitulates the findings reported for mammalian cells [102]. Therefore, accumulation of IBs by the N88S mutation is not related to defects in autophagy. Rather, the N88S mutation leads to misfolding of seipin in the ER, resulting in ER stress and activation of the autophagy system, possible as a homeostatic mechanism to accelerate the degradation of mutant seipin species, in concert with the UPR and ERAD, and prevent IB accumulation and their potential toxic effects.

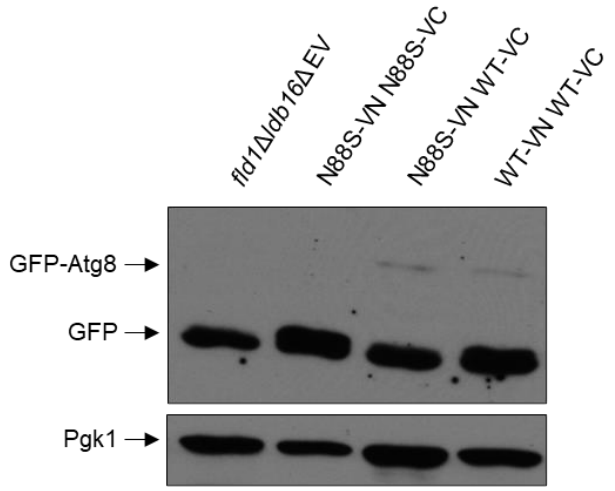

Figure 19. Autophagy is induced in the N88S-VN N88S-VC strain. Cells with the indicated genotypes carrying pRS315-GFP-*ATG8* were grown in SC-glucose lacking histidine and leucine to PDS phase. Protein extracts were analyzed by western blot using anti-GFP as primary antibody. Pgk1p was used as a loading control. A representative experiment of three is shown.

3.6. ROS levels and lipid peroxidation are increased in cells expressing N8SS-N88S homomers

Neurodegenerative disorders are commonly associated with cellular stress due to protein misfolding, aggregation and redox imbalance [134].

Studies have also indicated that ER stress events are correlated with ROS production within cells [127, 169, 170]. Changes in the protein-folding environment can cause accumulation of misfolded proteins in the ER that profoundly affect redox homeostasis and apoptosis. Several studies revealed that redox dyshomeostasis in the ER is sufficient to cause ER stress, which could, in turn, induce the production of intracellular ROS [127, 170]. Thus, we investigated if ER stress associated with the N88S seipin mutation is accompanied by oxidative stress. For this, cells were grown to stationary phase and labeled with dihydroethidium (DHE), a ROS probe, and ROS

accumulation was assessed by flow cytometry (Figure 20A). At stationary phase, approximately 25% cells expressing WT-VN WT-VC homomers displayed oxidative stress, but cells containing either N88S homomeric or heteromeric species displayed higher DHE staining (approximately 35-40%, Figure 20A).

Importantly, higher ROS content are associated with increased levels of lipid peroxides in N88S-VN N88S-VC, but not in N88S-VN WT-VC cells (Figure 20B). We then conclude that the toxicity associated with the formation of N88S homomers induces ER stress and oxidative modifications in aged cells, which can be modulated, at least in part, by WT seipin (Figures 15 and 20).

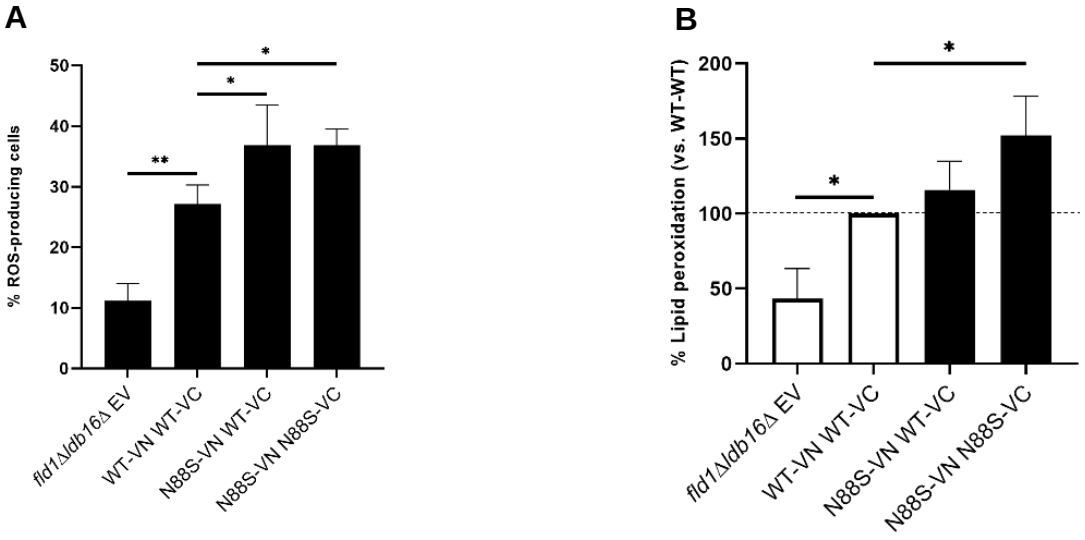

Figure 20. Cells expressing mutant homomeric species are associated with higher levels of ROS and an increase of lipid peroxidation during aging. **(A)** Cells with the indicated genotypes were grown in SC-glucose lacking histidine until stationary phase and ROS levels were assessed in cells labeled with dihydroethidium (DHE) and by flow cytometry using the FL3 channel. **(B)** Cells were grown in SC-glucose lacking histidine until stationary phase and lipid peroxidation levels were monitored using the TBARS (thiobarbituric acid reactive substance) assay. Values are mean ± SD of at least three independent experiments. *p<0.05. **p<0.01.

Next, we intended to identify the major source of ROS in N88S-VN WT-VC and N88S-VN N88S-VC strains. First, we decided to investigate the contribution of mitochondria in ROS production using rho^0 cells, which lack mitochondrial DNA [171]. These cells were then grown until stationary phase and labeled with DHE to assess ROS production by flow cytometry. We found that mitochondrial DNA depletion did not reduce ROS levels in all tested strains (Figure 21A). Instead, we observed a 40-60% increase in ROS levels in WT-VN WT-VC, N88S-VN WT-VC and N88S-VN N88S-VC rho^0 strains when compared to their RHO+ counterparts, whereas ROS accumulation in the *fld1*Δ*ldb16*Δ EV rho0 strain was slightly smaller (23% increase). This is in agreement with previous observations, showing that the ablation of mitochondrial DNA from WT cells induced higher levels of ROS [172]. Consistent with a non-mitochondrial source for ROS generation, all strains do not display obvious mitochondrial function

defects as they grow equally well on media containing glycerol, a non-fermentable carbon source (Figure 21B). Taken together, these results exclude the mitochondria as a potential major source for ROS accumulation.

We next examined possible non-mitochondrial candidates that may be responsible for ROS production in these cells. Recent studies have reported that the increase in superoxide generation could be attributed to the activity of the ER-localized NADPH oxidase Aim14p/Yno1p [133]. Therefore, we investigated whether the deletion of *AIM14* altered the ROS levels (Figure 21C).

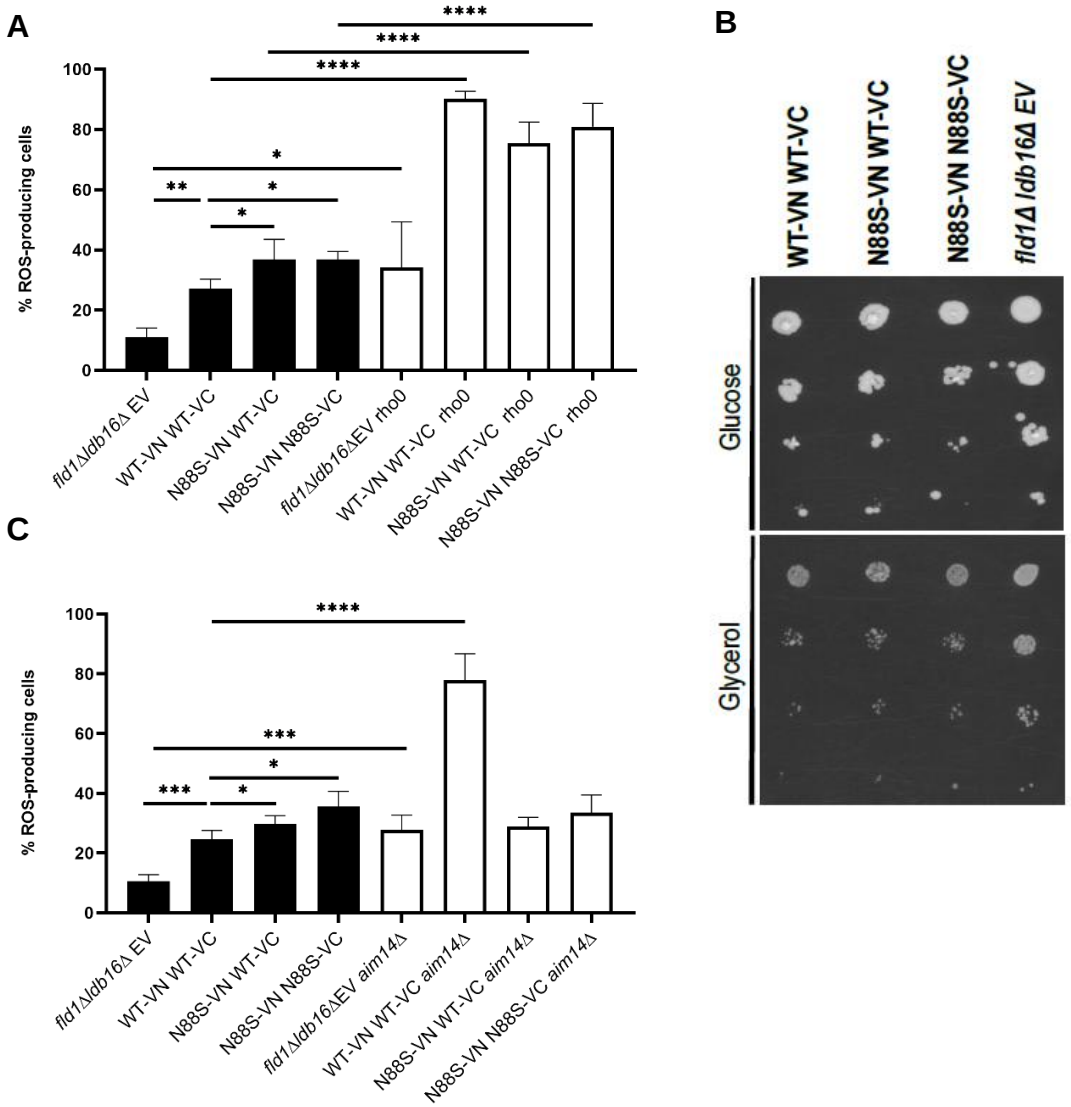

Figure 21. Mitochondria and ER-localized NADPH oxidase Yno1p are not the main sources of ROS accumulation in cells expressing the N88S mutation. (A) Cells with the indicated genotypes were grown in SC-glucose lacking histidine until stationary phase and ROS levels were monitored by flow cytometry using the FL3 channel, in cells stained with DHE. **(B)** Cells were grown to exponential phase in SC-glucose medium lacking histidine and 5-fold serial dilutions were plated in both SC-glucose and SC glycerol plates. One representative experiment out of three is shown. **(C)** Strains were grown in SC-glucose lacking histidine until stationary phase and ROS levels were monitored by flow cytometry using the FL3 channel, in cells labeled with DHE. Values are mean ± SD of at least three independent experiments. **p*<0.05. ***p*<0.01; ****p*<0.001. *****p*<0.0001.

The results showed no differences in ROS content when compared to the corresponding *aim14*Δ counterpart, except for the WT-VN WT-VC *aim14*Δ strain, where we found a 2.7-fold increase in ROS generation (Figure 21C). Overall, mitochondria and Yno1p are not major sources for ROS production in cells carrying the N88S mutation.

3.7. Yap1 pathway is hyperactivated in cells expressing N88S-N88S homomers

Yeast YAP1 is a bZIP transcription factor, which binds as a dimer to the YAP1 response element (YRE) [173]. The C-terminal domain of this transcription factor contains cysteine residues that, under oxidizing conditions, form an intramolecular disulfide bridge locking the molecule in a conformation where the nuclear export sequence is masked. Thus, YAP1 accumulates in the nucleus, promoting transcription of antioxidant genes [173]. Of interest to us here is the parallel made between yeast YAP1 and the mammalian KEAP-NRF2 pathways as major regulators of cytoprotective responses to stresses caused by ROS [173]. Since the Yap1 pathway is critical for oxidative stress tolerance in yeast, the induction of the pathway was monitored using a Yap1-dependent lacZ reporter (pRS415-AP-1-CYC1-LacZ) (Figure 22). The results showed a 1.4-fold increase of β-gal activity in cells expressing mutant homomers compared to the WT-VN WT-VC cells at PDS phase. Notably, in cells expressing WT-mutant heteromers, β-gal activity decreased to levels slightly lower to the observed in the WT-VN WT-VC cells (Figure 22).

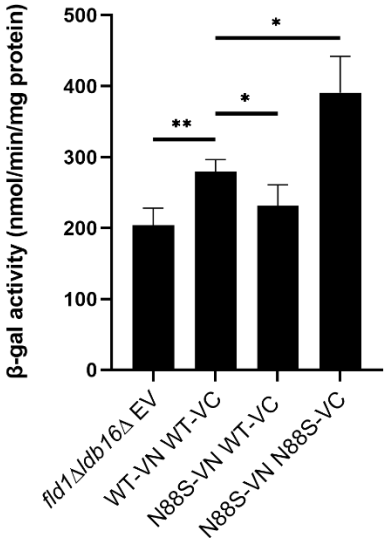

Figure 22. Yap1 pathway is hyperactivated in the mutant homomeric strain. Cells with the indicated genotypes expressing a Yap1-dependent LacZ reporter were grown in SC-glucose lacking histidine and leucine to PDS phase. β-galactosidase activity was determined with 70 µg of total protein. Values are represented as a mean ± SD of at least three independent experiments. *p<0.05. **p<0.01.

Taken together, these results suggest that Yap1 pathway is hyperactivated in cells expressing solely the N88S mutation, which displays higher level of toxicity (Figure 15) and reinforce the idea of acute oxidative stress experienced by the cells (Figure 20B), which is modulated, to some extent, by the WT form of seipin (Figures 15, 20B and 22).

Based on these results, we tested if ER and oxidative stress leads to loss of cell viability in cells carrying the N88S mutation. We found a ~10% and ~30% decrease in cell viability in N88S-VN WT-VC and N88S-VN N88S-VC cells respectively (Figure 23). Our work so far established that the N88S-N88S homo-oligomer is the species that actively contribute to enhance mutant seipin toxicity, resulting in severe cellular oxidative damages and induction of ER stress response with deleterious effects on cell viability.

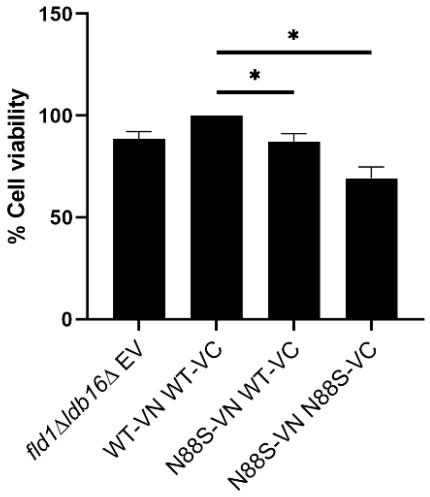

Figure 23. Loss of cell viability in cells expressing N88S-N88S homomers. Cells with the indicated genotypes were grown to exponential phase in SC-glucose medium lacking histidine. Cellular viability was measured as the percentage of the colony-forming unit. Values are represented as a mean ± SD of at least three independent experiments. **p*<0.05. Results were normalized to WT-VN WT-VC (considered 100%).

Overall, the increase in ROS production observed in cells expressing mutant homomers might explain the hyperactivation of the Yap1 pathway, as this pathway is activated under oxidizing conditions, leading to lipid peroxidation. Additionally, misfolding of mutant seipin leads to activation of UPR, ERAD and autophagy, probably as an adaptive stress mechanism to cope with the buildup of misfolded seipin in ER-localized IBs. The rapid loss of cell viability observed in cells expressing the N88S mutation solely can be explained by chronic activation of these homeostatic mechanisms, thus contributing to cell death. Importantly, all these alterations seem to be attenuated, at least to some degree, by the expression of WT seipin in cells containing N88S-WT heteromers.

3.8. The activity of antioxidant defenses is altered in cells expressing the N88S mutation

Increased ROS levels in cells may be also related to perturbations in ROS detoxification mechanisms, namely in the activity of antioxidant enzymes, such as catalase, superoxide dismutase (Sod) and glutathione [174]. Under normal conditions, these antioxidant mechanisms are able to maintain cellular ROS at basal level, preventing cytotoxicity. Catalase is one of the crucial antioxidant enzymes that relieves considerably oxidative stress through the decomposition of cellular hydrogen peroxide to water and oxygen [175]. Deficiency or malfunction of catalase is thought to be associated to the pathogenesis of many age-associated degenerative diseases [175]. Sod also plays a primary role in detoxification processes, through the conversion of superoxide radicals to hydrogen peroxide [176], while glutathione is a tripeptide and exists in cells in two different forms: reduced glutathione (GSH) (90-95% of the total glutathione) and oxidized glutathione (GSSG) [177]. The GSH/GSSG redox couple is used as a measure of the oxidative stress status, and the imbalance of GSH is reported in several human aliments such as atherosclerosis, cancer, neurodegenerative disease, and aging [178].

To monitor SOD activity, cells were grown to PDS phase and the two isoforms, Sod1p (cytosolic) and Sod2p (mitochondrial), were analyzed *in situ* using native PAGE and specific staining for SOD activity. We found no significant variations in Sod1p and Sod2p activities in all strains tested (Figure 24A), indicating that SOD activity is not compromised in cells expressing mutant seipin. Remarkably, we found a decrease of ~40-45% of catalase activity in cells expressing WT-mutant heteromers and mutant homomers (Figure 24B). Total reduced glutathione (GSH) levels, that represent up to 95% of the total glutathione in cells, were also measured. We observed a 3.7-fold and 2.6-fold increase in GSH levels in cells expressing WT-mutant heteromers and mutant homomers, respectively, when compared to WT-VN WT-VC cells (Figure 24C). This may indicate a compensatory ROS scavenging mechanism to counteract ROS generation or may reflect changes in the ERO1/PDI-mediated oxidative folding process in which GSH plays a crucial role in controlling the ER redox homeostasis [179]. Collectively, these results suggest that N88S mutation specifically impairs catalase

activity and increases GSH levels. The loss of catalase activity in cells expressing the N88S mutation may then contribute to ROS accumulation.

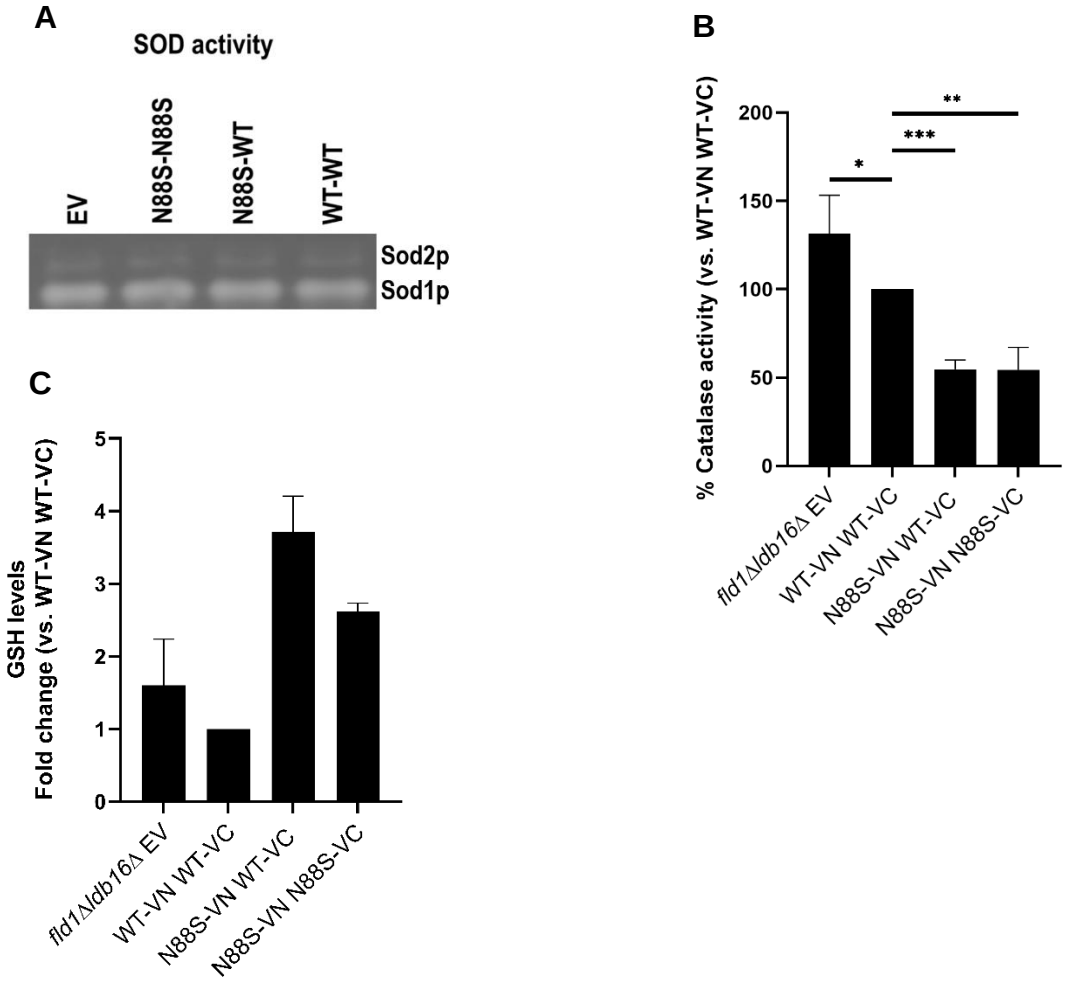

Figure 24. Catalase activity and glutathione levels are altered in cells expressing the N88S mutation. (A) Cells with the indicated genotypes were grown to PDS phase and activity of SOD was assessed *in situ* after native-PAGE, as described in Material and Methods. A representative experiment of three independent experiments is shown. **(B)** Quantification of catalase activity by measuring the degradation of H_2O_2 spectrophotometrically in cell lysates. Catalase activity was expressed as units of catalase per milligram of protein (U/mg). Values are mean ± SD of at least three independent experiments. **p*<0.05. ***p*<0.01; ****p*<0.001. **(C)** GSH levels were measured using the GSH/GSSG Ratio Detection Assay Kit. Values are mean ± SD of two independent experiments.

3.9. Crosstalk between oxidative stress, ER stress response and IB formation

Recent studies have revealed that ER stress is closely related to redox metabolism and ROS generation in several organisms [170, 180]. In order to establish a connection among ER stress, UPR, and oxidative stress in the context of N88S seipinopathy, we firstly tested if the antioxidant N-acetyl-L-cysteine (NAC) [181] could mitigate UPR induction in cells expressing the N88S mutation. Using the UPRE-LacZ reporter, we found that NAC supplementation did not alter UPR induction in N88S-VN

WT-VC and N88S-VN N88S-VC cells (Figure 25), indicating that ROS levels are not associated with induction of the ER stress response upon N88S mutation.

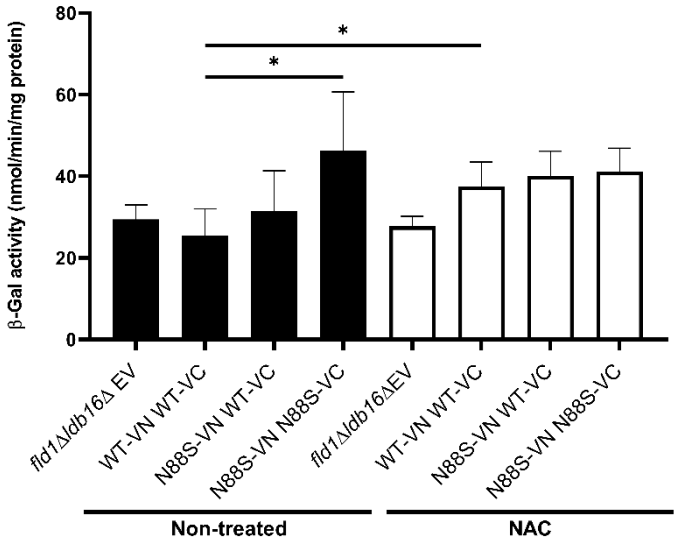

Figure 25. UPR induction is not altered in cells treated with NAC. Cells with the indicated genotypes harboring pJRS315-UPRE-LacZ reporter were grown in SC-glucose lacking histidine and leucine to PDS phase. Protein extracts were prepared, and specific β-galactosidase (β-Gal) activities, with o-nitrophenyl-β-D-galactopyranoside (ONPG) as a substrate, were determined by measuring the amount of o-nitrophenol released by the galactosidase-catalyzed hydrolysis process. Values are represented as a mean ± SD of at least three independent experiments. **p*<0.05.

In agreement with these findings, ablation of mitochondrial DNA, which was associated with a large increase in ROS levels in all tested strains (Figure 21A), had little effect on IB formation (as assessed by Venus fluorescence) in all rho^0 strains, except for WT-VN WT-VC rho^0 cells (Figure 26). Overall, ROS accumulation and oxidative stress is not the leading cause of UPR induction and IB formation, but it is more likely to be a consequence of protein misfolding imparted by expression of N88S seipin.

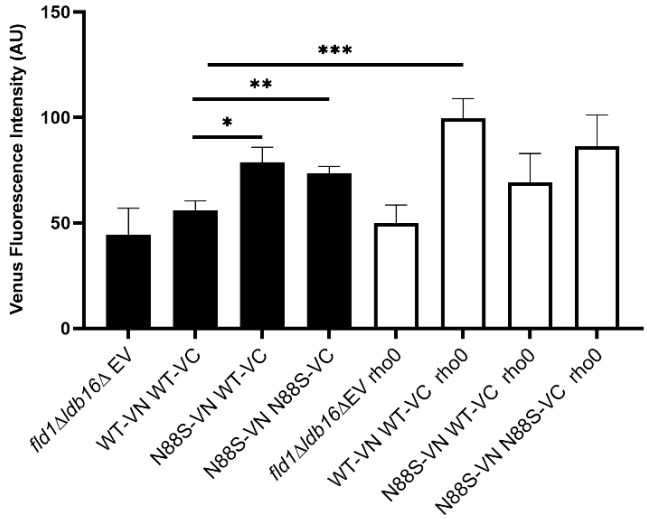

Figure 26. Ablation of mitochondrial DNA did not reduce the formation of IB. Cells with the indicated genotypes were grown until stationary phase and the formation of IBs was monitored by flow cytometry using the FL1 channel and quantification of the Venus fluorescence intensity, normalized to cell number. **p*<0.05. ***p*<0.01; ****p*<0.001

3.10. Disruption of control quality mechanisms enhances IB formation, ROS production and impairs growth in cells expressing N88S seipin

ERAD is an evolutionarily conserved process responsible for the clearance of misfolded proteins in the ER targeted for cytosolic proteasomal degradation, whereas UPR is activated in response to misfolded protein accumulation to reestablish ER redox balance and folding capacity [182].

Misfolded ER-lumenal proteins and some transmembrane proteins with misfolding lesions within the ER lumen, such as the N88S mutation located at the ER lumenal domain of seipin (Figure 7), are degraded by the ERAD-lumenal (ERAD-L) pathway. In yeast, ERAD-L and ERAD-M (membrane) substrates are targeted for degradation by the Hrd1p complex [121]. Since ERAD is functional in cells expressing the N88S mutant seipin (Figure 16), we questioned whether activation of ERAD regulates IB formation and the production of ROS in these cells. For this purpose, we performed the deletion of *HRD1* gene in N88S-VN WT-VC and N88S-VN N88S-VC cells. The results showed that loss of Hrd1p-mediated ERAD significantly increases the formation of intracellular inclusions (Figure 27A). Notably, a 2.5-fold increase in ROS levels was also observed (Figure 27B). Altogether, these data provide strong evidence that IB formation and oxidative stress are regulated by ERAD and suggest that this mechanism is required for protein degradation of mutant seipin and to fine-tune ROS buildup in response to accumulation of N88S misfolded proteins.

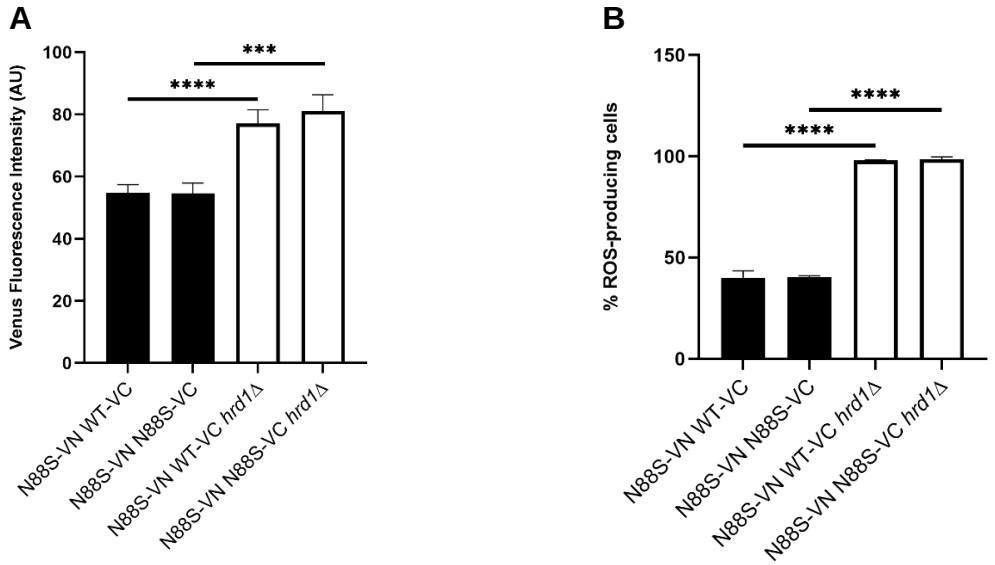

Figure 27. ERAD plays a key role in reducing IB formation and ROS production in cells expressing N88S mutant homomers. (A) Cells with the indicated genotypes were grown to stationary phase and the formation of IBs was monitored by flow cytometry using the FL1 channel and quantification of the Venus fluorescence intensity, normalized to cell number. **(B)** Cells were grown until stationary phase and ROS levels were monitored by flow cytometry using the FL3 channel, in cells labeled with DHE. Values are mean ± SD of at least three independent experiments. ***p<0.001; . ****p<0.0001.

The key UPR signal activator, Ire1p, senses the accumulation of misfolded proteins and responds to ER stress by propagating the UPR signal from the ER to the cytosol to restore the ER protein folding capacity [118]. Thus, we also investigated the contribution of the UPR in controlling IB formation in cells carrying the N88S mutation, (in N88S-VN WT-VC and N88S-VN N88S-VC cells) upon deletion of *IRE1*.

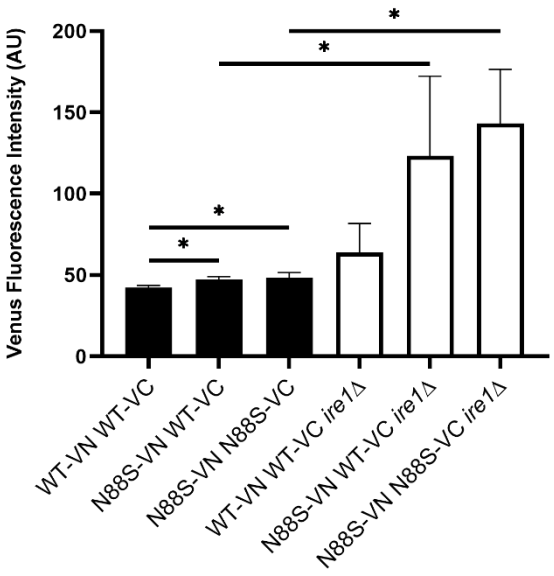

Figure 28. The UPR, like ERAD, has a cryoprotective role in preventing formation of IBs and ROS generation in cells expressing N88S mutant seipin. Cells with the indicated genotypes were grown to stationary phase and the formation of IBs was monitored by flow cytometry using the FL1 channel and quantification of the Venus fluorescence intensity was normalized to cell number. Values are mean ± SD of at least three independent experiments. **p*<0.05.

Here, we demonstrate that disruption of this pathway resulted in a 2.5-fold increase in the formation of intracellular inclusions in both strains expressing the N88S mutation when compared with cells expressing only WT seipin (Figure 28). Preliminary results indicate that ROS levels are also increased in N88S-VN WT-VC *ire1*Δ and N88S-VN N88S-VC *ire1*Δ cells (data not shown), similarly to what was observed for cells devoid of *HRD1* (Figure 27). Importantly, we observed a growth defect in cells lacking either *HRD1* or *IRE1* once they reached the stationary phase (Figure 29). Altogether, these results suggest that activation of Hrd1p-associated ERAD and the UPR pathways are essential for proper cell growth, and crucial to prevent accumulation of IBs and ROS in cells expressing the N88S mutation.

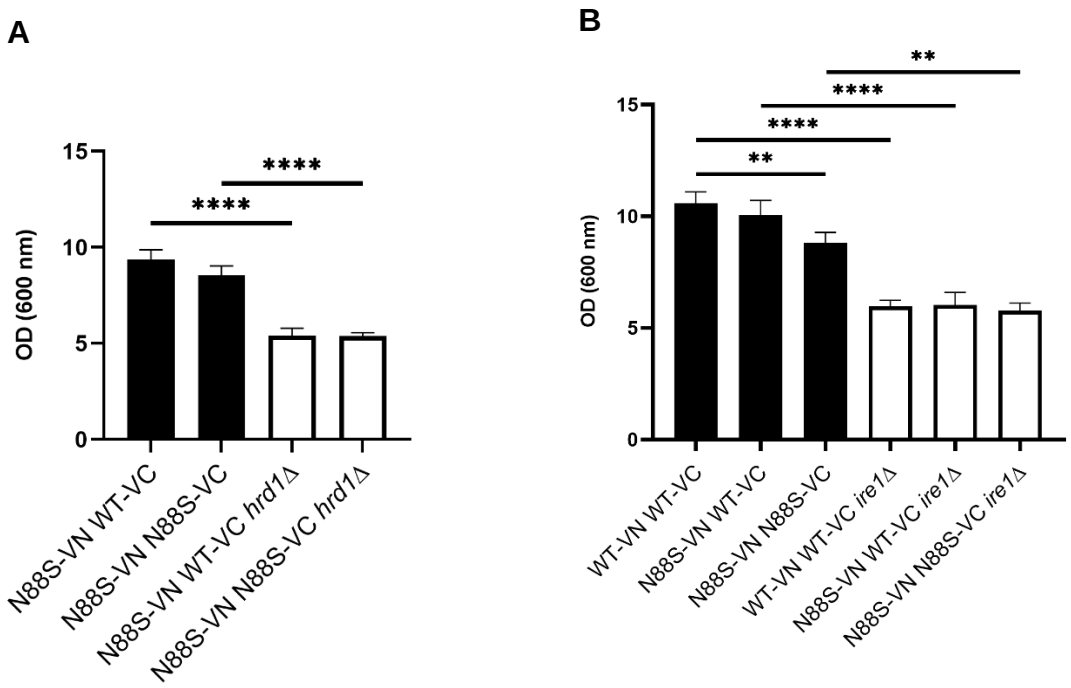

Figure 29. Disruption of major protein quality control mechanisms in cells expressing the N88S mutation results leads to defective growth. (A) and (B) Cells with the indicated genotypes were grown in SC-glucose medium lacking histidine until stationary phase and the growth rate was monitored by optical density (OD) at 600 nm. Values are represented as a mean ± SD of at least three independent experiments. ***p*<0.01; ****p*<0.0001.

3.11. Calcineurin signaling activation is impaired in cells expressing N88S-N88S homomers

Disruption of calcium homeostasis in the cell is one of the most adverse and immediate effects caused by ER stress produced by chronic accumulation of misfolded proteins [183]. Compared to other types of cells, this effect becomes even more deleterious to neurons, because of the important role of calcium waves in neuronal activity [184]. Alterations in calcium homeostasis have been reported in several neurodegenerative disorders associated with accumulation of misfolded aggregates [183, 185]. Previous studies have suggested increase of cytoplasmic Ca^{2+} due to ER stress in presence of misfolded proteins in various neurodegenerative diseases [183, 185]. The ER is the main intracellular Ca^{2+} store containing roughly 2 mM total Ca^{2+}, acting as a major buffering system that functions as a sink for Ca^{2+} storage. Loss of calcium ions during ER stress is mediated through activation/expression of calcium handling proteins localized in the ER and through Ca^{2+} release in the cytosol [186].

Among the consequences of protein misfolding mediated through ER stress and alterations in calcium homeostasis are changes on the activity of several phosphatases that play a crucial role in maintaining cellular functioning, namely the brain phosphatase calcineurin [184]. Ca^{2+} influx in the neuronal cytosol activates a myriad of proteins to

initiate the downstream signaling mechanism. Due to very high affinity (0.1-1nM) for Ca^{2+}/calmodulin and co-localization with N-methyl-D-aspartate receptor, calcineurin activates rapidly after cytoplasmic Ca^{2+} influx [184]. Upon activation, this phosphatase contributes to inhibit further Ca^{2+} influx into the cytosol [184].

One role of calcineurin is to activate gene expression through the regulation of the transcription factor Crz1p [187]. In yeast, calcineurin prevents cell death upon ER stress by regulating calcium influx through this transcription factor [187, 188]. In order to monitor calcineurin activation within the scope of N88S seipinopathy and ER stress, we transformed *fld1*Δ*ldb16*Δ EV, WT-VN WT-VC, N88S-VN WT-VC and N88S-VN N88S-VC strains with a calcineurin-dependent response element (CDRE)-LacZ reporter (Figure 30).

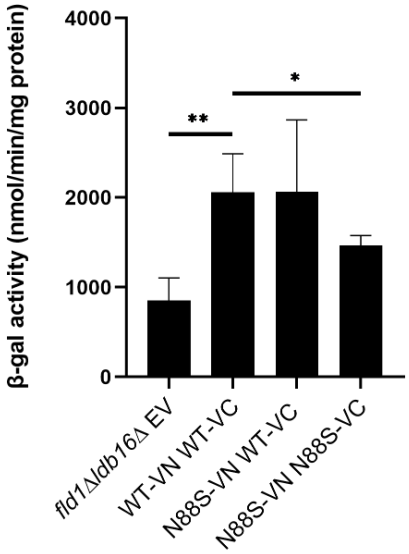

Figure 30. Impaired activation of calcineurin signaling in cells expressing mutant homomers. Cells with the indicated genotypes expressing a CDRE-lacZ reporter (YEplac181-CDRE-lacZ) were grown in SC-glucose lacking histidine and leucine to PDS phase. β-galactosidase activity was determined. Values are mean ± SD of at least three independent experiments. *p<0.05. **p<0.01.

We observed little changes in β-gal activity in cells expressing WT-mutant heteromers when compared to the WT-VN WT-VC cells (Figure 30). Surprisingly, cells expressing solely the N88S mutation exhibited a significant decrease in calcineurin activation (Figure 30), suggesting that calcineurin signaling is impaired in these cells.

Calcium signaling pathways interact with other cellular signaling systems such as ROS [189]. Previous studies have shown that Ca^{2+} is essential for production of ROS. Elevation of intracellular Ca^{2+} level is responsible for activation of ROS-generating enzymes and formation of free radicals by the mitochondria respiratory chain. In contrast, an increase in intracellular Ca^{2+} concentration may be stimulated by ROS [189]. Interestingly, there is evidence that calcineurin is required for survival under prolonged ER stress conditions through a mechanism that involves the control of ROS

production [190]. Dysfunction in either of the systems might affect their crosstalk, thus potentiating harmful effects, which might be on the basis of pathological alterations of various disorders.

To evaluate if the calcineurin pathway modulates ROS production and IB formation, we tested the effect of the deletion of *CNB1*, the regulatory subunit of calcineurin, which is required for functional calcineurin activity [191]. Abrogating calcineurin activity had no substantial effects on ROS levels in all strains tested (Figure 31A). However, disruption of this pathway leads to a partial increase in the formation of IBs in all strains tested (Figure 31B), suggesting a regulatory function of calcineurin in the accumulation of intracellular inclusions. This may indicate that lower calcineurin activation observed in N88S-VN N88S-VC cells (Figure 30) may be a contributing factor for the formation of these IBs.

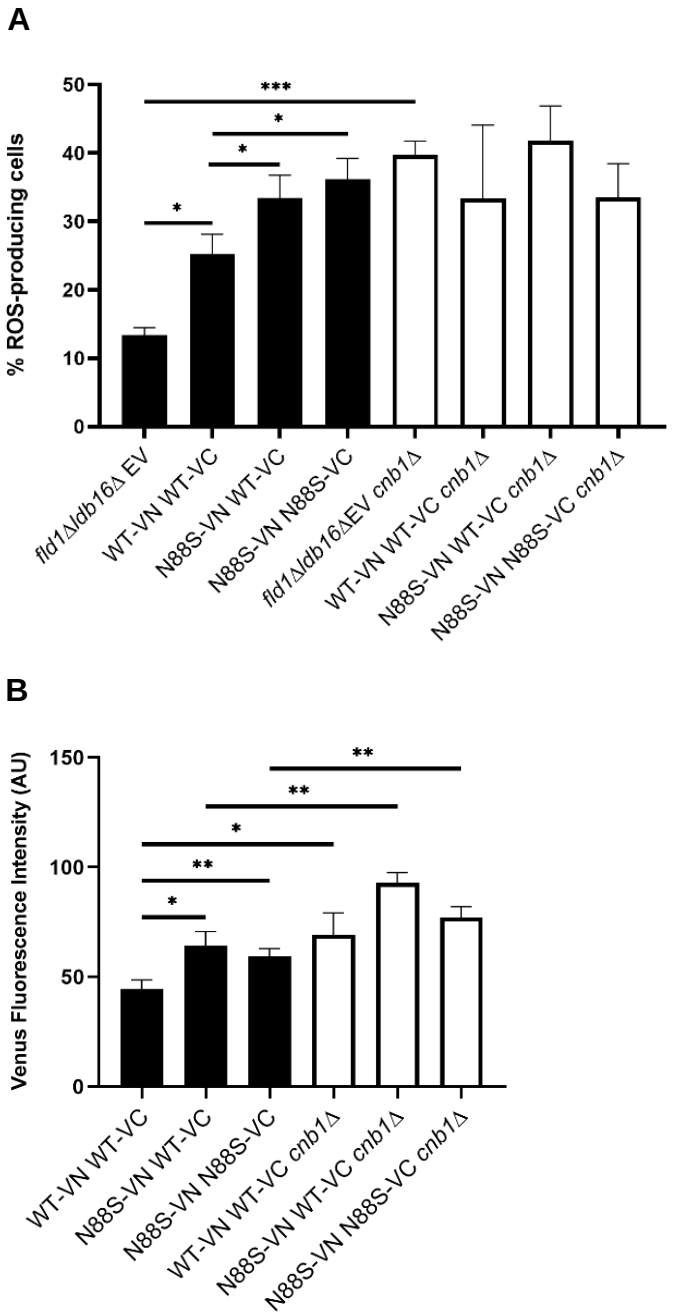

Figure 31. Abrogating calcineurin activity has no effect on ROS levels but stimulates IB generation in all strains tested. (A) Cells with the indicated genotypes were grown until stationary phase and ROS levels were monitored by flow cytometry using the FL3 channel, in cells labeled with DHE. **(B)** Cells were grown until stationary phase and the formation of IBs was monitored by flow cytometry using the FL1 channel and quantification of the Venus fluorescence intensity, normalized to cell number. Values are mean ± SD of at least three independent experiments. **p*<0.05. ***p*<0.01; ****p*<0.001.

Chapter 4

GENERAL DISCUSSION AND CONCLUSIONS

4. Discussion and conclusions

Seipin is a highly conserved and ubiquitous transmembrane protein that resides in the ER and concentrates at junctions between the ER and LDs [12]. Toxic gain-of-function mutations identified in the human seipin *BSCL2* gene, namely N88S and S90L, are functionally linked to the emergence of autosomal dominant motor neuron diseases, collectively known as seipinopathies [12]. Although the molecular pathogenesis of seipinopathies remains largely elusive, these diseases have been associated with impaired folding of seipin due to blocked *N*-glycosylation, seemingly contributing to IB formation, aberrant accumulation of the mutant protein in the ER and severe ER stress-mediated cell death [76, 89, 95]. Importantly, these observations were further substantiated by the development of mouse models of N88S seipin, which recapitulate many of the metabolic and neurological defects observed in patients [101]. Since seipinopathies are autosomal dominant MND, the existence of different combinations of this protein (homomers/heteromers) might modulate the phenotypic differences between patients.

From this point of view, this study aimed to define the model for formation and effects of homo- and heteromeric combinations of WT and human N88S mutant seipin in order to understand their contribution to disease, using *S. cerevisiae* as a model system of the disease. Our study showed that WT seipin can interact with itself and with the N88S mutant seipin to form oligomers, in line with previous observations made in mammalian systems [87, 192]. Consistent with this, our fluorescence microscopy and flow cytometry results showed that, during the exponential growth phase, cells expressing N88S mutant homomers and WT-mutant heteromers displayed approximately 30 and 40% of inclusions, respectively. Moreover, the inclusions formed by the heteromeric and mutant homomeric combination demonstrated a similar propensity to aggregate into numerous inclusions per cell (up to 3). Importantly, the formation of IBs was not observed in cells expressing only WT seipin. Although the formation of WT homomers is possible, it has not been detected in our system. This could be due to protein quality-control systems that would primarily eliminate less stable proteins. In the future, the characterization of the oligomerization state of WT and N88S mutant seipin would help to better understand the process of N88S seipin aggregation.

Previous studies in cultured cells have shown that expression of mutant N88S seipin activates the UPR pathway, suggesting that seipinopathies are closely associated with ER stress [95]. Importantly, these findings are confirmed by *in vivo* studies, which reported that expression of N88S seipin induces ER stress in affected neuronal tissue [101]. In our yeast model of seipinopathy, we observed higher induction

of the ER stress response during growth for all tested strains. In particular, N88S mutant homomeric formation was consistently associated with higher ER stress in cells grown to both exponential and PDS phase, which mirrors the activation of the UPR observed in mammalian cells carrying the N88S mutation. Importantly, activation of the UPR was required to prevent IB formation and ROS generation, denoting a cytoprotective rather than a toxic effect imparted by the UPR in cells expressing the N88S seipin mutation in our conditions. Alternatively, ROS accumulation potentiated by misfolding of N88S mutant seipin may be the leading cause of seipinopathy. However, we do not discard the possibility that chronic activation of ER stress may contribute to cell death.

Dysfunction of the ERAD protein quality-control system and ER stress are thought to be common features of pathological processes in neurological diseases [193]. This relationship between the ER and proteasomal system is essential for the maintenance of protein quality within the lumen of the ER. A defect in proteasomal degradation could result in the accumulation of misfolded proteins and subsequent aggregation rather than turnover [194]. Our data suggested that Hrd1p-mediated ERAD was functional and active in cells expressing N88S mutant seipin. In agreement, Kar2p, a HSP70 chaperone that integrates the Hdr1p complex, and the Hsp104p dissagregase colocalized with mutant seipin homomeric and heteromeric species. We then conceive a model in which Hsp104p may help to retrotranslocate the unstable seipin from the ER, as previously reported [195], in order to facilitate the removal of aggregation-prone, disease-causing N88S seipin, while preventing protein aggregation and prolonged ER stress.

Autophagy is one of the major systems for cytoplasmic protein degradation and several studies have reported that this degradation pathway also plays a critical role in the clearance of aggregate-prone proteins, such as polyglutamine and α-synuclein [196]. Moreover, previous studies in transgenic mice reported N88S overexpression to increase autophagy [102]. Our results confirm that the accumulation of IBs enhanced by the N88S mutation was not related to defects in autophagy, since the process is properly induced in cells expressing N88S mutant seipin. Instead, the N88S mutation seems to promote seipin misfolding in the ER, resulting in the activation of the UPR in response to ER stress, while both autophagic and ERAD processes may be induced in an attempt to prevent accumulation of mutant seipin aggregates and high levels of mutant seipin toxicity.

ER protein folding pathways are closely related with ROS production, especially in the context of neurodegeneration [169]. Moreover, oxidative stress has been linked to the progression of a number of neurodegenerative diseases, including Alzheimer's disease, Parkinson's disease and amyotrophic lateral sclerosis [197]. Therefore, we

investigated whether the response to oxidative stress was impaired in cells expressing the N88S mutant form of seipin, and if so, we aimed at identifying the main sources of ROS in these cells. Our results showed an increase of ROS accumulation in both strains expressing the N88S mutation and importantly, N88S mutant homomeric species strongly contributed to lipid peroxidation. Our findings also excluded both the mitochondria and the ER-localized NADPH oxidase Aim14p/Yno1p as major sources of ROS accumulation in cells expressing N88S mutant seipin. Instead, oxidative stress in cells expressing the N88S mutation was related to impairment of enzymatic antioxidant defenses. Although Sod1p and Sod2p activities were not altered in cells expressing mutant seipin, a loss of approximately 40-45% of catalase activity was observed in these cells. The loss of catalase activity is then likely responsible for the increase in ROS production also observed in cells expressing N88S mutant seipin. At this point, it is not clear how N88S seipin affects catalase activity. It is possible that the mutation provokes unanticipated changes in either catalase expression and/or protein stability. Nevertheless, the possibility that decreased catalase activity may be an underlying cause of seipinopathy (leading to increased ROS concentrations in the blood and neuronal tissues), as observed for different catalase mutations in patients [198], is very interesting and will serve as a molecular basis for future studies.

We also observed a substantial increase in GSH levels in N88S-VN WT-VC and N88S-VN N88S-VC cells. This may indicate a compensatory ROS scavenging mechanism to counteract the production of ROS, or may reveal changes in the ERO1/PDI-mediated oxidative folding process, which requires GSH to catalyze disulfide bond formation [179]. A bioinformatics analysis of seipin sequence reveals the presence of cysteine residues prone to form disulfide bonds (data not shown), and a cryo-electron microscopy structure of the *Drosophila melanogaster* seipin revealed two cysteines (C149 and C164) in close spatial proximity, consistent with the presence of a disulfide bond [85]. It is then possible that disulfide bond formation in mutant seipin is altered and stimulates Ero1p activity, which is significant cause of cellular ROS [141]. It would be interesting in the future to investigate the role of the ERO1/PDI protein folding pathway in the production of ROS in cells expressing the N88S mutation.

We also demonstrated that oxidative stress is not the contributing factor for intracellular inclusion formation. In fact, treatment with antioxidant NAC did not alter UPR induction and higher levels of ROS (observed in the rho^0 background) are not associated with higher IB formation in cells carrying the N88S mutant seipin. Instead, induction of the ER stress response during aging seems to derive from N88S seipin misfolding. The contribution of the ERAD and UPR quality control mechanisms in controlling the formation of IBs and the generation of ROS was also assessed in cells

expressing the N88S mutation. Deletion of *HRD1* drastically increased the formation of IB as well as the production of ROS in these cells, probably due to the toxic accumulation of N88S seipin species that are not properly degraded by this pathway. This indicates that ERAD is involved in the removal of N88S seipin and control of ROS generation to sustain proper growth. In addition, induction of the UPR is also required for growth and turnover of N88S mutant seipin, as disruption of *IRE1* significantly increased IB formation in cells expressing the N88S mutation.

Previous work has shown that following protein misfolding, prolonged ER stress leads to alterations in the protein folding and degradation machinery, disruption of calcium homeostasis, and activation of various intracellular signaling pathways [103, 185]. Among the many proteins affected by changes in calcium homeostasis is calcineurin, an important phosphatase in the brain, activated by ER stress during formation of misfolded aggregates [184]. The relationship between ER stress and calcineurin activation within the scope of N88S seipinopathy was evaluated by monitoring calcineurin activation. Curiously, our results revealed impaired activation of calcineurin signaling in the mutant homomeric strain but not in cells expressing WT-mutant heteromers. Furthermore, calcineurin is essential for survival under conditions of prolonged ER stress conditions through the control of mitochondrial ROS production [190]. Although abolishing calcineurin activity had no effect on ROS levels, it enhanced the formation of IB in all strains, which indicate that the phosphatase regulates the formation of intracellular inclusions. Whether calcineurin acts in concert with the ERAD and UPR pathways remains to be established.

Lastly, it would be interesting to investigate the involvement of lipid imbalance in seipinopathy, since seipin is directly involved in LD formation and TAG storage. Previous work in a zebrafish model has shown that expression of N88S seipin results in reduced TAG content in cells of the CNS origin as well as in the developing zebrafish brain, and that restoration of TAG storage reverses ER stress, possibly by allowing misfolded seipin protein to be sequestered from the ER to the surface of LDs [96].

Overall, our model recapitulates the major observations made in mammalian systems: the expression of N88S seipin in cells leads to formation of IBs associated with activation of the UPR pathway. Our study so far establishes that the N88S-N88S homo-oligomerization might actively contribute to enhance mutant seipin toxicity, resulting in IB formation, severe cellular oxidative damages caused by the increase in ROS production, concomitant with activation of the ER stress response, ERAD and autophagy. All these phenotypes described for N88S-VN/N88S-VC strain might explain the rapid loss of cell viability observed in these cells. Importantly, almost all of these alterations seem to be attenuated to some degree by the expression of WT seipin.

We then conceive a model for N88S seipinopathy as follows: when misfolded proteins appear but the cell's internal stress level is moderate, UPR is induced where active degradation or refolding prevents the formation of proteinaceous inclusions, along with activation of autophagy and ERAD. Alternatively, these inclusions are not directly toxic, but unfolded proteins stored in the ER can seed protein aggregation. During aging, gradual impairment of these homeostatic mechanisms elevate stress levels and increase the amount of misfolded seipin. Hence, more misfolded proteins are sequestered within the ER and may saturate and exhaust the quality control machinery or lead to prolonged activation of the ER stress response and ERAD. Therefore, protein degradation or refolding becomes impaired. Cytotoxic proteinaceous inclusions accumulate in the ER, and this toxicity may also arise from sequestration of other proteins involved in managing and processing misfolded proteins (e.g. Kar2p and the Hsp104p chaperones). The accumulation of N88S misfolded protein, particularly in cells expressing solely the N88S mutation, leads to a state of acute oxidative damage associated with higher ROS levels and lipid peroxidation, concomitant with reduced cellular antioxidant capacity (e.g. catalase). Prolonged ER stress and oxidative stress then contribute to increased apparent cytotoxicity and decreased cell viability. Importantly, severe oxidative stress is recognized by the oxidative stress sensor Yap1p, which shares functional similarity to the mammalian Keap1-Nrf2 signaling pathway. The involvement of this pathway and ROS accumulation, which we propose to be a hallmark of seipinopathy, should be explored in future studies using mammalian systems.

The pathogenic mechanisms of neuron dysfunction in seipinopathy and how therapy might be approached are yet to be established. Importantly, there is no effective treatment option for seipinopathy due to incomplete understanding of the pathogenesis of the disease. Within this scope, our study and future research will provide new insights into the molecular underpinnings of this disease.

Chapter 5

BIBLIOGRAPHY

5. Bibliography

1. Olzmann, J.A. and P. Carvalho, *Dynamics and functions of lipid droplets.* Nat Rev Mol Cell Biol, 2019. **20**(3): p. 137-155.
2. Jackson, C.L., *Lipid droplet biogenesis.* Curr Opin Cell Biol, 2019. **59**: p. 88-96.
3. Walther, T.C., J. Chung, and R.V. Farese, Jr., *Lipid Droplet Biogenesis.* Annu Rev Cell Dev Biol, 2017. **33**: p. 491-510.
4. Jarc, E. and T. Petan, *Lipid Droplets and the Management of Cellular Stress.* Yale J Biol Med, 2019. **92**(3): p. 435-452.
5. Teixeira, V., P. Maciel, and V. Costa, *Leading the way in the nervous system: Lipid Droplets as new players in health and disease.* Biochim Biophys Acta Mol Cell Biol Lipids, 2021. **1866**(1): p. 158820.
6. Mejhert, N., et al., *Partitioning of MLX-Family Transcription Factors to Lipid Droplets Regulates Metabolic Gene Expression.* Mol Cell, 2020. **77**(6): p. 1251-1264 e9.
7. Herker, E., et al., *Lipid Droplet Contact Sites in Health and Disease.* Trends Cell Biol, 2021. **31**(5): p. 345-358.
8. Welte, M.A., *Expanding roles for lipid droplets.* Curr Biol, 2015. **25**(11): p. R470-81.
9. Melvin, A., A. Stears, and D.B. Savage, *Recent developments in lipodystrophy.* Curr Opin Lipidol, 2019. **30**(4): p. 284-290.
10. Henne, W.M., M.L. Reese, and J.M. Goodman, *The assembly of lipid droplets and their roles in challenged cells.* EMBO J, 2018. **37**(12).
11. Krahmer, N., R.V. Farese, Jr., and T.C. Walther, *Balancing the fat: lipid droplets and human disease.* EMBO Mol Med, 2013. **5**(7): p. 973-83.
12. Magre, J., et al., *Identification of the gene altered in Berardinelli-Seip congenital lipodystrophy on chromosome 11q13.* Nat Genet, 2001. **28**(4): p. 365-70.
13. Lodhi, I.J. and C.F. Semenkovich, *Peroxisomes: a nexus for lipid metabolism and cellular signaling.* Cell Metab, 2014. **19**(3): p. 380-92.
14. Long, A.P., et al., *Lipid droplet de novo formation and fission are linked to the cell cycle in fission yeast.* Traffic, 2012. **13**(5): p. 705-14.
15. Thiam, A.R. and L. Foret, *The physics of lipid droplet nucleation, growth and budding.* Biochim Biophys Acta, 2016. **1861**(8 Pt A): p. 715-22.
16. Yen, C.L., et al., *Thematic review series: glycerolipids. DGAT enzymes and triacylglycerol biosynthesis.* J Lipid Res, 2008. **49**(11): p. 2283-301.
17. Kassan, A., et al., *Acyl-CoA synthetase 3 promotes lipid droplet biogenesis in ER microdomains.* J Cell Biol, 2013. **203**(6): p. 985-1001.
18. Kennedy, E.P., *Metabolism of lipides.* Annu Rev Biochem, 1957. **26**: p. 119-48.
19. Dahlqvist, A., et al., *Phospholipid:diacylglycerol acyltransferase: an enzyme that catalyzes the acyl-CoA-independent formation of triacylglycerol in yeast and plants.* Proc Natl Acad Sci U S A, 2000. **97**(12): p. 6487-92.

20. Sorger, D. and G. Daum, *Synthesis of triacylglycerols by the acyl-coenzyme A:diacyl-glycerol acyltransferase Dga1p in lipid particles of the yeast Saccharomyces cerevisiae.* J Bacteriol, 2002. **184**(2): p. 519-24.

21. Sorger, D., et al., *A yeast strain lacking lipid particles bears a defect in ergosterol formation.* J Biol Chem, 2004. **279**(30): p. 31190-6.

22. Bohnert, M., *New friends for seipin - Implications of seipin partner proteins in the life cycle of lipid droplets.* Semin Cell Dev Biol, 2020. **108**: p. 24-32.

23. Thiam, A.R., R.V. Farese, Jr., and T.C. Walther, *The biophysics and cell biology of lipid droplets.* Nat Rev Mol Cell Biol, 2013. **14**(12): p. 775-86.

24. Ben M'barek, K., et al., *ER Membrane Phospholipids and Surface Tension Control Cellular Lipid Droplet Formation.* Dev Cell, 2017. **41**(6): p. 591-604 e7.

25. Choudhary, V., et al., *Seipin and Nem1 establish discrete ER subdomains to initiate yeast lipid droplet biogenesis.* J Cell Biol, 2020. **219**(7).

26. Chung, J., et al., *LDAF1 and Seipin Form a Lipid Droplet Assembly Complex.* Dev Cell, 2019. **51**(5): p. 551-563 e7.

27. Hayes, M., et al., *Fat storage-inducing transmembrane (FIT or FITM) proteins are related to lipid phosphatase/phosphotransferase enzymes.* Microb Cell, 2017. **5**(2): p. 88-103.

28. Becuwe, M., et al., *FIT2 is an acyl-coenzyme A diphosphatase crucial for endoplasmic reticulum homeostasis.* J Cell Biol, 2020. **219**(10).

29. Gross, D.A., C. Zhan, and D.L. Silver, *Direct binding of triglyceride to fat storage-inducing transmembrane proteins 1 and 2 is important for lipid droplet formation.* Proc Natl Acad Sci U S A, 2011. **108**(49): p. 19581-6.

30. Choudhary, V., et al., *Architecture of Lipid Droplets in Endoplasmic Reticulum Is Determined by Phospholipid Intrinsic Curvature.* Curr Biol, 2018. **28**(6): p. 915-926 e9.

31. Wang, S., et al., *Seipin and the membrane-shaping protein Pex30 cooperate in organelle budding from the endoplasmic reticulum.* Nat Commun, 2018. **9**(1): p. 2939.

32. Joshi, A.S., et al., *Lipid droplet and peroxisome biogenesis occur at the same ER subdomains.* Nat Commun, 2018. **9**(1): p. 2940.

33. Santinho, A., et al., *Membrane Curvature Catalyzes Lipid Droplet Assembly.* Curr Biol, 2020. **30**(13): p. 2481-2494 e6.

34. Wilfling, F., et al., *Lipid droplet biogenesis.* Curr Opin Cell Biol, 2014. **29**: p. 39-45.

35. Adeyo, O., et al., *The yeast lipin orthologue Pah1p is important for biogenesis of lipid droplets.* J Cell Biol, 2011. **192**(6): p. 1043-55.

36. Fei, W., et al., *A role for phosphatidic acid in the formation of "supersized" lipid droplets.* PLoS Genet, 2011. **7**(7): p. e1002201.

37. Skinner, J.R., et al., *Diacylglycerol enrichment of endoplasmic reticulum or lipid droplets recruits perilipin 3/TIP47 during lipid storage and mobilization.* J Biol Chem, 2009. **284**(45): p. 30941-8.

38. Kadereit, B., et al., *Evolutionarily conserved gene family important for fat storage.* Proc Natl Acad Sci U S A, 2008. **105**(1): p. 94-9.

39. Choudhary, V., et al., *A conserved family of proteins facilitates nascent lipid droplet budding from the ER.* J Cell Biol, 2015. **211**(2): p. 261-71.

40. Kimmel, A.R. and C. Sztalryd, *The Perilipins: Major Cytosolic Lipid Droplet-Associated Proteins and Their Roles in Cellular Lipid Storage, Mobilization, and Systemic Homeostasis.* Annu Rev Nutr, 2016. **36**: p. 471-509.

41. Itabe, H., et al., *Perilipins: a diversity of intracellular lipid droplet proteins.* Lipids Health Dis, 2017. **16**(1): p. 83.

42. Thiam, A.R. and M. Beller, *The why, when and how of lipid droplet diversity.* J Cell Sci, 2017. **130**(2): p. 315-324.

43. Gao, Q., et al., *Pet10p is a yeast perilipin that stabilizes lipid droplets and promotes their assembly.* J Cell Biol, 2017. **216**(10): p. 3199-3217.

44. Wang, H., et al., *Seipin is required for converting nascent to mature lipid droplets.* Elife, 2016. **5**.

45. Salo, V.T., et al., *Seipin Facilitates Triglyceride Flow to Lipid Droplet and Counteracts Droplet Ripening via Endoplasmic Reticulum Contact.* Dev Cell, 2019. **50**(4): p. 478-493 e9.

46. Salo, V.T., et al., *Seipin regulates ER-lipid droplet contacts and cargo delivery.* EMBO J, 2016. **35**(24): p. 2699-2716.

47. Grippa, A., et al., *The seipin complex Fld1/Ldb16 stabilizes ER-lipid droplet contact sites.* J Cell Biol, 2015. **211**(4): p. 829-44.

48. Fei, W., et al., *Fld1p, a functional homologue of human seipin, regulates the size of lipid droplets in yeast.* J Cell Biol, 2008. **180**(3): p. 473-82.

49. Pagac, M., et al., *SEIPIN Regulates Lipid Droplet Expansion and Adipocyte Development by Modulating the Activity of Glycerol-3-phosphate Acyltransferase.* Cell Rep, 2016. **17**(6): p. 1546-1559.

50. Yan, R., et al., *Human SEIPIN Binds Anionic Phospholipids.* Dev Cell, 2018. **47**(2): p. 248-256 e4.

51. Talukder, M.M., et al., *Seipin oligomers can interact directly with AGPAT2 and lipin 1, physically scaffolding critical regulators of adipogenesis.* Mol Metab, 2015. **4**(3): p. 199-209.

52. Teixeira, V., et al., *Regulation of lipid droplets by metabolically controlled Ldo isoforms.* J Cell Biol, 2018. **217**(1): p. 127-138.

53. Eisenberg-Bord, M., et al., *Identification of seipin-linked factors that act as determinants of a lipid droplet subpopulation.* J Cell Biol, 2018. **217**(1): p. 269-282.

54. Romanauska, A. and A. Kohler, *The Inner Nuclear Membrane Is a Metabolically Active Territory that Generates Nuclear Lipid Droplets.* Cell, 2018. **174**(3): p. 700-715 e18.

55. Wilfling, F., et al., *Triacylglycerol synthesis enzymes mediate lipid droplet growth by relocalizing from the ER to lipid droplets.* Dev Cell, 2013. **24**(4): p. 384-99.

56. Wanner, G. and R.R. Theimer, *Membranous appendices of spherosomes (oleosomes) : Possible role in fat utilization in germinating oil seeds.* Planta, 1978. **140**(2): p. 163-9.

57. Klemm, R.W., et al., *A conserved role for atlastin GTPases in regulating lipid droplet size.* Cell Rep, 2013. **3**(5): p. 1465-75.

58. Wilfling, F., et al., *Arf1/COPI machinery acts directly on lipid droplets and enables their connection to the ER for protein targeting.* Elife, 2014. **3**: p. e01607.

59. Thiam, A.R., et al., *COPI buds 60-nm lipid droplets from reconstituted water-phospholipid-triacylglyceride interfaces, suggesting a tension clamp function.* Proc Natl Acad Sci U S A, 2013. **110**(33): p. 13244-9.

60. Krahmer, N., et al., *Phosphatidylcholine synthesis for lipid droplet expansion is mediated by localized activation of CTP:phosphocholine cytidylyltransferase.* Cell Metab, 2011. **14**(4): p. 504-15.

61. Bostrom, P., et al., *SNARE proteins mediate fusion between cytosolic lipid droplets and are implicated in insulin sensitivity.* Nat Cell Biol, 2007. **9**(11): p. 1286-93.

62. Jambunathan, S., et al., *FSP27 promotes lipid droplet clustering and then fusion to regulate triglyceride accumulation.* PLoS One, 2011. **6**(12): p. e28614.

63. Guo, Y., et al., *Functional genomic screen reveals genes involved in lipid-droplet formation and utilization.* Nature, 2008. **453**(7195): p. 657-61.

64. Kounakis, K., et al., *Emerging Roles of Lipophagy in Health and Disease.* Front Cell Dev Biol, 2019. **7**: p. 185.

65. Smirnova, E., et al., *ATGL has a key role in lipid droplet/adiposome degradation in mammalian cells.* EMBO Rep, 2006. **7**(1): p. 106-13.

66. Schweiger, M., et al., *Adipose triglyceride lipase and hormone-sensitive lipase are the major enzymes in adipose tissue triacylglycerol catabolism.* J Biol Chem, 2006. **281**(52): p. 40236-41.

67. Taschler, U., et al., *Monoglyceride lipase deficiency in mice impairs lipolysis and attenuates diet-induced insulin resistance.* J Biol Chem, 2011. **286**(20): p. 17467-77.

68. Singh, R., et al., *Autophagy regulates lipid metabolism.* Nature, 2009. **458**(7242): p. 1131-5.

69. Zechner, R., F. Madeo, and D. Kratky, *Cytosolic lipolysis and lipophagy: two sides of the same coin.* Nat Rev Mol Cell Biol, 2017. **18**(11): p. 671-684.

70. van Zutphen, T., et al., *Lipid droplet autophagy in the yeast Saccharomyces cerevisiae.* Mol Biol Cell, 2014. **25**(2): p. 290-301.

71. Schulze, R.J., A. Sathyanarayan, and D.G. Mashek, *Breaking fat: The regulation and mechanisms of lipophagy.* Biochim Biophys Acta Mol Cell Biol Lipids, 2017. **1862**(10 Pt B): p. 1178-1187.

72. Schott, M.B., et al., *Lipid droplet size directs lipolysis and lipophagy catabolism in hepatocytes.* J Cell Biol, 2019. **218**(10): p. 3320-3335.

73. Cartwright, B.R. and J.M. Goodman, *Seipin: from human disease to molecular mechanism.* J Lipid Res, 2012. **53**(6): p. 1042-55.

74. Windpassinger, C., et al., *Heterozygous missense mutations in BSCL2 are associated with distal hereditary motor neuropathy and Silver syndrome.* Nat Genet, 2004. **36**(3): p. 271-6.

75. Szymanski, K.M., et al., *The lipodystrophy protein seipin is found at endoplasmic reticulum lipid droplet junctions and is important for droplet morphology.* Proc Natl Acad Sci U S A, 2007. **104**(52): p. 20890-5.

76. Ito, D. and N. Suzuki, *Seipinopathy: a novel endoplasmic reticulum stress-associated disease.* Brain, 2009. **132**(Pt 1): p. 8-15.

77. Rowe, E.R., et al., *Conserved Amphipathic Helices Mediate Lipid Droplet Targeting of Perilipins 1-3.* J Biol Chem, 2016. **291**(13): p. 6664-78.

78. Craveiro Sarmento, A.S., et al., *Exploring Seipin: From Biochemistry to Bioinformatics Predictions.* Int J Cell Biol, 2018. **2018**: p. 5207608.

79. Sanchez-Iglesias, S., et al., *Skipped BSCL2 Transcript in Celia's Encephalopathy (PELD): New Insights on Fatty Acids Involvement, Senescence and Adipogenesis.* PLoS One, 2016. **11**(7): p. e0158874.

80. Agarwal, A.K. and A. Garg, *Seipin: a mysterious protein.* Trends Mol Med, 2004. **10**(9): p. 440-4.

81. Lundin, C., et al., *Membrane topology of the human seipin protein.* FEBS Lett, 2006. **580**(9): p. 2281-4.

82. Wang, C.W., Y.H. Miao, and Y.S. Chang, *Control of lipid droplet size in budding yeast requires the collaboration between Fld1 and Ldb16.* J Cell Sci, 2014. **127**(Pt 6): p. 1214-28.

83. Chapman, K.D., et al., *Mechanisms of lipid droplet biogenesis.* Biochem J, 2019. **476**(13): p. 1929-1942.

84. Henne, M., J.M. Goodman, and H. Hariri, *Spatial compartmentalization of lipid droplet biogenesis.* Biochim Biophys Acta Mol Cell Biol Lipids, 2020. **1865**(1): p. 158499.

85. Sui, X., et al., *Cryo-electron microscopy structure of the lipid droplet-formation protein seipin.* J Cell Biol, 2018. **217**(12): p. 4080-4091.

86. Bohnert, M., *Wrapping up the fats-a structure of the lipid droplet biogenesis protein seipin.* J Cell Biol, 2018. **217**(12): p. 4053-4054.

87. Fei, W., et al., *Molecular characterization of seipin and its mutants: implications for seipin in triacylglycerol synthesis.* J Lipid Res, 2011. **52**(12): p. 2136-47.

88. Van Maldergem, L., et al., *Genotype-phenotype relationships in Berardinelli-Seip congenital lipodystrophy.* J Med Genet, 2002. **39**(10): p. 722-33.

89. Ito, D., T. Yagi, and N. Suzuki, *[BSCL2-related neurologic disorders/seipinopathy: endoplasmic reticulum stress in neurodegeneration].* Rinsho Shinkeigaku, 2011. **51**(11): p. 1186-8.

90. Miranda, D.M., et al., *Novel mutations of the BSCL2 and AGPAT2 genes in 10 families with Berardinelli-Seip congenital generalized lipodystrophy syndrome.* Clin Endocrinol (Oxf), 2009. **71**(4): p. 512-7.

91. Foster, L.A. and M.K. Salajegheh, *Motor Neuron Disease: Pathophysiology, Diagnosis, and Management.* Am J Med, 2019. **132**(1): p. 32-37.

92. Auer-Grumbach, M., et al., *Phenotypes of the N88S Berardinelli-Seip congenital lipodystrophy 2 mutation.* Ann Neurol, 2005. **57**(3): p. 415-24.

93. Patni, N. and A. Garg, *Congenital generalized lipodystrophies--new insights into metabolic dysfunction.* Nat Rev Endocrinol, 2015. **11**(9): p. 522-34.

94. Guillen-Navarro, E., et al., *A new seipin-associated neurodegenerative syndrome.* J Med Genet, 2013. **50**(6): p. 401-9.

95. Ito, D. and N. Suzuki, *Molecular pathogenesis of seipin/BSCL2-related motor neuron diseases.* Ann Neurol, 2007. **61**(3): p. 237-50.

96. Holtta-Vuori, M., et al., *Alleviation of seipinopathy-related ER stress by triglyceride storage.* Hum Mol Genet, 2013. **22**(6): p. 1157-66.

97. Ito, D., et al., *Characterization of seipin/BSCL2, a protein associated with spastic paraplegia 17.* Neurobiol Dis, 2008. **31**(2): p. 266-77.

98. Pennuto, M., et al., *Ablation of the UPR-mediator CHOP restores motor function and reduces demyelination in Charcot-Marie-Tooth 1B mice.* Neuron, 2008. **57**(3): p. 393-405.

99. Zhang, K. and R.J. Kaufman, *The unfolded protein response: a stress signaling pathway critical for health and disease.* Neurology, 2006. **66**(2 Suppl 1): p. S102-9.

100. Turner, B.J. and J.D. Atkin, *ER stress and UPR in familial amyotrophic lateral sclerosis.* Curr Mol Med, 2006. **6**(1): p. 79-86.

101. Yagi, T., et al., *N88S seipin mutant transgenic mice develop features of seipinopathy/BSCL2-related motor neuron disease via endoplasmic reticulum stress.* Hum Mol Genet, 2011. **20**(19): p. 3831-40.

102. Guo, J., et al., *Motor neuron degeneration in a mouse model of seipinopathy.* Cell Death Dis, 2013. **4**: p. e535.

103. Schroder, M. and R.J. Kaufman, *ER stress and the unfolded protein response.* Mutat Res, 2005. **569**(1-2): p. 29-63.

104. Back, S.H., et al., *ER stress signaling by regulated splicing: IRE1/HAC1/XBP1.* Methods, 2005. **35**(4): p. 395-416.

105. Mori, K., et al., *A transmembrane protein with a cdc2+/CDC28-related kinase activity is required for signaling from the ER to the nucleus.* Cell, 1993. **74**(4): p. 743-56.

106. Cox, J.S., C.E. Shamu, and P. Walter, *Transcriptional induction of genes encoding endoplasmic reticulum resident proteins requires a transmembrane protein kinase.* Cell, 1993. **73**(6): p. 1197-206.

107. Mori, K., et al., *A 22 bp cis-acting element is necessary and sufficient for the induction of the yeast KAR2 (BiP) gene by unfolded proteins.* EMBO J, 1992. **11**(7): p. 2583-93.

108. Zhao, L. and S.L. Ackerman, *Endoplasmic reticulum stress in health and disease.* Curr Opin Cell Biol, 2006. **18**(4): p. 444-52.

109. Pineau, L. and T. Ferreira, *Lipid-induced ER stress in yeast and beta cells: parallel trails to a common fate.* FEMS Yeast Res, 2010. **10**(8): p. 1035-45.

110. Gardner, B.M., et al., *Endoplasmic reticulum stress sensing in the unfolded protein response.* Cold Spring Harb Perspect Biol, 2013. **5**(3): p. a013169.

111. Riaz, T.A., et al., *Role of Endoplasmic Reticulum Stress Sensor IRE1alpha in Cellular Physiology, Calcium, ROS Signaling, and Metaflammation.* Cells, 2020. **9**(5).

112. Siwecka, N., et al., *The Structure, Activation and Signaling of IRE1 and Its Role in Determining Cell Fate.* Biomedicines, 2021. **9**(2).

113. Zhang, K. and R.J. Kaufman, *Signaling the unfolded protein response from the endoplasmic reticulum.* J Biol Chem, 2004. **279**(25): p. 25935-8.

114. Bertolotti, A., et al., *Dynamic interaction of BiP and ER stress transducers in the unfolded-protein response.* Nat Cell Biol, 2000. **2**(6): p. 326-32.

115. Hong, M., et al., *Underglycosylation of ATF6 as a novel sensing mechanism for activation of the unfolded protein response.* J Biol Chem, 2004. **279**(12): p. 11354-63.

116. Shen, X., K. Zhang, and R.J. Kaufman, *The unfolded protein response--a stress signaling pathway of the endoplasmic reticulum.* J Chem Neuroanat, 2004. **28**(1-2): p. 79-92.

117. Xia, X., *Translation Control of HAC1 by Regulation of Splicing in Saccharomyces cerevisiae.* Int J Mol Sci, 2019. **20**(12).

118. Travers, K.J., et al., *Functional and genomic analyses reveal an essential coordination between the unfolded protein response and ER-associated degradation.* Cell, 2000. **101**(3): p. 249-58.

119. Friedlander, R., et al., *A regulatory link between ER-associated protein degradation and the unfolded-protein response.* Nat Cell Biol, 2000. **2**(7): p. 379-84.

120. Kaneko, M. and Y. Nomura, *ER signaling in unfolded protein response.* Life Sci, 2003. **74**(2-3): p. 199-205.

121. Sun, Z. and J.L. Brodsky, *Protein quality control in the secretory pathway.* J Cell Biol, 2019. **218**(10): p. 3171-3187.

122. Vembar, S.S. and J.L. Brodsky, *One step at a time: endoplasmic reticulum-associated degradation.* Nat Rev Mol Cell Biol, 2008. **9**(12): p. 944-57.

123. Xie, W. and D.T. Ng, *ERAD substrate recognition in budding yeast.* Semin Cell Dev Biol, 2010. **21**(5): p. 533-9.

124. Habeck, G., et al., *The yeast ERAD-C ubiquitin ligase Doa10 recognizes an intramembrane degron.* J Cell Biol, 2015. **209**(4): p. 621.

125. Carvalho, P., V. Goder, and T.A. Rapoport, *Distinct ubiquitin-ligase complexes define convergent pathways for the degradation of ER proteins.* Cell, 2006. **126**(2): p. 361-73.

126. Schoebel, S., et al., *Cryo-EM structure of the protein-conducting ERAD channel Hrd1 in complex with Hrd3.* Nature, 2017. **548**(7667): p. 352-355.

127. Cao, S.S. and R.J. Kaufman, *Endoplasmic reticulum stress and oxidative stress in cell fate decision and human disease.* Antioxid Redox Signal, 2014. **21**(3): p. 396-413.

128. Shergalis, A.G., et al., *Role of the ERO1-PDI interaction in oxidative protein folding and disease.* Pharmacol Ther, 2020. **210**: p. 107525.

129. Osellame, L.D., T.S. Blacker, and M.R. Duchen, *Cellular and molecular mechanisms of mitochondrial function.* Best Pract Res Clin Endocrinol Metab, 2012. **26**(6): p. 711-23.

130. Santos, R.X., et al., *Mitochondrial DNA oxidative damage and repair in aging and Alzheimer's disease.* Antioxid Redox Signal, 2013. **18**(18): p. 2444-57.

131. Zhao, R.Z., et al., *Mitochondrial electron transport chain, ROS generation and uncoupling (Review).* Int J Mol Med, 2019. **44**(1): p. 3-15.

132. Laurindo, F.R., T.L. Araujo, and T.B. Abrahao, *Nox NADPH oxidases and the endoplasmic reticulum.* Antioxid Redox Signal, 2014. **20**(17): p. 2755-75.

133. Rinnerthaler, M., et al., *Yno1p/Aim14p, a NADPH-oxidase ortholog, controls extramitochondrial reactive oxygen species generation, apoptosis, and actin cable formation in yeast.* Proc Natl Acad Sci U S A, 2012. **109**(22): p. 8658-63.

134. Plaisance, V., et al., *Endoplasmic Reticulum Stress Links Oxidative Stress to Impaired Pancreatic Beta-Cell Function Caused by Human Oxidized LDL.* PLoS One, 2016. **11**(9): p. e0163046.

135. Hasanain, M., et al., *alpha-Solanine induces ROS-mediated autophagy through activation of endoplasmic reticulum stress and inhibition of Akt/mTOR pathway.* Cell Death Dis, 2015. **6**: p. e1860.

136. Tu, B.P. and J.S. Weissman, *Oxidative protein folding in eukaryotes: mechanisms and consequences.* J Cell Biol, 2004. **164**(3): p. 341-6.

137. van der Vlies, D., et al., *Oxidation of ER resident proteins upon oxidative stress: effects of altering cellular redox/antioxidant status and implications for protein maturation.* Antioxid Redox Signal, 2003. **5**(4): p. 381-7.

138. Malhotra, J.D., et al., *Antioxidants reduce endoplasmic reticulum stress and improve protein secretion.* Proc Natl Acad Sci U S A, 2008. **105**(47): p. 18525-30.

139. Chakravarthi, S. and N.J. Bulleid, *Glutathione is required to regulate the formation of native disulfide bonds within proteins entering the secretory pathway.* J Biol Chem, 2004. **279**(38): p. 39872-9.

140. Benham, A.M., et al., *Ero1-PDI interactions, the response to redox flux and the implications for disulfide bond formation in the mammalian endoplasmic reticulum.* Philos Trans R Soc Lond B Biol Sci, 2013. **368**(1617): p. 20110403.

141. Sevier, C.S. and C.A. Kaiser, *Ero1 and redox homeostasis in the endoplasmic reticulum.* Biochim Biophys Acta, 2008. **1783**(4): p. 549-56.

142. Chong, W.C., M.D. Shastri, and R. Eri, *Endoplasmic Reticulum Stress and Oxidative Stress: A Vicious Nexus Implicated in Bowel Disease Pathophysiology.* Int J Mol Sci, 2017. **18**(4).

143. Botstein, D. and G.R. Fink, *Yeast: an experimental organism for 21st Century biology.* Genetics, 2011. **189**(3): p. 695-704.

144. Menezes, R., et al., *From the baker to the bedside: yeast models of Parkinson's disease.* Microb Cell, 2015. **2**(8): p. 262-279.

145. Guan, J., et al., *Cvt18/Gsa12 is required for cytoplasm-to-vacuole transport, pexophagy, and autophagy in Saccharomyces cerevisiae and Pichia pastoris.* Mol Biol Cell, 2001. **12**(12): p. 3821-38.

146. Wilkinson, B.M., et al., *Distinct domains within yeast Sec61p involved in post-translational translocation and protein dislocation.* J Biol Chem, 2000. **275**(1): p. 521-9.

147. Stathopoulos, A.M. and M.S. Cyert, *Calcineurin acts through the CRZ1/TCN1-encoded transcription factor to regulate gene expression in yeast.* Genes Dev, 1997. **11**(24): p. 3432-44.

148. Maeta, K., et al., *Activity of the Yap1 transcription factor in Saccharomyces cerevisiae is modulated by methylglyoxal, a metabolite derived from glycolysis.* Mol Cell Biol, 2004. **24**(19): p. 8753-64.

149. Ng, D.T., E.D. Spear, and P. Walter, *The unfolded protein response regulates multiple aspects of secretory and membrane protein biogenesis and endoplasmic reticulum quality control.* J Cell Biol, 2000. **150**(1): p. 77-88.

150. Swinnen, E., et al., *The protein kinase Sch9 is a key regulator of sphingolipid metabolism in Saccharomyces cerevisiae.* Mol Biol Cell, 2014. **25**(1): p. 196-211.

151. Yofe, I. and M. Schuldiner, *Primers-4-Yeast: a comprehensive web tool for planning primers for Saccharomyces cerevisiae.* Yeast, 2014. **31**(2): p. 77-80.

152. Longtine, M.S., et al., *Additional modules for versatile and economical PCR-based gene deletion and modification in Saccharomyces cerevisiae.* Yeast, 1998. **14**(10): p. 953-61.

153. Janke, C., et al., *A versatile toolbox for PCR-based tagging of yeast genes: new fluorescent proteins, more markers and promoter substitution cassettes.* Yeast, 2004. **21**(11): p. 947-62.

154. Gietz, R.D. and R.H. Schiestl, *High-efficiency yeast transformation using the LiAc/SS carrier DNA/PEG method.* Nat Protoc, 2007. **2**(1): p. 31-4.

155. Steels, E.L., R.P. Learmonth, and K. Watson, *Stress tolerance and membrane lipid unsaturation in Saccharomyces cerevisiae grown aerobically or anaerobically.* Microbiology (Reading), 1994. **140 (Pt 3)**: p. 569-76.

156. Chen, J., et al., *A simple technique for the simultaneous determination of molecular weight and activity of superoxide dismutase using SDS-PAGE.* J Biochem Biophys Methods, 2001. **47**(3): p. 233-7.

157. Goth, L., *A simple method for determination of serum catalase activity and revision of reference range.* Clin Chim Acta, 1991. **196**(2-3): p. 143-51.

158. Sung, M.K. and W.K. Huh, *Bimolecular fluorescence complementation analysis system for in vivo detection of protein-protein interaction in Saccharomyces cerevisiae.* Yeast, 2007. **24**(9): p. 767-75.

159. Wickner, S., M.R. Maurizi, and S. Gottesman, *Posttranslational quality control: folding, refolding, and degrading proteins.* Science, 1999. **286**(5446): p. 1888-93.

160. Ahner, A. and J.L. Brodsky, *Checkpoints in ER-associated degradation: excuse me, which way to the proteasome?* Trends Cell Biol, 2004. **14**(9): p. 474-8.

161. Bays, N.W., et al., *Hrd1p/Der3p is a membrane-anchored ubiquitin ligase required for ER-associated degradation.* Nat Cell Biol, 2001. **3**(1): p. 24-9.

162. Lajoie, P., et al., *Kar2p availability defines distinct forms of endoplasmic reticulum stress in living cells.* Mol Biol Cell, 2012. **23**(5): p. 955-64.

163. Mokry, D.Z., J. Abrahao, and C.H. Ramos, *Disaggregases, molecular chaperones that resolubilize protein aggregates.* An Acad Bras Cienc, 2015. **87**(2 Suppl): p. 1273-92.

164. Mehnert, M., et al., *The interplay of Hrd3 and the molecular chaperone system ensures efficient degradation of malfolded secretory proteins.* Mol Biol Cell, 2015. **26**(2): p. 185-94.

165. Nakatsukasa, K., *Potential Physiological Relevance of ERAD to the Biosynthesis of GPI-Anchored Proteins in Yeast.* Int J Mol Sci, 2021. **22**(3).

166. Yorimitsu, T., et al., *Protein kinase A and Sch9 cooperatively regulate induction of autophagy in Saccharomyces cerevisiae.* Mol Biol Cell, 2007. **18**(10): p. 4180-9.

167. Shintani, T. and D.J. Klionsky, *Autophagy in health and disease: a double-edged sword.* Science, 2004. **306**(5698): p. 990-5.

168. Wang, Z., et al., *Antagonistic controls of autophagy and glycogen accumulation by Snf1p, the yeast homolog of AMP-activated protein kinase, and the cyclin-dependent kinase Pho85p.* Mol Cell Biol, 2001. **21**(17): p. 5742-52.

169. Zeeshan, H.M., et al., *Endoplasmic Reticulum Stress and Associated ROS.* Int J Mol Sci, 2016. **17**(3): p. 327.

170. Bhandary, B., et al., *An involvement of oxidative stress in endoplasmic reticulum stress and its associated diseases.* Int J Mol Sci, 2012. **14**(1): p. 434-56.

171. Dunn, C.D., et al., *A genomewide screen for petite-negative yeast strains yields a new subunit of the i-AAA protease complex.* Mol Biol Cell, 2006. **17**(1): p. 213-26.

172. Leadsham, J.E., et al., *Loss of cytochrome c oxidase promotes RAS-dependent ROS production from the ER resident NADPH oxidase, Yno1p, in yeast.* Cell Metab, 2013. **18**(2): p. 279-86.

173. Simaan, H., S. Lev, and B.A. Horwitz, *Oxidant-Sensing Pathways in the Responses of Fungal Pathogens to Chemical Stress Signals.* Front Microbiol, 2019. **10**: p. 567.

174. Farrugia, G. and R. Balzan, *Oxidative stress and programmed cell death in yeast.* Front Oncol, 2012. **2**: p. 64.

175. Nandi, A., et al., *Role of Catalase in Oxidative Stress- and Age-Associated Degenerative Diseases.* Oxid Med Cell Longev, 2019. **2019**: p. 9613090.

176. Wang, Y., et al., *Superoxide dismutases: Dual roles in controlling ROS damage and regulating ROS signaling.* J Cell Biol, 2018. **217**(6): p. 1915-1928.

177. Gaucher, C., et al., *Glutathione: Antioxidant Properties Dedicated to Nanotechnologies.* Antioxidants (Basel), 2018. **7**(5).

178. Presnell, C.E., et al., *Computational insights into the role of glutathione in oxidative stress.* Curr Neurovasc Res, 2013. **10**(2): p. 185-94.

179. Fu, J., et al., *PDI-Regulated Disulfide Bond Formation in Protein Folding and Biomolecular Assembly.* Molecules, 2020. **26**(1).

180. Ozgur, R., et al., *Interplay between the unfolded protein response and reactive oxygen species: a dynamic duo.* J Exp Bot, 2018. **69**(14): p. 3333-3345.

181. Kwolek-Mirek, M., et al., *Yeast Saccharomyces cerevisiae devoid of Cu,Zn-superoxide dismutase as a cellular model to study acrylamide toxicity.* Toxicol In Vitro, 2011. **25**(2): p. 573-9.

182. Hwang, J. and L. Qi, *Quality Control in the Endoplasmic Reticulum: Crosstalk between ERAD and UPR pathways.* Trends Biochem Sci, 2018. **43**(8): p. 593-605.

183. Hetz, C.A. and C. Soto, *Stressing out the ER: a role of the unfolded protein response in prion-related disorders.* Curr Mol Med, 2006. **6**(1): p. 37-43.

184. Mukherjee, A. and C. Soto, *Role of calcineurin in neurodegeneration produced by misfolded proteins and endoplasmic reticulum stress.* Curr Opin Cell Biol, 2011. **23**(2): p. 223-30.

185. Lindholm, D., H. Wootz, and L. Korhonen, *ER stress and neurodegenerative diseases.* Cell Death Differ, 2006. **13**(3): p. 385-92.

186. Deniaud, A., et al., *Endoplasmic reticulum stress induces calcium-dependent permeability transition, mitochondrial outer membrane permeabilization and apoptosis.* Oncogene, 2008. **27**(3): p. 285-99.

187. Cyert, M.S., *Calcineurin signaling in Saccharomyces cerevisiae: how yeast go crazy in response to stress.* Biochem Biophys Res Commun, 2003. **311**(4): p. 1143-50.

188. Hernandez-Elvira, M., et al., *The Unfolded Protein Response Pathway in the Yeast Kluyveromyces lactis. A Comparative View among Yeast Species.* Cells, 2018. **7**(8).

189. Gorlach, A., et al., *Calcium and ROS: A mutual interplay.* Redox Biol, 2015. **6**: p. 260-271.

190. Bonilla, M., K.K. Nastase, and K.W. Cunningham, *Essential role of calcineurin in response to endoplasmic reticulum stress.* EMBO J, 2002. **21**(10): p. 2343-53.

191. Cyert, M.S. and J. Thorner, *Regulatory subunit (CNB1 gene product) of yeast Ca2+/calmodulin-dependent phosphoprotein phosphatases is required for adaptation to pheromone.* Mol Cell Biol, 1992. **12**(8): p. 3460-9.

192. Binns, D., et al., *Seipin is a discrete homooligomer.* Biochemistry, 2010. **49**(50): p. 10747-55.

193. Remondelli, P. and M. Renna, *The Endoplasmic Reticulum Unfolded Protein Response in Neurodegenerative Disorders and Its Potential Therapeutic Significance.* Front Mol Neurosci, 2017. **10**: p. 187.

194. Hamdan, N., P. Kritsiligkou, and C.M. Grant, *ER stress causes widespread protein aggregation and prion formation.* J Cell Biol, 2017. **216**(8): p. 2295-2304.

195. Doonan, L.M., et al., *Hsp104 facilitates the endoplasmic-reticulum-associated degradation of disease-associated and aggregation-prone substrates.* Protein Sci, 2019. **28**(7): p. 1290-1306.

196. Knaevelsrud, H. and A. Simonsen, *Fighting disease by selective autophagy of aggregate-prone proteins.* FEBS Lett, 2010. **584**(12): p. 2635-45.

197. Barnham, K.J., C.L. Masters, and A.I. Bush, *Neurodegenerative diseases and oxidative stress.* Nat Rev Drug Discov, 2004. **3**(3): p. 205-14.

198. Glorieux, C. and P.B. Calderon, *Catalase, a remarkable enzyme: targeting the oldest antioxidant enzyme to find a new cancer treatment approach.* Biol Chem, 2017. **398**(10): p. 1095-1108.